ABSTRACT

Title of dissertation: PHOTON THERMALIZATION IN DRIVEN OPEN QUANTUM SYSTEMS

Chiao-Hsuan Wang
Doctor of Philosophy, 2018

Dissertation directed by: Professor Jacob M. Taylor
Department of Physics

Light is a paradigmatic quantum field, with individual excitations—photons—that are the most accessible massless particles known. However, their lack of mass and extremely weak interactions mean that typically the thermal description of light is that of blackbody radiation. As the temperature of the light decreases, the overall number of photons approaches zero. Therefore, efforts for quantum optics and optical physics have mostly focused on driving systems far from equilibrium to populate sufficient numbers of photons. While lasers provide a severe example of a nonequilibrium problem, recent interests in the near-equilibrium physics of so-called photon gases, such as in Bose condensation of light or in attempts to make photonic quantum simulators, suggest one re-examine near-equilibrium cases.

In this thesis, we consider peculiar driven open quantum system scenarios where near-equilibrium dynamics can lead to equilibration of photons with a finite number, following a thermal description closer to that of an ideal gas than to blackbody radiation. Specifically, we show how laser cooling of a well-isolated mechanical

mode or atomic motion can provide an effective bath which enables control of both the chemical potential and temperature of the resulting grand canonical ensemble of photon. We then theoretically demonstrate that Bose condensation of photons can be realized by cooling an ensemble of two-level atoms inside a cavity. Finally, we find that the engineered chemical potential for light not only admits future applications in many-body quantum simulations, facilitates preparation of near-equilibrium photonic states, but also enables an analogous voltage bias for photonic circuit elements.

PHOTON THERMALIZATION IN DRIVEN OPEN QUANTUM SYSTEMS

by

Chiao-Hsuan Wang

Dissertation submitted to the Faculty of the Graduate School of the
University of Maryland, College Park in partial fulfillment
of the requirements for the degree of
Doctor of Philosophy
2018

Advisory Committee:
Professor Christopher Jarzynski, Chair
Professor Jacob M. Taylor, Co-Chair/Advisor
Professor Alexey V. Gorshkov
Professor Mohammad Hafezi
Professor Luis A. Orozco
Professor J. V. Porto

Acknowledgments

Foremost, I would like to thank Prof. Jacob Taylor for being an exceptional advisor and an amazing mentor. I sincerely appreciate his keen scientific insights, his encouragement and recognition, and his continuous guidance and support especially at difficult times.

I am truly grateful and feel blessed to collaborate with Prof. William Phillips, Prof. Trey Porto and Dr. Michael Gullans. For me, our joint projects on photon thermalization and Bose condensation via laser cooling of atoms is the highlight of my graduate work. This collaboration experience also reminds me of the key reason why I dreamed of an academic career since young: Being able to work with wonderful people who have talented minds, kind hearts and endless curiosities.

I want to acknowledge my dissertation committee: Prof. Christopher Jarzynski, Prof. Alexey Gorshkov, Prof. Mohammad Hafezi, and Prof. Luis Orozco for their support and valuable inputs. I would also like to thank Prof. Jay Sau for serving on my candidacy presentation committee in 2015.

The work in this thesis also benefits from helpful conversations with other scientists: Prof. Steven Girvin, Prof. Vladan Vuletić, Prof. Martin Weitz, Prof. Howard Carmichael, Garnett Bryant, Eric Shirley, Elizabeth Goldschmidt, Julian Stirling, Michael Zwolak, and Eric Benck.

I owe my gratitude to the entirety of Jake's research group: Vanita Srinavasa, Tom Purdy, Shelby Kimmel, Jim Garrison, Jianxin Chen, Xingyao Wu, Justyna Zwolak, Dan Carney, Xunnong Xu, Dvir Kafri, Haitan Xu, Prabin Adhikari, Stephen

Ragole, Andrew Glaudell, Minh Tran, Shangjie Guo, Brittany Richman, Yiping Wang, Sandesh Kalantre, and Sohitri Ghosh. It has been a tremendous pleasure to be part of the group, and I greatly appreciate all the stimulating discussions. I would also like to thank many friends from JQI and QuICS, including Setiawan, Zhe-Xuan Gong, Guanyu Zhu, Yen-Hsiang Lin, Mohammad Maghrebi, Yidan Wang, Yi-Hsieh Wang, Chunxiao Liu, Wenchao Ge, Haoquan Fan, Penghui Yao, Tongyang Li, Aaron Ostrander, and Amir Kalev. These past six years would have been impossible without their friendships and supports.

This dissertation would not have been possible without funding support from the National Science Foundation through the Physics Frontier Center at the Joint Quantum Institute.

My final and deepest thanks go to my family. Your unconditional love gives me the courage to pursue all my wildest dreams.

Table of Contents

List of Figures

Chapter 1: Introduction

1.1 Near-Equilibrium Physics of Light: A Revisit

The thermal distribution of light was first deduced by Planck more than a century ago [1, 2]. Following the efforts to understand the spectral distribution of electromagnetic radiation emitted by a object in thermal equilibrium [3–5], Planck successfully derived his famous blackbody radiation law by postulating discrete energy elements proportional to the frequencies of a set of resonators. Planck's theory resolved the problem of high frequency divergences in Rayleigh's classical physics prediction of the thermal radiation emission spectrum [5], which was later referred to as the ultraviolet catastrophe by Ehrenfest [6], and led to the first appearance of the Planck constant h and the determination of the Boltzmann constant k_B. People marked the publication of the revolutionary blackbody radiation formula as the beginning of quantum theory, and Planck was awarded the Nobel Prize in Physics 1918 for "his discovery of energy quanta".

The modern understanding of matter-light interactions is based upon quantum electrodynamics (QED) pioneered by the work of Dirac [7]. In QED, photons are gauge massless bosons for electromagnetic fields, i.e. the quanta of excitation carrying electromagnetic forces. Unlike usual massive particles, gauge massless bosons

including photons are not governed by particle conservation during their typical interaction with matter even at low energies, and thus are described in equilibrium by the canonical ensemble – they have no chemical potential. This peculiar nature explains why the spectrum of thermal radiation only depends upon the temperature but not other properties of the blackbody material. At low temperatures, rather than forming a condensate as massive bosons do, the occupation number of photons drops significantly as described by the theory of blackbody radiation, and the vacuum is the typical ground state of such systems. As a consequence, major efforts of quantum optics has been focused mostly on nonthermal states of light such as lasers or coherent states, and non-classical squeezed states.

On the other hand, the quantized degree of freedom of light provides one promising avenue for quantum simulation [8, 9] by examining the phases of matter that can arise with the inclusion of interactions between photons [10–14]. Perhaps the most dramatic possibilities arise in circuit QED [15], where the Josephson effect provides a strong microwave nonlinearity, though similar improvements are now becoming available in semiconductor, molecular, and atomic nonlinearities in the optical domain [16–19]. These photonic systems are particularly interesting given our ability to control the dispersion relation of the particles, including, e.g., the creation of effective mass [20, 21] or synthetic gauge fields [22–24] as well as the character of their interaction. Simple examples of photonic quantum simulations include observations quasiequilibrium Bose-Einstein condensate of photons in recent experiments using cavity polaritons [20, 25–27] or with dye microcavities [21] under pumping and loss process, and self-organization of atoms and open Dicke model

phase transition in the setting of cavity quantum electrodynamics [28–31]. More complex versions now include driven arrays of Josephson-junction-based devices [32]. To provide a sufficient number of photons to create an interesting many-body state of light, current experiments either use approximate number conservation [33, 34] (enabling an effective chemical potential description with a phenomenological temperature) or are far from equilibrium and instead described by a steady-state, while the behavior of which is challenging to predict [35, 36].

Recent attempts to generate and describe complex many-body phenomena with photons suggest one revisit near-equilibrium physics of light. In particular, statistical mechanics has laid a firm foundation for addressing complicated problems with standard thermodynamic ensembles introduced by Gibbs [37]. It has been recently proposed that in parametrically driven systems, near-equilibrium dynamics can lead to equilibration of photons into a thermodynamic ensemble with a finite number of photons [38]. This Gibbs-like ensemble then has an adjustable effective chemical potential, and the dynamics admits a near-equilibrium description without solving the full driven-dissipative nonequilibrium quantum problem. This approach left open a key challenge of developing a robust source of photons that will populate the nonlinear system at a desired temperature and number.

In this thesis, we explore photon thermalization in driven open quantum systems whose long-time dynamics admit thermodynamic descriptions with a finite photon number, which may open up new opportunities in quantum optics, quantum simulations, and photonic statistics. The nonequilibrium nature in driven systems poses crucial challenges in predicting their dynamics and simulating equilibrium

many-body states while at the same time provides distinct opportunities to explore dynamical quantum phases. Here we show that the ability to cool a massive harmonic oscillator to its ground state, via optomechanics, as well as the advent of laser cooling and trapping of cold atoms, provides the necessary tools to realize the dream of many-body quantum simulation with photons. Specifically, photons in microwave or optical cavities can reach a steady-state mimicking a grand-canonical ensemble at the temperature of the laser-cooled motions and with a chemical potential close to the energy of a single laser photon. We then find that Bose condensation of photons is also possible via our proposed thermalization mechanism, and construct a phase diagram suggesting our ability to access different phases of cavity photons, including condense, gain, thermal, and quasi-thermal, by simply adjusting the frequency and intensity of the laser. Moreover, the photon flow between a parametric bath to another photon bath can be formulated as nonequilibrium transport analogous to electronic current driven by a voltage imbalance. Potential implementations of our approaches are built upon available technologies today, and the thermodynamic detailed-balance arguments could be directly generalized to include nonlinear interactions [38]. We are looking forward to future applications including manipulating nonlinear photonics in circuit QED, thermalization of Rydberg-polariton, superfluidities of light, nonequilibrium phase transitions, as well as predicting and controlling photon flow in photonic circuits.

1.2 Chemical Potential of Light by Parametric Thermalization

A general approach to engineering a *controllable* chemical potential for light is highly desirable to provide an adjustable parameter in exploring phase diagrams as well as a photonic analog to voltage bias in directing photon transport. We now briefly review the idea of generating an chemical potential of light by parametric thermalization proposed in Ref. [38]. Consider a photonic system with Hamiltonina H_S coupled parametrically via $2\lambda\cos(\omega_p t)H_{SB}$ to a low-temperature, low-frequency thermal bath with Hamiltonian H_B (see Fig. 1.1). Assuming the system and the bath are initially uncorrelated with the density matrix of the bath of the Boltzmann form $\rho_B \propto \exp(-\beta H_B)$ [39], where β is the inverse temperature of the bath, the authors of Ref. [38] find the parametric system-bath coupling will lead to a controlled chemical potential of the photons.

Specifically, assuming a bi-near interaction of the form

$$H_{SB} = \sum_j (\hat{a}_j + \hat{a}_j^\dagger)\hat{B}_j, \tag{1.1}$$

where $\hat{B}_j$ is a bath operator, $\hat{a}_j^\dagger$ is the creation operator of photonic mode j, and the total photon number is $\hat{N} = \sum_j \hat{n}_j = \sum_j \hat{a}_j^\dagger \hat{a}_j$. Moving to the rotating corresponding to an unitary operation $U = \exp\left(-it\omega_p \hat{N}\right)$, the total Hamiltonian $H = H_S + 2\lambda\cos(\omega_p t)H_{SB} + H_B$ becomes

$$U^\dagger H U - i\hbar U^\dagger \frac{\partial}{\partial t} U \approx H_S{}' - \hbar\omega_p \hat{N} + \lambda H_{SB} + H_B, \tag{1.2}$$

where $H_S{}'$ is the total number conserving part of the original system Hamiltonian, $\left[H_S{}', \hat{N}\right] = 0$. In the above approximate sign we have made the rotating wave ap-

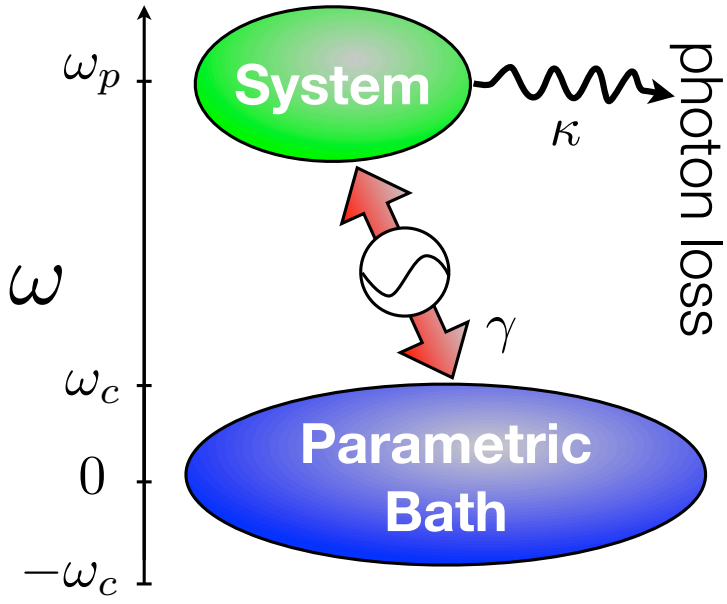

Figure 1.1: Schematic diagram of engineering a controllable chemical potential for light by parametric thermalization [38].

proximation by assuming $||H_S - H_S'||, \hbar\omega_c \ll \hbar\omega_p$, where ω_c is the cutoff frequency of the bath response function. We now have a time-independent total Hamiltonian in this rotating frame and under the rotating wave approximation. For weak coupling λ and an infinite thermal bath, one will expect the system thermalize to the temperature of the bath with a system density matrix

$$\rho_S \propto e^{-\beta(H_S' - \omega_p \hat{N})}. \tag{1.3}$$

Comparing Eq. (1.3) to the Gibbs state of a grand canonical ensemble, we have identified an effective chemical potential $\mu \equiv \hbar\omega_p$, which is directly controlled by the frequency of the parametric coupling. The key challenges for this approach include introducing an appropriate bath to the photonic system via a parametric coupling, and examining photon flow when the system is coupled to an additional

bath corresponding to photon loss.

1.3 Outline of Thesis

Chap. 2 builds upon the general concept of an effective chemical potential in driven systems with an implementation appropriate for a photon-based quantum simulator via quantum optomechanics. The canonical parametric process we consider is the generation of sidebands of light by the motion of a mirror. We show how laser cooling of a well-isolated mechanical mode can provide an effective low-frequency bath for the quantum simulator system, and that the use of auxiliary photon modes, coupled by the mechanical system, enables control of both the chemical potential and temperature of the resulting grand canonical ensemble of the photonic quantum simulator.

Chap. 3 studies the emitted light during laser cooling of atoms and find that noninteracting photons can thermalize with the atoms to a grand canonical ensemble. This thermalization is accomplished via scattering of light between different optical modes, mediated by the laser cooling process. While optically thin modes lead to traditional laser cooling of the atoms, the dynamics of multiple scattering in optically thick modes has been more challenging to describe. We carefully treat the atomic motion and the two sets of modes with quantum master equations and develop a theoretical tool called self-consistent Fermi's golden rule (see Appendix. A) to examine the optically thick modes. We then find that in an appropriate set of limits, multiple scattering leads to thermalization of the light with the atomic mo-

tion in a manner that approximately conserves total photon number between the laser beams and optically thick modes, leading to a grand canonical ensemble of the optically thick subsystem with a chemical potential nearly equal to the energy of a single laser photon. We consider the realization of this regime using two-level atoms in Doppler cooling, and find physically realistic conditions for rare-earth atoms.

Chap. 4 addresses the open question of the possibility of a BEC of photons in the laser cooling scenario presented in Chap. 3 and theoretically demonstrate that a Bose condensation of photons can be realized by cooling an ensemble of two-level atoms (realizable with alkaline earth atoms) inside a long, curved Fabry-Perot cavity. We consider the potential realization using rare-earth atoms in Doppler cooling, and construct a phase diagram as a function of laser frequency and field strength, showing gain, condensate, thermal and quasi-thermal regimes for cavity photons.

Finally, Chap. 5 considers how a sinusoidal parametric coupling between two semi-infinite photonic transmission lines leads to the creation and flow of photons between the two lines. Our approach provides a photonic analog to the Landauer transport formula, and using nonequilbrium Green's functions, we can extend it to the case of an interacting region between two photonic leads where the sinusoid frequency plays the role of a voltage bias. Crucially, we identify both the mathematical framework and the physical regime in which photonic transport is directly analogous to electronic transport and regimes in which other behavior such as two-mode squeezing can emerge.

Chapter 2: Optomechanical approach to controlling the temperature and chemical potential of light[1]

2.1 Quantum Optomechanics

Optomechanics, a rapidly growing research frontier investigating the interaction between light and motion, has paved the way for preparation and manipulation of nonclassical states of light and macroscopic mechanical resonators [40–43]. The development and advancement of optomechanical cooling techniques [44–47], recently reaching the quantum backaction limit [48], have made possible the preparation of the quantum ground state of a mechanical resonator [49–51], squeezed states of light [52–54], realization of nonlinear optics [55–60], and bath engineering for photons using the mechanical degree of freedom [61] in optomechanical platforms.

Here we build upon the general concept of chemical potential in driven systems with an optomechanical implementation appropriate for a nonlinear photonic or microwave quantum simulator, taking full advantage of the advances in laser cooling and related techniques in optomechanics to control the effective bath for the photonic system. The parametric optomechanical interaction between the optical

[1]This chapter has part of "Optomechanical approach to controlling the temperature and chemical potential of light," by C.-H. Wang and J. M. Taylor in Phys. Rev. A **97**, 033850 (2018)

system and the low-frequency bath is provided through a beam-splitter coupling between the optical system and another laser-driven mode, which can be realized in a Michelson-Sagnac interferometer [62, 63]. The use of multiple photon modes enables control of both the chemical potential, by drive frequency, and temperature, by drive amplitude, of the resulting photonic grand canonical ensemble.

2.2 Optomechanical Implementation of a Parametric Bath for Photons

Here we propose an optomechanical implementation for a controllable bath that leads to a grand canonical ensemble of photons with definite temperature and chemical potential by parametric coupling in a driven system. One natural candidate to engineer the parametric coupling is through optomechanics, where thermal (mechanical) excitation can create sideband photons from a pump laser, leading to an effective photonic bath. Consider a beam-splitter-type coupling, which is common in so-called mirror-in-the-middle systems [64–66] and can also be realized in the Michaelson-Sagnac geometry [62, 63], between optical modes $\hat{a}$ and $\hat{b}$ and the motion of the mechanical resonator $\hat{q}$, $\hat{V}_{qa} = -\hbar G_{a0}(\hat{b}^\dagger\hat{a} + \hat{a}^\dagger\hat{b})\hat{q}$, where G_{a0} is the coupling parameter between $\hat{a}$, $\hat{b}$, and $\hat{q}$. By driving the photonic mode $\hat{b}$ with a strong laser of frequency ν_b, we can expand $\hat{b}$ as a small quantum fluctuation $\delta\hat{b}$ around a large steady-state mean value b_s, $\hat{b}(t) = b_s e^{-i\nu_b t} + \delta\hat{b}(t)$, and the interaction can be linearized by neglecting the quantum fluctuations $\delta\hat{b}(t)$,

$$\hat{V}_{qa}(t) \approx -\hbar G_{a0} b_s(\hat{a}e^{i\nu_b t} + \hat{a}^\dagger e^{-i\nu_b t})\hat{q}. \tag{2.1}$$

We assume that the coupling strength is weak compared to optical energies, $\hbar g_a \ll \hbar\nu_b$, which is typically true for optomechanical interactions. Here $g_a = G_{a0} b_s q_{\mathrm{ZPF}}$ is the pump enhanced coupling between $\hat{q}$, $\hat{a}$, and $\hat{b}$ in the unit of frequency and $q_{\mathrm{ZPF}} = \sqrt{\frac{\hbar}{2M\omega_m}}$ is the mechanical zero-point fluctuation. Given this weak parametric coupling and sufficiently small optical losses, one expects the system to reach an equilibrium state describable by a grand canonical ensemble with chemical potential $\hbar\nu_b$, as shown in Ref. [38].

In practice, there are three fundamental limits to this optomechanical approach. First, the response of a high quality factor resonator is narrow band, characterized by its mechanical damping rate, leading to thermalization for transitions only very near the mechanical resonances. Second, the mechanical temperature may be too high even in cryogenic settings, compared to, for example, the relevant photonic nonlinear terms around 100 MHz one may be using to implement a many-body Hamiltonian [see Fig. 2.1(a)-2.1(c)]. Third, the optomechanical interaction requires a strong pump field in mode $\hat{b}$, which we would like to not pollute our many-body optical system $\hat{a}$. That is, we want no steady-state coherence generated in our optical system $\hat{a}$ by the pump ($a_s = 0$).

To conquer the first two challenges, we propose adding an additional optical cooling mode $\hat{c}$ to broaden the mechanical bandwidth and lower the temperature via laser cooling [see Fig. 2.1(d)-2.1(f)]. Specifically, the quantum Brownian motion theory applies to the coupled three optical modes and one mechanical mode by treating $\hat{b}$, $\hat{c}$, $\hat{q}$ all together as an effective heat bath for the system $\hat{a}$ as we show below. The last problem we solve only technically via a potential experimental

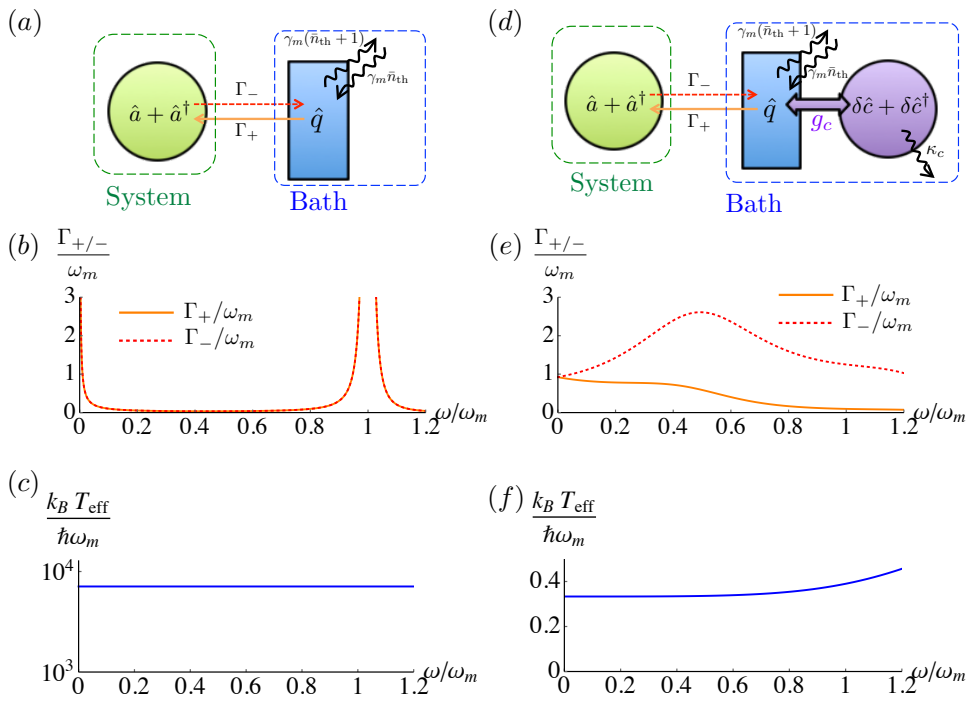

Figure 2.1: Comparison between cases of (a)-(c) a mechanical resonator as a bath and (d)-(f) a laser-cooled mechanical resonator as a bath for the many-body photonic system. (a) Schematic diagram of a mechanical resonator $\hat{q}$ serving as an effective bath for the many-body photonic system $\hat{a}$ through optomechanical interaction. (b) Photon emission coefficient Γ_+ (orange solid line) and absorption coefficient Γ_- (red dashed line) due to coupling with the mechanical resonator. The coefficients have an out-of-range peak centered at the mechanical resonant frequency ω_m, with a small width characterized by the mechanical damping rate γ_m, leading to efficient thermalization only within the narrowband around ω_m. (c) Effective bath temperature $k_B T_{\rm eff}$ of the mechanical resonator. (d) Schematic diagram of a mechanical resonator $\hat{q}$, laser-cooled by a cooling mode $\hat{c}$, serving as a thermal bath to the photonic many-body system $\hat{a}$ through optomechanical interaction. (e) Photon emission coefficient Γ_+ (orange solid line) and absorption coefficient Γ_- (red dashed line) due to coupling with the laser-cooled mechanical resonator, suggesting a much broader bandwidth towards low frequencies. (f) Effective bath temperature $k_B T_{\rm eff}$ of a laser-cooled mechanical resonator, which is lowered by a factor of 10^{-5} in comparison to the case without laser-cooling. These plots are generated with the parameters $\Delta_c = -\omega_m = -\sqrt{\frac{3}{4}}\kappa_c$, $\beta = 10^{-4}\omega_m$, $\gamma_m = 10^{-6}\omega_m$, the cavity-enhanced system-bath coupling $g_a = 0.45\omega_m$, and the mechanical resonator-cooling cavity coupling $g_c = 0.45\omega_m$.

design using the Michelson-Sagnac geometry [62, 63], but the underlying concept of using beam-splitter optomechanical interactions for pump rejection should be extensible to many other configurations.

We now focus on our solutions to the first two challenges. Specifically, we consider how the correlation functions, which describe the full dynamics of the mechanical system, including its bath, are modified by laser cooling using, e.g., an additional photonic mode $\hat{c}$. This allows us to connect the full non-Markovian theory that describes the original mechanical system to a new effective bath that includes the laser cooling and is close to Markovian. Thus the $\hat{q}$ degree of freedom is effectively promoted to a bath operator $\hat{B}$ whose correlation functions mimic the desired bath (including chemical potential) for the many-body photonic system $\hat{a}$. We will show how $\hat{b}$, $\hat{c}$, $\hat{q}$, and their dissipative environments all together serve as a bath for the many-body system $\hat{a}$ (see Fig. 2.2). Specifically, the Hamiltonian reads

$$\begin{aligned}\hat{H} =&\hat{H}_a + \hat{H}_0 + \hat{V}_{qa} + \hat{V}_{qc} + \hat{H}_{\text{drive,b}} + \hat{H}_{\text{drive,c}} \\ &+ \hat{H}_{\kappa_b} + \hat{H}_{\kappa_c} + \hat{H}_{\gamma_m},\end{aligned} \tag{2.2}$$

where $\hat{H}_a$ is some general system Hamiltonian for $\hat{a}$ and might contain nonlinear terms. We have

$$\hat{H}_0 = \hbar\omega_a \hat{a}^\dagger \hat{a} + \hbar\omega_b \hat{b}^\dagger \hat{b} + \hbar\omega_c \hat{c}^\dagger \hat{c} + \frac{\hat{p}^2}{2M} + \frac{M\omega_m^2(\hat{q} - q_0)^2}{2}, \tag{2.3}$$

$$\hat{V}_{qa} = -\hbar G_{a0}(\hat{b}^\dagger \hat{a} + \hat{a}^\dagger \hat{b})\hat{q}, \tag{2.4}$$

$$\hat{V}_{qc} = -\hbar G_{c0}(\hat{c}^\dagger \hat{c})\hat{q}, \tag{2.5}$$

$$\hat{H}_{\mathrm{drive,b}} = i\hbar\sqrt{\kappa_b}\left(\hat{b}^\dagger \hat{b}_{\mathrm{in}} e^{-i\nu_b t} - \hat{b}\hat{b}_{\mathrm{in}}^\dagger e^{i\nu_b t}\right), \tag{2.6}$$

$$H_{\mathrm{drive,c}} = i\hbar\sqrt{\kappa_c}\left(\hat{c}^\dagger \hat{c}_{\mathrm{in}} e^{-i\nu_c t} - \hat{c}\hat{c}_{\mathrm{in}}^\dagger e^{i\nu_c t}\right). \tag{2.7}$$

Here ω_a, ω_b, and ω_c are the frequencies of the optical modes $\hat{a}$, $\hat{b}$, and $\hat{c}$; M, ω_m, and $\hat{p}$ are the mass, mode frequency, and momentum of the mechanical resonator; G_{c0} is the coupling parameter between the optical mode $\hat{c}$ and the mechanical resonator $\hat{q}$; H_{κ_b}, H_{κ_c}, and H_{γ_m} are the dissipative interactions of the cavity modes $\hat{b}$ and $\hat{c}$ and mechanical modes $\hat{q}$ with the environment with damping rates κ_b, κ_c, and γ_m respectively. Note that we have assumed the perfect cavity limit, i.e., no internal losses inside the high quality factor cavities, such that the dissipation in cavity modes comes solely from the coupling to the external drive. The loss rate of the system $\hat{a}$ is zero, $\kappa_a = 0$, since we are driving $\hat{b}$ and $\hat{c}$ modes only. The interaction $\hat{V}_{qc}$ between the mechanical mode and cooling mode $\hat{c}$ can also be beam-splitter-like.

We now move to a rotating frame through $U = e^{i(\nu_b \hat{a}^\dagger \hat{a} + \nu_b \hat{b}^\dagger \hat{b} + \nu_c \hat{c}^\dagger \hat{c})t}$. H_a can be decomposed into $H_{a0} + H_{a,\perp}$. Here H_{a0} is the particle-number conserving part (comprising of $\hat{a}\hat{a}^\dagger$ and $\hat{a}^\dagger\hat{a}$ pairs) while $H_{a,\perp}$ includes all terms that do not conserve the total number of particles. Assuming $||H_{a,\perp}|| \ll \hbar\nu_b$ and weak beam-splitter coupling $\hbar G_{a0} q_{\mathrm{ZPF}} \ll \hbar\nu_b$, we can make the rotating wave approximation such that $H_a^r(t) = U(t)H_a U^\dagger(t) \approx H_{a0}$. The full quantum Langevin equations of motion based

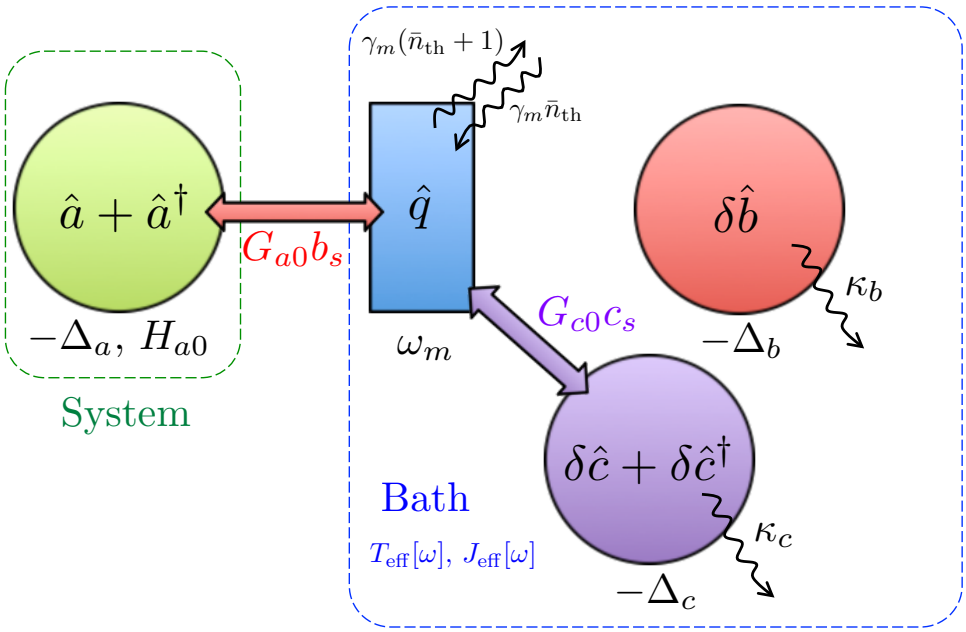

Figure 2.2: Schematic diagram of the optomechanical implementation of a parametric bath for photons. Here, $\hat{b}$, $\hat{c}$, $\hat{q}$, and their dissipative environments all together serve as a bath for the photonic system $\hat{a}$ as described in the linearized Heisenberg-Langevin equations (2.12).

on the input-output formalism (following [67]; see also [42, 68]) now read

$$\begin{aligned}
\dot{\hat{a}} =& \frac{i}{\hbar}\left[H_{a0}, \hat{a}\right] + i\Delta_a \hat{a} + iG_{a0}\hat{q}\hat{b}, \\
\dot{\hat{b}} =& i(\Delta_a - \frac{\kappa_b}{2})\hat{b} + iG_{a0}\hat{q}\hat{a} + \sqrt{\kappa_b}\hat{b}_{\rm in}(t), \\
\dot{\hat{c}} =& i(\Delta_c - \frac{\kappa_c}{2})\hat{c} + iG_{c0}\hat{q}\hat{c} + \sqrt{\kappa_c}\hat{c}_{\rm in}(t), \\
\dot{\hat{q}} =& \frac{\hat{p}}{M}, \\
\dot{\hat{p}} =& -M\omega_m^2(\hat{q} - q_0) - \gamma_m \hat{p} + \hbar G_{a0}(\hat{b}^\dagger\hat{a} + \hat{a}^\dagger\hat{b}) + \hbar G_{c0}\hat{c}^\dagger\hat{c} + \hat{F}_{\rm in}(t).
\end{aligned} \tag{2.8}$$

We have defined the optical detunings $\Delta_a = \nu_b - \omega_a$, $\Delta_b = \nu_b - \omega_b$, and $\Delta_c = \nu_c - \omega_c$. The cavity input fields $\hat{b}_{\rm in} = b_{\rm in,s} + \delta\hat{b}_{\rm in}$ and $\hat{c}_{\rm in} = c_{\rm in,s} + \delta\hat{c}_{\rm in}$ have classical drive amplitudes $b_{\rm in,s}$ and $c_{\rm in,s}$ and quantum vacuum noise parts $\delta\hat{b}_{\rm in}$ and $\delta\hat{c}_{\rm in}$, respectively, while the mechanical motion is affected by a Brownian stochastic force $\hat{F}_{\rm in}(t)$ [68–71]. The baths are described by the noise correlators,

$$\begin{aligned}
\left\langle \delta\hat{b}_{\rm in}(t)\delta\hat{b}_{\rm in}^\dagger(t')\right\rangle &= \delta(t-t'), \\
\left\langle \delta\hat{b}_{\rm in}(t)\delta\hat{b}_{\rm in}(t')\right\rangle &= \left\langle \delta\hat{b}_{\rm in}^\dagger(t)\delta\hat{b}_{\rm in}(t')\right\rangle = 0,
\end{aligned} \tag{2.9}$$

$$\begin{aligned}
\left\langle \delta\hat{c}_{\rm in}(t)\delta\hat{c}_{\rm in}^\dagger(t')\right\rangle &= \delta(t-t'), \\
\langle \delta\hat{c}_{\rm in}(t)\delta\hat{c}_{\rm in}(t')\rangle &= \left\langle \delta\hat{c}_{\rm in}^\dagger(t)\delta\hat{c}_{\rm in}(t')\right\rangle = 0,
\end{aligned} \tag{2.10}$$

$$\begin{aligned}
\left\langle \hat{F}_{\rm in}(t)\hat{F}_{\rm in}(t')\right\rangle =& \frac{\hbar}{\pi}\int_0^\infty {\rm d}\omega J[\omega]\{e^{-i\omega(t-t')}(1+\bar{n}_{\rm th}[\omega]) + e^{i\omega(t-t')}\bar{n}_{\rm th}[\omega]\} \\
=& \frac{\hbar}{\pi}\int_0^\infty {\rm d}\omega J[\omega]\left[\coth\left(\frac{\beta\hbar\omega}{2}\right)\cos[\omega(t-t')] - i\sin[\omega(t-t')]\right].
\end{aligned} \tag{2.11}$$

Here $\bar{n}_{\rm th}[\omega] = \frac{1}{e^{\beta\hbar\omega}-1}$ is the bosonic occupation function at thermal equilibrium for the mechanical thermal environment, and for specificity we assume the spectral

density $J[\omega] = \gamma_m \omega M e^{-\omega/\omega_a}$ for Ohmic damping, though other baths work as well. In the end, the laser cooling changes the correlation functions sufficiently to eliminate these effects. However, putting in the Ohmic form of $J[\omega]$ now helps us connect this system to the effective spectral density $J_{\text{eff}}[\omega]$ we obtain later by looking at the correlation functions of $\hat{q}$ in the laser cooling regime.

Assuming that the laser fields are strong, we now separate the dynamics of the operators into their semiclassical steady-state values and quantum fluctuations, $\hat{\mathcal{O}} = \mathcal{O}_s + \delta\hat{\mathcal{O}}$ and $\hat{\mathcal{O}} = \hat{a}, \hat{a}^\dagger, \hat{b}, \hat{b}^\dagger, \hat{c}, \hat{c}^\dagger, \hat{q}, \hat{p}$. We are interested in the case $\sqrt{\langle \hat{a}^\dagger \hat{a} \rangle} = 0$ such that the occupation of the system is not driven by the laser pump. Note that we need to set $q_0 = -\hbar G_{c0} |c_s|^2 / M\omega_m^2$ to balance the displacement induced by the constant radiation pressure force and make $q_s = 0$ such that the vanishing steady-state solution for the system $a_s = 0$ is allowed in the coupled equation of motion. Solving for the steady-state solution through Eq. (2.8) with the above condition, we have $b_s = \sqrt{\kappa_b} b_{\text{in,s}} / (i\Delta_d - \kappa_b/2)$, $c_s = \sqrt{\kappa_c} c_{\text{in,s}} / (i\Delta_c - \kappa_c/2)$, and $a_s = q_s = p_s = 0$. We can take b_s and c_s to be real by absorbing the complex phase into the definition of the laser amplitudes. Since $a_s = q_s = p_s = 0$, our system $\hat{a}$ and the resonator mode $\hat{q}$ are not displaced.

By keeping only the linear terms in fluctuations, though making no assumption about H_a for the many-body system of interest, we arrive at the linearized

Heisenberg-Langevin equations for the quantum dynamics:

$$\begin{aligned}
\dot{\hat{a}} &= \frac{i}{\hbar}\left[H_{a0}, \hat{a}\right] + i\Delta_a \hat{a} + iG_{a0} b_s \hat{q}, \\
\delta\dot{\hat{b}} &= (i\Delta_b - \frac{\kappa_b}{2})\delta\hat{b} + \sqrt{\kappa_b}\delta\hat{b}_{\text{in}}(t), \\
\delta\dot{\hat{c}} &= (i\Delta_c - \frac{\kappa_c}{2})\delta\hat{c} + iG_{c0} c_s \hat{q} + \sqrt{\kappa_c}\delta\hat{c}_{\text{in}}(t), \\
\dot{\hat{q}} &= \frac{\hat{p}}{M}, \\
\dot{\hat{p}} &= -M\omega_m^2 \hat{q} - \gamma_m \hat{p} + \hbar G_{a0} b_s (\hat{a} + \hat{a}^\dagger) + \hbar G_{c0} c_s (\delta\hat{c} + \delta\hat{c}^\dagger) + \hat{F}_{\text{in}}(t).
\end{aligned} \tag{2.12}$$

One can see that the optical field $\delta\hat{b}$ now decouples from all the other modes, only entering the dynamics with its steady-state value b_s as an enhancement of the coupling between $\hat{q}$ and $\hat{a}$.

Note that one can see explicitly the form of a parametric coupling between $\hat{a}$ and $\hat{q}$ by rotating back to the laboratory frame of the system c, $\hat{V}_{qa}^{\text{lin.,lab}}(t) = -\hbar G_{a0} b_s (\hat{a} e^{i\nu_b t} + \hat{a}^\dagger e^{-i\nu_b t})\hat{q}$. We stress that the original beam-splitter-type coupling between $\hat{a}$ and $\hat{b}$ is essential for the pump rejection purpose such that the classical amplitude of $\hat{b}$ mediated the sinusoidal parametric coupling without pumping the system directly.

2.3 Effective Bath Spectral Density and Temperature

The system-bath coupling is proportional to $\hat{a} + \hat{a}^\dagger$, which will lead to a force-like term as in quantum Brownian motion. We show that the correlation function

of the mechanical resonator can be expressed in a form analogous to Eq. (2.11) as

$$C_{qq}(t) \equiv \langle \hat{q}_I(t)\hat{q}_I(0)\rangle = \frac{\hbar}{\pi}\int_0^\infty \mathrm{d}\omega J_{\mathrm{eff}}[\omega]\left[\coth\left(\frac{\hbar\omega\beta_{\mathrm{eff}}[\omega]}{2}\right)\cos(\omega t) - i\sin(\omega t)\right], \tag{2.13}$$

where $\hat{q}_I(t) = e^{iH_B t}\hat{q}e^{-iH_B t}$ is the coordinate field in the interaction picture. The evolution of the many-body system $\hat{a}$ can be described as Langevin equations [71, 72]:

$$\begin{aligned}
\dot{\hat{X}}_a =& -\Delta_a\hat{Y}_a + \frac{i}{\hbar}\left[H_{a0}, \hat{X}_a\right], \\
\dot{\hat{Y}}_a =& \Delta_a\hat{X}_a + \frac{i}{\hbar}\left[H_{a0}, \hat{Y}_a\right] + \hat{\xi}_{Y_a}(t) - 2\hbar G_{a0}^2 b_s^2\int_0^t \mathrm{d}t'\hat{X}_a(t')\frac{\mathrm{d}}{\mathrm{d}t}\gamma_{\mathrm{eff}}(t-t'),
\end{aligned} \tag{2.14}$$

with a Langevin force-like term

$$\hat{\xi}_{Y_a}(t) = \sqrt{2}G_{a0}b_s\hat{q}_I(t). \tag{2.15}$$

Here we have introduced cavity mode quadratures $\hat{X}_a = \frac{\hat{a}+\hat{a}^\dagger}{\sqrt{2}}$ and $\hat{Y}_a = \frac{i(\hat{a}^\dagger-\hat{a})}{\sqrt{2}}$. The effective damping kernel is defined as $\gamma_{\mathrm{eff}}(t) = \Theta(t)\frac{2}{\pi}\int_0^\infty \frac{J_{\mathrm{eff}}[\omega]}{\omega}\cos(\omega t)\,\mathrm{d}\omega$, and $\hat{q}_I(t)$ determines the properties of the stochastic force $\hat{\xi}_{Y_a}(t)$.

To find the interaction operator $\hat{q}_I(t)$, it is equivalent to solve a set of coupled equations of motion for $\delta\hat{c}$ and $\hat{q}$ as in Eq. (2.12) but without the system-bath coupling terms. Solving the equations in the Fourier domain $\tilde{\mathcal{O}}[\omega] = \int_{-\infty}^\infty \mathrm{d}t e^{i\omega t}\delta\hat{\mathcal{O}}_I(t)$ and defining the pump-enhanced coupling $G_c = G_{c0}c_s$, we now have

$$\begin{aligned}
-i\omega\tilde{c}[\omega] =& (i\Delta_c - \frac{\kappa_c}{2})\tilde{c}[\omega] + \sqrt{\kappa_c}\tilde{c}_{\mathrm{in}}[\omega] + iG_c\tilde{q}[\omega], \\
-i\omega\tilde{c}^\dagger[\omega] =& (-i\Delta_c - \frac{\kappa_c}{2})\tilde{c}^\dagger[\omega] + \sqrt{\kappa_c}\tilde{c}_{\mathrm{in}}^\dagger[\omega] - iG_c\tilde{q}[\omega], \\
-i\omega\tilde{q}[\omega] =& \frac{\tilde{p}[\omega]}{M}, \\
-i\omega\tilde{p}[\omega] =& -M\omega_m^2\tilde{q}[\omega] - \gamma_m\tilde{p}[\omega] + \tilde{F}_{\mathrm{in}}[\omega] + \hbar G_c(\tilde{c}[\omega] + \tilde{c}^\dagger[\omega]).
\end{aligned} \tag{2.16}$$

We define the bare mechanical susceptibility

$$\chi_{q,0}^{-1}[\omega] = -M\omega^2 + M\omega_m^2 - iM\omega\gamma_m, \tag{2.17}$$

and the optomechanical modification from the cooling mode $\hat{c}$,

$$\Sigma[\omega] = \hbar G_c^2 \left(\frac{1}{(\Delta_c + \omega) + i\kappa_c/2} + \frac{1}{(\Delta_c - \omega) - i\kappa_c/2} \right), \tag{2.18}$$

such that $\chi_q^{-1}[\omega] = \chi_{q,0}^{-1}[\omega] + \Sigma[\omega]$. Note that $\chi_q[-\omega] = (\chi_q[\omega])^*$. We have

$$\begin{aligned} \tilde{q}[\omega] &= \chi_q[\omega] \left[\tilde{F}_{\text{in}}[\omega] + \left(\frac{\hbar G_c \sqrt{\kappa_c} \tilde{c}_{\text{in}}[\omega]}{-i(\Delta_c + \omega) + \kappa_c/2} + \frac{\hbar G_c \sqrt{\kappa_c} \tilde{c}_{\text{in}}^\dagger[\omega]}{i(\Delta_c - \omega) + \kappa_c/2} \right) \right] \\ &= \chi_q[\omega](\tilde{F}_{\text{in}}[\omega] + \tilde{C}_{\text{in}}[\omega]). \end{aligned} \tag{2.19}$$

The position autocorrelation function thus has two contributions: $C_{qq}(t) = C_{qq,F}(t) + C_{qq,c}(t)$. One contribution is from the Ohmic mechanical bath,

$$C_{qq,F}(t) = \int_0^\infty \mathrm{d}\omega \frac{\hbar J[\omega] |\chi_q[\omega]|^2}{\pi} \left[\coth\left(\frac{\beta\hbar\omega}{2} \right) \cos(\omega t) - i \sin(\omega t) \right], \tag{2.20}$$

and the other is from the optical cooling and counter-rotating (heating) terms:

$$C_{qq,c}(t) = \int_0^\infty \mathrm{d}\omega \hbar^2 G_c^2 |\chi_q[\omega]|^2 \left(e^{-i\omega t} L[\omega] + e^{i\omega t} L[-\omega] \right). \tag{2.21}$$

Here $L[\omega]$ is a Lorentzian function of frequency centered at $-\Delta_c$ with a width κ_c,

$$L[\omega] \equiv \frac{\kappa_c/2\pi}{(\omega + \Delta_c)^2 + \kappa_c^2/4}. \tag{2.22}$$

Compared with Eq. (2.13), we arrive at a new quantum Brownian motion bath with a modified spectral density $J_{\text{eff}}[\omega]$, a frequency-dependent temperature $T_{\text{eff}}[\omega]$, and an in general non-Markovian damping kernel $\gamma_{\text{eff}}(t)$. The effective spectral density is

$$J_{\text{eff}}[\omega] = |\chi_q[\omega]|^2 \left\{ J[\omega] + \pi\hbar G_c^2 (L[\omega] - L[-\omega]) \right\}, \tag{2.23}$$

and the effective temperature $T_{\text{eff}}[\omega] = 1/k_B\beta_{\text{eff}}[\omega]$ is given implicitly by

$$\coth\left(\frac{\beta_{\text{eff}}[\omega]\hbar\omega}{2}\right) = \frac{J[\omega]\coth\left(\frac{\beta\hbar\omega}{2}\right) + \pi\hbar G_c^2\left(L[\omega] + L[-\omega]\right)}{J[\omega] + \pi\hbar G_c^2\left(L[\omega] - L[-\omega]\right)}, \tag{2.24}$$

or equivalently by a detailed-balance-like condition

$$e^{\hbar\omega\beta_{\text{eff}}[\omega]} = \frac{J[\omega](\bar{n}[\omega]+1) + \pi\hbar G_c^2 L[\omega]}{J[\omega]\bar{n}[\omega] + \pi\hbar G_c^2 L[-\omega]}. \tag{2.25}$$

We note that working in the red-detuned regime such that $\Delta_c < 0$, when $\frac{L[\omega]}{L[-\omega]} > e^{\hbar\omega\beta}$, we have $\beta_{\text{eff}}[\omega] > \beta$, consistent with the cooling mechanism.

The effective temperature and spectral density determine the equilibrium distribution of the photons through a detailed-balance condition [42]. Specifically, consider the quantum noise spectrum defined as

$$S_{qq}[\omega] = \int_{-\infty}^{\infty} \mathrm{d}t e^{i\omega t} C_{qq}(t). \tag{2.26}$$

If the $\hat{a}$ mode is at a frequency $\Omega = -\Delta_a = \omega_a - \nu_b$, then the corresponding Fermi's golden rule transition rates of emitting one photon by absorbing energy from the effective bath $R_{\text{n}\to\text{n}+1}[\Omega]$ and losing one photon to the effective bath $R_{\text{n}\to\text{n}-1}[\Omega]$ can be expressed in terms of the quantum noise spectrum as

$$\begin{aligned} R_{\text{n}\to\text{n}+1}[\Omega] &= (n+1)\frac{g_a^2}{q_{\text{ZPF}}^2} S_{qq}[-\Omega] = (n+1)\Gamma_+[\Omega], \\ R_{\text{n}\to\text{n}-1}[\Omega] &= n\frac{g_a^2}{q_{\text{ZPF}}^2} S_{qq}[\Omega] = n\Gamma_-[\Omega]. \end{aligned} \tag{2.27}$$

According to Eq. (2.13), the photon emission (absorption) coefficient $\Gamma_{+(-)}$ can be expressed with the effective temperature and spectral density as

$$\begin{aligned} \Gamma_+[\Omega] &= \frac{g_a^2}{q_{\text{ZPF}}^2} S_{qq}[-\Omega] = 4g_a^2 M\omega_m J_{\text{eff}}[\Omega]\frac{1}{e^{\hbar\Omega\beta_{\text{eff}}[\Omega]} - 1}, \\ \Gamma_-[\Omega] &= \frac{g_a^2}{q_{\text{ZPF}}^2} S_{qq}[\Omega] = 4g_a^2 M\omega_m J_{\text{eff}}[\Omega]\frac{e^{\hbar\Omega\beta_{\text{eff}}[\Omega]}}{e^{\hbar\Omega\beta_{\text{eff}}[\Omega]} - 1}. \end{aligned} \tag{2.28}$$

At equilibrium, the photon occupation number should satisfy the detailed-balance condition according to the ratio

$$\frac{\bar{n}[\Omega]+1}{\bar{n}[\Omega]}=\frac{\Gamma_{-}[\Omega]}{\Gamma_{+}[\Omega]}=e^{\hbar\Omega\beta_{\mathrm{eff}}[\Omega]}=e^{\hbar(\omega_a-\nu_b)\beta_{\mathrm{eff}}[\omega_a-\nu_b]}. \tag{2.29}$$

Note that since we are working in the rotating frame, the detailed-balance condition leads to the grand canonical distribution of photons associated with a frequency-dependent effective temperature, as predicted. Here $\hbar\nu_b$ takes the role of an effective chemical potential set by the driving frequency on the auxiliary beam-splitter mode $\hat{b}$.

The effective spectral density that determines the coupling strength and the actual value of transition rates also matters. So far we have been working in the perfect cavity limit and neglecting the internal loss of the cavity. If the thermalization rates of the effective bath $R_{\mathrm{n}\to\mathrm{n}+1}[\Omega]$ and $R_{\mathrm{n}\to\mathrm{n}-1}[\Omega]$ are too slow such that one can no longer ignore the small cavity loss, the equilibrium condition becomes

$$\frac{\bar{n}[\Omega]+1}{\bar{n}[\Omega]}=\frac{\Gamma_{-}[\Omega]+\kappa_a}{\Gamma_{+}[\Omega]}. \tag{2.30}$$

The finite loss effect of the cavity will eventually destroy the desired grand canonical distribution. A strong enough coupling (determined by J_{eff}) and enhanced coupling g_a (determined by the power of the driving field $\hat{b}_{\mathrm{in}}$) within the photonic bandwidth is therefore required to achieve efficient thermalization towards the grand canonical distribution.

To generate the equilibrium photonic state of interest, we aim at a well-defined (frequency-independent) bath temperature T_B within the operating frequency bandwidth of interest $0\leq\omega\lesssim|\Delta_a|\ll\omega_a$ and study the bath property within that range.

We note again here that it is crucial to include the cooling mode $\hat{c}$ to broaden the resonator linewidth and provide a lower effective temperature.

2.4 Laser-Cooling-Dominated Limit

First we look for an idealized case under the laser-cooling-dominated limit, $\gamma_m \approx 0$, such that one can achieve the minimum effective temperature by omitting the mechanical thermal environment and consider the laser cooling effect only. We then study the minimum effective temperature $T_{\text{eff}}^{\text{opt}}[\omega]$ and spectral density $J_{\text{eff}}^{\text{opt}}[\omega]$ under this limit, especially at low frequencies $\omega \ll |\Delta_c|, \kappa_c$ (see Fig. 2.3). Note that we are working with the red-detuned regime $\Delta_c < 0$ for cooling process. Specifically, according to the detailed-balance-like condition (2.25),

$$e^{\hbar\omega\beta_{\text{eff}}^{\text{opt}}[\omega]} = \frac{\pi\hbar G_c^2 L[\omega]}{\pi\hbar G_c^2 L[-\omega]} = \frac{(\omega-\Delta_c)^2+\kappa_c^2/4}{(\omega+\Delta_c)^2+\kappa_c^2/4}. \tag{2.31}$$

Expanding this equation around $\omega = 0$, we have

$$\hbar\beta_{\text{eff}}^{\text{opt}}[\omega] = \frac{-4\Delta_c}{\Delta_b^2+\kappa_c^2/4} - \frac{\Delta_c(4\Delta_c^2-3\kappa_c^2)}{3(\Delta_c^2+\kappa_c^2/4)^3}\omega^2 + O(\omega^4). \tag{2.32}$$

Thus we have an optimal choice of detuning $4\Delta_c^2 = 3\kappa_c^2$ to make the ω^2 coefficient vanish. Note that Eq. (2.32) corresponds to a positive temperature for $\Delta_c < 0$ associated with the cooling process. For a blue-detuned laser, the effective temperature is negative, representing a gain in the optomechanical system.

At low frequencies, the effective spectral density under the laser-cooling-dominated limit is

$$\lim_{\omega\to 0} J_{\text{eff}}^{\text{opt}}[\omega] = \frac{-4g_c^2\Delta_c\kappa_c}{M\omega_m[\omega_m(\Delta_c^2+\kappa_c^2/4)+4g_c^2\Delta_c]^2}\omega = \eta_{\text{eff}}^{\text{opt}}\omega. \tag{2.33}$$

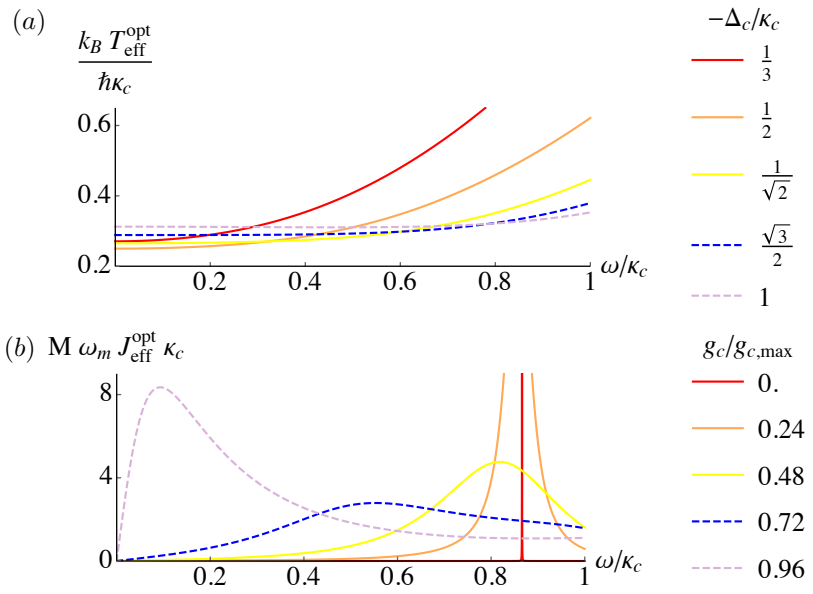

Figure 2.3: (a) Effective temperature of the laser-cooled mechanical resonator as a bath under laser-cooling-dominated limit. (b) Effective spectral density of the bath under laser-cooling-dominated limit with the parameters $-\Delta_c = \omega_m = \sqrt{3}\kappa_c/2$ and $g_{\text{c,max}} = \kappa_c/2$, and we have included $\beta = 10^{-4}\omega_m$ and $\gamma_m = 10^{-6}\omega_m$ for the $g_c = 0$ case. Note that there are out-of-range peaks centered around the mechanical resonance ω_m in (b) for $g_c/g_{\text{c,max}} = 0, 0.24$.

We have introduced $g_c = G_c q_{\mathrm{ZPF}} = G_{c0} c_s q_{\mathrm{ZPF}}$ to express the pump-enhanced coupling strength as a frequency. Recall that the effective spectral density controls the induced damping rate by defining the effective damping kernel for the many-body system $\gamma_{\mathrm{eff}}(t) = \Theta(t)\frac{2}{\pi}\int_0^\infty \frac{J_{\mathrm{eff}}[\omega]}{\omega}\cos(\omega t)\mathrm{d}\omega$. The effective spectral density is Ohmic in this regime, leading to an effective damping kernel $\gamma_{\mathrm{eff}}^{\mathrm{opt}}(t) = 2\eta_{\mathrm{eff}}^{\mathrm{opt}}\delta(t)$ corresponding to a memoryless Markovian-like damping term $-4M\omega_m g_a^2 \eta_{\mathrm{eff}}^{\mathrm{opt}} \delta\dot{\hat{X}}_c$ in Eq. (2.14) at low frequencies. Here $g_a = G_{a0} b_s q_{\mathrm{ZPF}}$ is the pump-enhanced coupling between $\hat{q}$, $\hat{a}$, and $\hat{b}$ in the unit of frequency.

Note that for the red-detuned regime $\Delta_c < 0$, $\eta_{\mathrm{eff}}^{\mathrm{opt}}$ diverges when $\omega_m(\Delta_c^2 + \kappa_c^2/4) + 4g_c^2\Delta_c$ approaches zero, which defines a critical value $g_{c,\max}^2 = \omega_m(\Delta_c^2 + \kappa_c^2/4)/(4|\Delta_c|)$. An arbitrarily strong cooling rate can be achieved by increasing $g_c \lesssim g_{c,\max}$ towards the critical value. On the other hand, when one drives the cavity-enhanced coupling g_c above this threshold value, the form of the low-frequency spectral density suggests a negative damping rate and the system is no longer stable. We will explore the detailed stability criteria for the system in the next section.

We remark that the initial mechanical thermal bath does not contribute to these equations as we are working in the laser-cooling-dominated limit. In reality, the resonator is always coupled to some thermal environment with finite dissipation γ_m and we have seen that one cannot drive the laser intensity all the way to infinity before reaching a dynamical instability. We are going to examine the maximum g_c that ensures a stable perturbation around the steady-state solutions and then revisit the properties of the effective spectrum and temperature for a system with finite γ_m.

2.5 Stability Criteria

When the pump intensity driving the photonic mode is too strong, an optomechanical system may no longer be stable [43]. Here we study the stability criteria for the coupled linearized Heisenberg-Langevin equations (2.8) in order to find the maximum pump intensities, or equivalently the maximum pump enhanced optomechanical coupling strengths, such that the steady-state solutions are stable and expansions around those solutions are still valid.

First we solve for the stability condition for the $\hat{b}$ and $\hat{q}$ modes only before the interaction with the many-body system $\hat{a}$ turns on. We introduce dimensionless quadratures $\hat{X}_c = \frac{1}{\sqrt{2}}(\delta\hat{c} + \delta\hat{c}^\dagger)$, $\hat{Y}_c = \frac{i}{\sqrt{2}}(\delta\hat{c}^\dagger - \delta\hat{c})$, $\hat{Q} = \sqrt{\frac{M\omega_m}{\hbar}}\hat{q}$, $\hat{P} = \sqrt{\frac{1}{\hbar M\omega_m}}\hat{p}$, and the normalized stochastic force $\hat{\xi}(t) = \frac{\hat{F}_{\rm in}(t)}{\sqrt{\hbar M\omega_m}}$. The equations of motions becomes

$$\dot{\hat{X}}_c = -\frac{\kappa_c}{2}\hat{X}_c - \Delta_c\hat{Y}_c + \sqrt{\kappa_c}\hat{X}_{c,\rm in}(t), \tag{2.34}$$

$$\dot{\hat{Y}}_c = \Delta_c\hat{X}_c - \frac{\kappa_c}{2}\hat{Y}_c + 2g_c\hat{Q} + \sqrt{\kappa_c}\hat{Y}_{c,\rm in}(t), \tag{2.35}$$

$$\dot{\hat{Q}} = \omega_m\hat{P}, \tag{2.36}$$

$$\dot{\hat{P}} = -\omega_m\hat{Q} - \gamma_m\hat{P} + 2g_c\hat{X}_c + \hat{\xi}(t), \tag{2.37}$$

corresponding to a matrix form

$$\begin{pmatrix} \dot{\hat{Q}}(t) \\ \dot{\hat{P}}(t) \\ \dot{\hat{X}}_c(t) \\ \dot{\hat{Y}}_c(t) \end{pmatrix} = \begin{pmatrix} 0 & \omega_m & 0 & 0 \\ -\omega_m & -\gamma_m & 2g_c & 0 \\ 0 & 0 & -\frac{\kappa_c}{2} & -\Delta_c \\ 2g_c & 0 & \Delta_c & -\frac{\kappa_c}{2} \end{pmatrix} \begin{pmatrix} \hat{Q}(t) \\ \hat{P}(t) \\ \hat{X}_c(t) \\ \hat{Y}_c(t) \end{pmatrix} + \begin{pmatrix} 0 \\ \hat{\xi}(t) \\ \sqrt{\kappa_c}\hat{X}_{\rm c,in}(t) \\ \sqrt{\kappa_c}\hat{Y}_{\rm c,in}(t) \end{pmatrix}. \tag{2.38}$$

According to the Routh-Hurwitz criterion, the stability condition for the red-detuned

cooling pump $\Delta_c < 0$ is

$$4g_c^2\Delta_c + (\Delta_c^2 + \kappa_c^2/4)\omega_m > 0. \tag{2.39}$$

Applying the optimal detuning for a fixed effective temperature around low frequencies $-\Delta_c = \sqrt{3}\kappa_c/2$, the condition sets an upper bound for the optical enhanced coupling $g_c^2 \lesssim \frac{1}{2\sqrt{3}}\kappa_c\omega_m$. Recall that $g_c = G_{c0}c_s q_{\mathrm{ZPF}}$, $c_s = \sqrt{\kappa_c}c_{\mathrm{in,s}}/(i\Delta_c - \kappa_c/2)$, and the criterion sets the maximum intensity for the driving field c_{in}.

We then further examine the stability condition when the coupling G_{a0} is turned on. We omit H_{a0} here and express the coupling in terms of the optical enhanced frequency $g_a = G_{a0}b_s q_{\mathrm{ZPF}}$, where g_a is limited by buckling phase transitions [73]:

$$\begin{pmatrix} \dot{\hat{Q}}(t) \\ \dot{\hat{P}}(t) \\ \dot{\hat{X}}_c(t) \\ \dot{\hat{Y}}_c(t) \\ \dot{\hat{X}}_a(t) \\ \dot{\hat{Y}}_a(t) \end{pmatrix} = \begin{pmatrix} 0 & \omega_m & 0 & 0 & 0 & 0 \\ -\omega_m & -\gamma_m & 2g_c & 0 & 2g_a & 0 \\ 0 & 0 & -\frac{\kappa_c}{2} & -\Delta_c & 0 & 0 \\ 2g_c & 0 & \Delta_c & -\frac{\kappa_c}{2} & 0 & 0 \\ 0 & 0 & 0 & 0 & 0 & -\Delta_a \\ 2g_a & 0 & 0 & 0 & \Delta_a & 0 \end{pmatrix} \begin{pmatrix} \hat{Q}(t) \\ \hat{P}(t) \\ \hat{X}_c(t) \\ \hat{Y}_c(t) \\ \hat{X}_a(t) \\ \hat{Y}_a(t) \end{pmatrix} + \begin{pmatrix} 0 \\ \hat{\xi}(t) \\ \sqrt{\kappa_c}\hat{X}_{c,\mathrm{in}}(t) \\ \sqrt{\kappa_c}\hat{Y}_{c,\mathrm{in}}(t) \\ 0 \\ 0 \end{pmatrix}. \tag{2.40}$$

Under optimal detuning $-\Delta_c = \sqrt{3}\kappa_c/2$, and taking the limit $\gamma_m = 0$ since additional decay only enhances stability, the nontrivial stability conditions now read

$$\begin{aligned} s_1 &= \omega_m\kappa_c > 2\sqrt{3}g_c^2, \\ s_2 &= -\Delta_a > 0, \\ s_3 &= 2\sqrt{3}\Delta_a g_c^2 - 4g_a^2\kappa_c - \Delta_a\kappa_c\omega_m > 0. \end{aligned} \tag{2.41}$$

The condition s_1 is the same condition as before the interaction g_a turned on. A negative detuning is necessary as suggested by s_2, and s_3 requires $\Delta_a < 0$ and sets a more stringent upper bound for g_c, $\omega_m\kappa_c > 2\sqrt{3}g_c^2 + \frac{4g_a^2\kappa_c}{|\Delta_a|}$. Considering a weak system-bath coupling g_a such that $\frac{4g_a^2}{|\Delta_a|\omega_m} \ll 1$, one recovers the upper bound $g_{c,max}^2 \lesssim \frac{1}{2\sqrt{3}}\kappa_c\omega_m$.

2.6 Beyond the Laser-Cooling-Dominated Limit

We now revisit the effective low-frequency temperature and spectrum to include corrections from the mechanical dissipative environment. With finite γ_m and G_c, according to Eq. (2.25), the effective inverse temperature at low frequencies is

$$\lim_{\omega\to 0}\hbar\beta_{\text{eff}}[\omega] = \frac{\hbar\beta[\gamma_m(\Delta_c^2+\kappa_c^2/4)^2 - 4g_c^2\Delta_c\kappa_c\omega_m]}{(\Delta_c^2+\kappa_c^2/4)[\gamma_m(\Delta_c^2+\kappa_c^2/4)+g_c^2\beta\hbar\kappa_c\omega_m]}. \tag{2.42}$$

To approach the laser-cooling-dominated limit, the conditions are $\gamma_m(\Delta_c^2 + \kappa_c^2/4)^2 \ll 4g_c^2|\Delta_c|\kappa_c\omega_m$ and $\gamma_m(\Delta_c^2+\kappa_c^2/4) \ll g_c^2\beta\hbar\kappa_c\omega_m$. Taking g_c such that $g_{c,max}^2 \lesssim \frac{1}{2\sqrt{3}}\kappa_c\omega_m$ with the optimal detuning, the conditions become $Q_m \gg \kappa_c/\omega_m$ and $\frac{4}{\sqrt{3}}\pi Q_m f_m \gg k_B T/\hbar$; these conditions are satisfied for a high-Q resonator in a quantum optomechanical regime.

Note that the optimal laser-cooling-dominated limit is achieved in the regime $\omega_m \approx \kappa_c$ in contrast to the usual side-band resolved cooling limit $\omega_m \gg \kappa_c$ to achieve the quantum ground state of the resonator. The different choice here is due to the fact that, while in the usual cooling process one hopes to have a narrow spectrum around the mechanical side band for efficient cooling, instead we are taking the low-frequency part of the resonator as a bath and thus require a larger linewidth

$\kappa_c \sim \omega_m$ to broaden the noise spectrum from its center ω_m towards low frequencies $\omega \sim 0$.

Around the laser-cooling-dominated limit, the correction to the temperature due to the mechanical environment is

$$\lim_{\omega\to 0} \hbar\beta_{\text{eff}}[\omega] \approx -\frac{4\Delta_c}{\Delta_b^2 + \kappa_c^2/4} + \frac{4\Delta_c + \hbar\beta(\Delta_c^2 + \kappa_c^2/4)}{g_c^2\hbar\beta\kappa_c\omega_m}\gamma_m + O(\gamma_m^2). \tag{2.43}$$

With this thermal correction, the effective temperature increases since $\hbar\beta(\Delta_c^2 + \kappa_c^2/4)/|\Delta_c|$ is typically small.

The effective spectral density including the thermal environment is

$$\lim_{\omega\to 0} J_{\text{eff}}[\omega] = \frac{\gamma_m(\Delta_c^2 + \kappa_c^2/4)^2 - 4g_c^2\Delta_c\kappa_c\omega_m}{M\omega_m(\omega_m(\Delta_c^2 + \kappa_c^2/4) + 4g_c^2\Delta_c)^2}\omega = \eta_{\text{eff}}\omega. \tag{2.44}$$

Note that this expression is exact without expansions in γ_m. At low frequencies the noise spectrum still behaves as an Ohmic heat bath and γ_m contributes an extra damping rate to the system.

2.7 Physical Design

With our theoretical analysis in place, we look for a potential physical design to realize our optomechanical implementation. One essential component of the theory is the purely beam-splitter-type coupling between our system $\hat{a}$, the mechanical resonator $\hat{q}$, and the beam-splitter auxiliary optical mode $\hat{b}$. To achieve a near-equilibrium grand canonical ensemble of photons, we require the drive to enter as a classical amplitude of $\hat{b}$ mediating the sinusoidal parametric coupling, without driving the many-body system ($\hat{a}$) directly. While a beam-splitter-type interaction

is common in the so-called mirror-in-the-middle systems [64–66], the strong driving field on $\hat{b}$ inevitably leaks into the system $\hat{a}$ through the translucent middle mirror and generates unwanted steady-state coherence in $\hat{a}$ in the simple mirror-in-the-middle geometry.

Here we suggest a potential experimental design via a Michaelson-Sagnac interferometer (MSI). This topology was first proposed to apply power and signal recycling techniques on translucent membrane resonators for accessing a quantum radiation pressure noise regime [62] and can be used to realize generalized optomechanical coupling and cooling [63]. In the interferometer geometry (see Fig. 2.4), one uses a translucent (with reflectivity r_m and transmissivity t_m) subwavelength mechanical resonator (for example, thin SiN membranes) as a common end mirror for the two arms of the Michelson interferometer, while the transmitted light through the resonator forms a Sagnac mode. Note that the Sagnac mode is insensitive to the resonator position. This set up is equivalent to placing a fixed mirror at equal lengths between two high quality factor cavity end mirrors while the effective reflectivity ρ and transmissivity τ of the middle mirror change with the resonator motion $\hat{q}$.

For pump rejection, we operate the inteferometer at its dark fringe condition: At the equilibrium position of the resonator, the Michelson and Sagnac modes form a total destructive interference at the output end, with $|\rho(\hat{q}=0)| = 1$ and $\tau(\hat{q} = 0) = 0$. The two cavity modes are initially decoupled for zero displacement of the mechanical resonator. Using the transfer matrix method, following the supplemental material of Ref. [63], and applying the boundary condition at the two cavity end

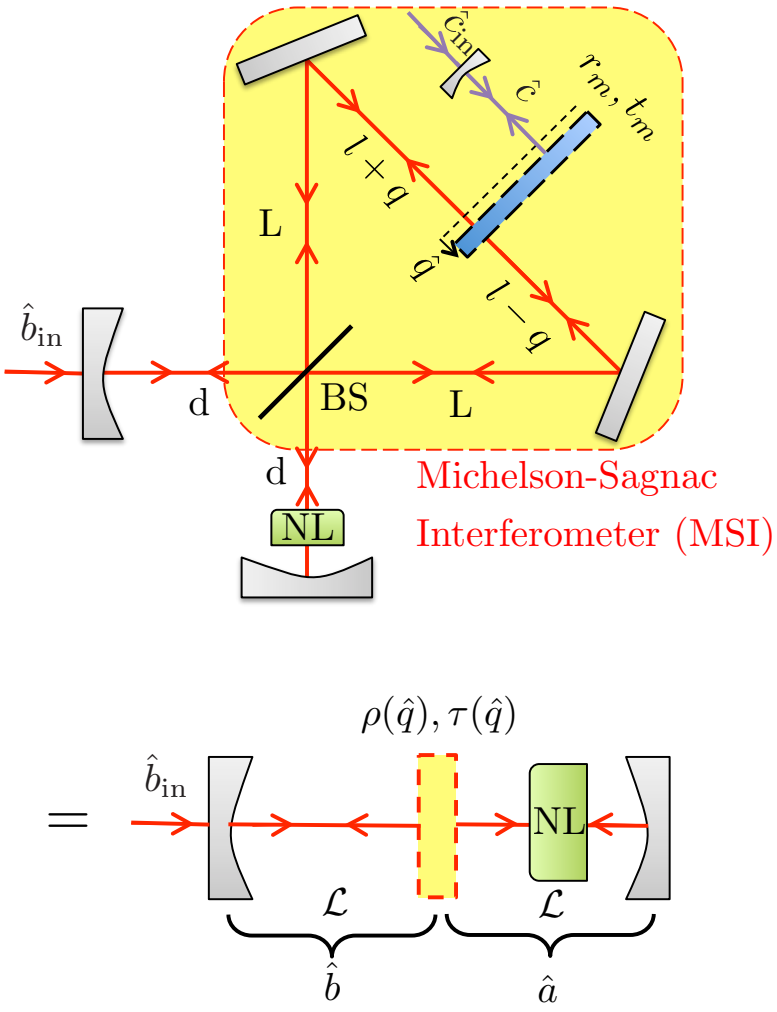

Figure 2.4: Physical implementation that includes both pump rejection (via two red pathways of a Michelson-Sagnac interferometer) and reasonable optomechanical coupling even for small reflectivity mirrors, such as thin SiN membranes. The equivalent two cavity modes showing the nonlinear (marked NL) media that forms part of the quantum simulator and the pumped mode are shown in the lower section. Another spatially independent cavity $\hat{c}$ (purple pathway), which takes the resonator as one of the end mirrors and is driven by a red-detuned laser field $\hat{c}_{\rm in}$, is added to laser cool the resonator.

mirrors to solve for normal mode eigenvalues [64], we find that the Hamiltonian of the composite system reads

$$\hat{H}_{\mathrm{MSI}} = \omega_0 \hat{a}^\dagger \hat{a} + \hbar\omega_0 \hat{b}^\dagger \hat{b} + \frac{\hat{p}^2}{2M} + \frac{M\omega_m^2 \hat{q}^2}{2} + \frac{r_m \omega_0}{\mathcal{L}} \hat{q}(\hat{a}^\dagger \hat{b} + \hat{b}^\dagger \hat{a}), \tag{2.45}$$

Here $\omega_a = \omega_b = \omega_0$ is the resonant frequency of the cavity modes $\hat{a}$ and $\hat{b}$, r_m is the complex reflectivity of the mechanical resonator, and $\mathcal{L} = d + L + l$ is the effective cavity length.

Thus we arrive at a purely beam-splitter-type coupling between the mechanical system and the cavity modes. In the symmetric MSI geometry at the dark fringe condition, the driving field on $\hat{b}$ merely mediates the parametric coupling without pumping the many-body photonic system $\hat{a}$ directly. One can include an additional laser cooling mode $\hat{c}$, for example, by adding another spatially independent cavity to complete the bath engineering story as described in Fig. 2.2. This concept of using purely beam-splitter optomechanical interactions for pump rejection should be extensible to many other configurations.

2.8 Outlook

Our approach for controlling the chemical potential and temperature of light suggests a path forward for creating equilibrium many-body states of photon-based quantum simulators. However, key questions remain, including the best way to create nonlinear optical or microwave terms as well as methods in the microwave domain for determining the photonic statistics to confirm our grand canonical ensemble prediction. Furthermore, intriguing new challenges await, particularly with regard to

other conserved quantities and their associated thermodynamic Lagrange multipliers. The general approach used here may be extensible to other such scenarios, which may allow for the exploration of a wide range of thermodynamic ensembles. We also note that our technical implementation may have the many-mode extension necessary to generate thermodynamic equilibrium in a macroscopic system, which is left for future work.

Chapter 3: Photon thermalization via laser cooling of atoms[1]

3.1 Introduction

The laser cooling and trapping of atoms [74–79] provides a variety of powerful tools for exploring the physics of light and matter [80–82]. While many discussions focus on the atomic behavior, including the thermalization of the motion of a single atom without collisions [74], curious possibilities regarding the light have also emerged [31]. Simple questions, such as the description of scattered light in optically thick atomic clouds, remain incompletely explored. Another key question is how modification of the photon density of states can change the scattering process. For example, this enables novel regimes of laser cooling in cavities [83–91], and, in interacting systems, the observation of Bose-Einstein condensation (BEC) of light in semiconductors [20, 25, 26, 92] and molecular dyes [21, 33, 93–99]. In those cases, the strength of incoherent pumping of excitations determines the photon number and sets a nonzero chemical potential for light [100, 101]. By contrast, in traditional laser cooling, we have a coherent, periodic drive oscillating at the laser frequency. This scenario has been suggested in a general setting as a possible regime of thermal-

[1]This chapter has part of "Photon thermalization via laser cooling of atoms," by C.-H. Wang, M. J. Gullans, J. V. Porto, W. D. Phillips and J. M. Taylor in Phys. Rev. A **98**, 013834 (2018)

ization in a driven system [102–104] – leading to a controllable chemical potential for light [38]. This leads to the natural question of whether similar phenomena can occur in optically thick, laser-cooled atomic systems, where multiple scattering, or cavity confinement, allows laser photons emitted from the atoms to continue to interact with the atomic cloud and potentially thermalize.

Here we partially answer this question by exploring the thermodynamic properties of the photons emitted in the laser-cooling process in samples with at least one optically thick axis, comprising many modes. We show that in this driven-dissipative system the thermalization of these photons arises directly from atomic laser cooling and they are described by a detailed balance condition corresponding to a grand canonical ensemble. These results apply even though the photons are noninteracting, the atoms are noninteracting, and neither is in thermal equilibrium with an external bath. As an illustrative example, this approach allows thermalization of cavity photons with a single atom trapped in an optical cavity. The thermodynamic arguments presented in this work, which are based on the microscopic theory of atom-light interactions, do not rely on specific assumptions about the interaction Hamiltonian or the photonic kinetic energy and, thus, apply to a broad class of many-body photonic systems that can be realized with ultracold atoms.

The laser-cooling configuration we focus on in this paper is illustrated in Fig. 3.1(a). We consider two-level atoms interacting with Doppler-cooling laser beams and two sets of photon modes. One set represents a macroscopic collection of lossy (optically thin), free-space modes and is associated with modes that allow the atom to Doppler cool; we call these "bath" modes. The photons in the other set

of (optically thick) modes are distinguished by the high probability that they will be re-absorbed by the atomic cloud before being lost, either due to intrinsic optical depth (OD) or the existence of a cavity [see Fig. 3.1(a)]. As described above we find that these high OD modes have intriguing thermodynamic properties, and we call them "system" modes in what follows.

To study the emission and absorption of the system modes during Doppler cooling, we use the quantum jump formalism [105, 106], but modify it to achieve self-consistent rates with effective elimination of the bath modes. This allows us to treat the Doppler-cooled atoms as a thermal bath. We then show that the detailed balance condition for photon emission and absorption of the system modes leads to a grand canonical ensemble description of photons at equilibrium, with a chemical potential nearly equal to the energy of a single laser photon. We conclude by examining rare-earth atoms as a practical two-level system that can laser cool even at high power. We suggest that the rare-earth atoms provide a good platform for realizing thermalization of light using this approach.

The structure of the paper is as follows: Section 3.2 gives an overview of how photons thermalize in an optically thick laser-cooled atomic ensemble using simple thermodynamic arguments, and contrast this thermalization mechanism with prior work. Section 3.3 lays out a detailed theoretical formulation of laser cooling with two sets of modes. Section 3.4 presents a self-consistent analysis of the steady state distribution of system photons, carefully treating the finite lifetime of the atoms as well as possible photon loss mechanisms. Section 3.5 characterizes the photon steady state by examining rare-earth atoms as practical two-level atoms to realize the grand

canonical ensemble of photons. Section 3.6 concludes by motivating the potential theoretical and experimental extensions of our results, including Bose condensation of photons and interacting photonic systems with ultracold atoms.

3.2 Overview of theoretical analysis

In the conventional theory of laser cooling the electromagnetic field is treated as a Markovian bath, which neglects the back-action of the laser-cooling process on the photonic environment. This approximation becomes unjustified when the emitted light from an atom has a high probability of being rescattered by another atom. Such effects are known to play an important role in laser cooling of high optical depth atomic ensembles and are a key limitation in efforts to directly laser cool atoms to quantum degeneracy [107]. This regime is theoretically challenging because one has to solve self-consistently for the evolution of the atoms and the rescattered photons. However, the corresponding interplay between the atom and photon dynamics is central to their thermalization.

To capture this essential physics we work in the low-excitation limit, such that the nominal Rabi frequency of the cooling laser (2Ω) can be treated perturbatively in $\Omega/|\Delta_L + i\Gamma/2|$ for a laser detuning $\Delta_L = \omega_L - \omega_A$ to an atomic transition with frequency ω_A and linewidth Γ. In this regime, photons from the cooling laser scatter from the atoms at the rate $\Omega^2\Gamma/(\Delta_L^2 + \Gamma^2/4)$. When the coupling of the system photons to the atoms is much weaker than the overall coupling of the bath photons to the atoms, this represents the dominant dynamical process. This cools the atomic

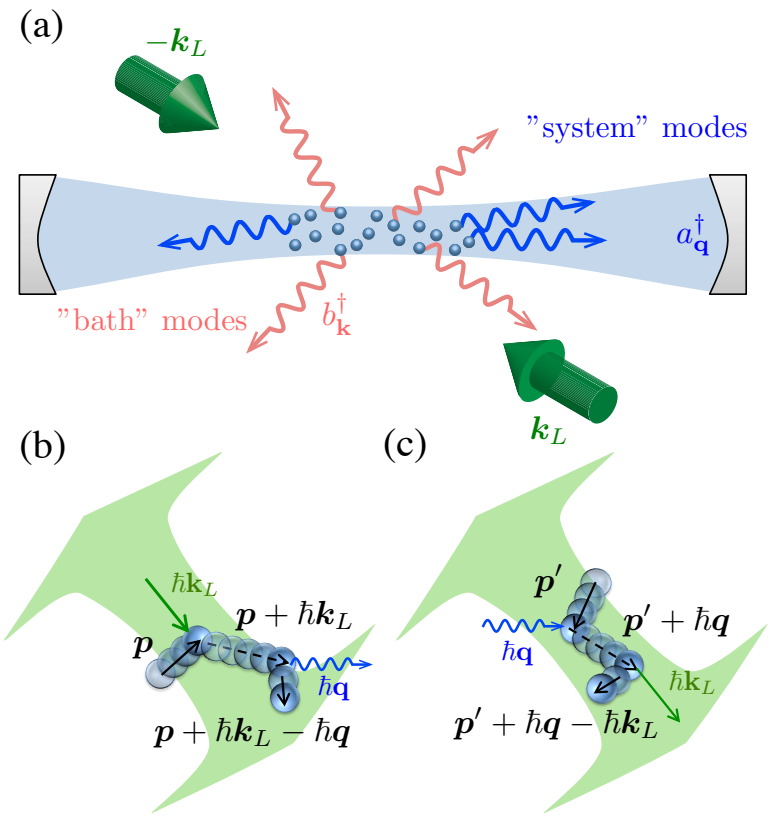

Figure 3.1: (a) Schematic of an ensemble of Doppler-cooled two-level atoms interacting with long-lived cavity (system) photon modes $a_{\boldsymbol{q}}$ [blue (dark-gray) wavy arrows within the light-blue (light-gray) region] and lossy (bath) photon modes $b_{\boldsymbol{k}}$ [red (gray) wavy arrows]. Traditional laser cooling arises via loss into the bath modes, while scattering into and out of the blue modes leads to our projected regime of photon thermalization. (b),(c) The dominant atom-photon scattering processes that lead to a grand canonical ensemble of system photons. (b) The atom is excited by the laser field then emits a system photon. (c) The atom absorbs a system photon then scatters back into the laser field. Effective system plus pump photon number conservation applies due to adiabatic elimination of the atomic excited state and the rotating wave approximation.

motion via loss of photons emitted into bath modes, leading to a thermal ensemble with a temperature set by the Doppler limit $k_B T = \hbar(\Delta_L^2 + \frac{\Gamma^2}{4})/2|\Delta_L|$.

As the atoms approach the Doppler limit, there remains the slower dynamics of the system photons. These photons can undergo a variety of scattering processes including absorption of system photons and reemission into either bath modes or the cooling laser mode, as well as absorption of cooling laser photons and re-emission into system modes. In general, the rate for each of these processes can vary widely depending on the regime of operation, as discussed in Secs. 3.3 and 3.4. For large detunings, however, (corresponding to the high-temperature limit for the atoms) we can understand the steady-state distribution of the system photons by appealing to thermodynamic arguments based on detailed balance between the laser-cooled atoms and the emitted system photons.

3.2.1 Photon thermalization with a nonzero chemical potential

In our hierarchy of bath and system modes, the rate of the system scattering processes is small compared to the overall bath photon-laser photon scattering rate which leads to Doppler cooling of atoms. For a sufficiently high OD, at large detuning and high power $|\Delta_L| \gg \Omega \gg \Gamma$, the key processes that determine the slow dynamics of the system photons are the absorption of cooling laser photons and reemission into system modes [Fig. 3.1(b)], and vice versa [Fig. 3.1(c)].

For a given system mode with label $\boldsymbol{q}$ and frequency $\omega_{\boldsymbol{q}}$, these emission and absorption processes are associated with an energy transfer of $|\hbar\omega_L - \hbar\omega_{\boldsymbol{q}}|$ between

the atoms and system photons. Furthermore, when these processes dominate over the loss of the system photons (typically into bath modes), these photons effectively equilibrate with the atoms. In this limit, the atoms approach a thermal distribution with temperature T due to the laser-cooling process, and we have the detailed balance condition, $(\bar{n}_{\boldsymbol{q}}+1)\Lambda^{+}_{\boldsymbol{q},L} = \bar{n}_{\boldsymbol{q}}\Lambda^{-}_{\boldsymbol{q},L}$, which leads to

$$\frac{\bar{n}_{\boldsymbol{q}}+1}{\bar{n}_{\boldsymbol{q}}} = \frac{\Lambda^{-}_{\boldsymbol{q},L}}{\Lambda^{+}_{\boldsymbol{q},L}} = e^{\beta\hbar(\omega_{\boldsymbol{q}}-\omega_L)}, \tag{3.1}$$

where $\beta^{-1} = k_B T$, $\bar{n}_{\boldsymbol{q}}$ is the mean photon number in mode $\boldsymbol{q}$, $\Lambda^{+}_{\boldsymbol{q},L}$ is the rate of absorption of laser photons and subsequent emission into the system modes, and $\Lambda^{-}_{\boldsymbol{q},L}$ is the rate of absorption of system photons and subsequent emission into the cooling laser mode. These scattering rates $\Lambda^{\pm}_{\boldsymbol{q},L}$ are proportional to the population of the initial momentum states of the atoms and therefore pick up the Boltzmann factor for the atomic temperature. For $\omega_{\boldsymbol{q}} > \omega_L$, we will have $\bar{n}_{\boldsymbol{q}} = \frac{1}{e^{\beta\hbar(\omega_{\boldsymbol{q}}-\omega_L)}-1}$, which corresponds to a bosonic grand canonical distribution with the temperature of the atomic motion and an effective chemical potential $\hbar\omega_L$. Effectively, the system photons have come to a thermal equilibrium with the atoms, but in a frame rotating with the laser frequency so that the energy of a laser photon plays the role of the chemical potential. This detailed balance argument applies to interacting photons as well [38].

A nonzero chemical potential for photons occurs because these dominating processes conserve the total number of system photons plus cooling-laser photons. The system photons are thermalized through number exchange between laser photons and system photons when scattered from ground-state atoms. This implies

that the cooling laser acts as a number reservoir for the system photons, while the atoms play the role of the energy reservoir in the grand canonical ensemble. There are modifications to this picture, derived below, arising from effects such as the finite lifetime of the system photons, that lead to perturbative shifts in the effective temperature and chemical potential. These corrections arise because the underlying system is still a nonequilibrium, mesoscopic one. We emphasize that this picture of a grand canonical ensemble for system photons is distinct from the trivial effect whereby the scattered light reflects the temperature of the atoms [108]. In this case, the Gaussian spectrum of scattered light reflects the Maxwell-Boltzmann distribution of the laser-cooled atoms, as opposed to being in a Bose distribution, as we find here.

For $\omega_{\boldsymbol{q}} < \omega_L$, in contrast to the case above, there is a runaway process and we expect gain or lasing instead of an equilibrium steady state since it is more probable to emit photons into such system modes than absorb photons from the mode. In an optically thick medium, the system photons are diffusive and become trapped for a finite time related to the OD; however, due to runaway processes the steady state may become dominated by saturation effects, which we do not account for in this work. Restricting the system photon states to $\omega_{\boldsymbol{q}} > \omega_L$ by a cavity or other means will prevent gain. For simplicity, we focus on the cavity model in the later discussions.

Reaching the regime where we can safely neglect the loss of the system photons, due to scattering into bath modes or other decay mechanisms, requires a careful consideration of those other, lossy, emission and absorption processes that occur

during the laser-cooling dynamics. The above arguments based on detailed balance require energy conservation during the microscopic energy transfer process between atoms and system photons, while the finite lifetime of the atomic ground state due to the Doppler-cooling process potentially violates this condition. To incorporate the mechanisms leading to Doppler cooling, with the mechanisms leading to detailed balance, we develop a theoretical tool called the self-consistent Fermi's golden rule (SC-FGR). Under the framework of SC-FGR, we can treat Doppler cooling of atoms, all emission and absorption processes of system photons, and the loss mechanisms in a self-consistent manner as described in the following sections. We find that the finite lifetime of the dressed atomic ground state due to Doppler cooling, a necessary ingredient for atomic thermalization, modifies the simple detailed balance argument presented above. Specifically, at high detuning and high laser power, where the atomic temperature is far from the Doppler limit, we see grand canonical ensemble (GCE) and other behavior, as summarized in the phase diagram of Fig. 3.2.

3.2.2 Comparison to previous work

It is helpful to contrast the results of this paper with previous work on photon thermalization with a nonzero chemical potential, which has a long history. Such work can be broadly classified into two categories that rely (i) on interactions between light and matter where the matter is in thermal equilibrium with an external reservoir, or (ii) multiple photon-photon collisions mediated by matter. The former includes the earliest theoretical proposal of photon BEC in a plasma [110], photon

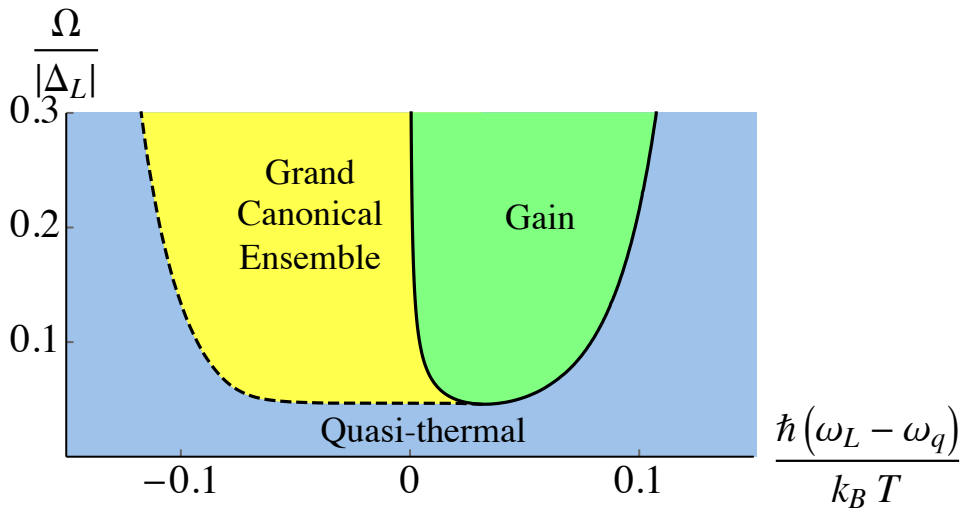

Figure 3.2: Characterization of system photon regimes for a single mode cavity with laser Rabi frequency (Ω) and the laser detuning from the system photon energy ($\hbar(\omega_L - \omega_{\boldsymbol{q}})$) as parameters. At higher powers, photon generation can exceed loss as per Eq. (3.1), leading to either gain [green (gray)] and possibly lasing, or the formation of a grand canonical ensemble for light [yellow (light gray)]. For low powers or large laser detunings from the system photon, photon loss prevents detailed balance with the atomic motion and only quasithermal light is expected [blue (dark gray)]. In this diagram we use the physical parameters for the Yb $^1S_0 - {}^3P_1$ narrow cooling transition [109] with $\omega_A/2\pi = 539$ THz, $\Gamma/2\pi = 180$ kHz, $\bar{\Delta}_L \approx -157\,\Gamma$, and assume $|\boldsymbol{k}_L - \boldsymbol{q}| = \sqrt{2}k_L$.

thermalization and condensation in a dye-filled microcavity [21, 93, 95, 100, 111], as well as recent proposals in quantum optomechanics [33, 112]; the latter includes photon BEC through photon-photon scattering in a nonlinear resonator [113] and BEC of exciton polaritons [20, 25, 26] and stationary-light polaritons [92]. Our approach has the most in common with (i), however, it falls outside this category because the bath for the photons (i.e., the atoms) is not in thermal equilibrium with an external reservoir but rather driven to a nonequilibrium steady state with a thermal description. In optically thick atomic media, the dynamics of the system photons, which are generated during the laser-cooling process, must then be treated self-consistently with the equilibration dynamics of the atoms.

A related class of studies is concerned with characterizing the nonequilibrium steady state of driven-dissipative photonic systems [114–119]. In many instances, these systems are driven towards an effectively thermal state at long times. However, statistical mechanical arguments do not guarantee such emergence of one of the standard thermodynamic ensembles, making the results dependent on underlying assumptions about the system. In cases where universal results can be obtained using the renormalization group [116–119], the thermal behavior is only guaranteed to apply at long-time and long-wavelength scales. Although the analysis from these studies does not apply to our system, we find a similar conclusion that, under a broad range of conditions, laser cooling in optically thick media acts as an effectively thermal driven-dissipative system. This result is surprising in the context of laser cooling because one might expect that multiple scattering in such driven optically thick atomic media leads to complicated many-body effects and nonthermal steady

states [120–123].

3.3 Laser Cooling with Optically Thick and Thin Modes

Here we study light scattering in dilute, optically thick atomic gases and neglect radiative dipole-dipole interactions between atoms. The Hamiltonian for a two-level atom interacting with a single laser and two sets of photonic modes H_S, H_B is

$$H = H_S + H_B + H_{AS} + H_{AB} + H_{AL}(t) + H_A, \tag{3.2}$$

$$H_A = \frac{\boldsymbol{p}^2}{2m} + \hbar\omega_A \left|e\right\rangle \left\langle e\right|, \tag{3.3}$$

$$H_S = \sum_{\boldsymbol{q}} \hbar\omega_{\boldsymbol{q}} a^\dagger_{\boldsymbol{q}} a_{\boldsymbol{q}},\ H_B = \sum_{\boldsymbol{k}} \hbar\omega_{\boldsymbol{k}} b^\dagger_{\boldsymbol{k}} b_{\boldsymbol{k}}, \tag{3.4}$$

$$H_{AS} = -\sum_{\boldsymbol{q}} \hbar\alpha_{\boldsymbol{q}} a_{\boldsymbol{q}} e^{i\boldsymbol{q}\cdot\boldsymbol{r}} \left|e\right\rangle \left\langle g\right| + \text{H.c.}, \tag{3.5}$$

$$H_{AB} = -\sum_{\boldsymbol{k}} \hbar\beta_{\boldsymbol{k}} b_{\boldsymbol{k}} e^{i\boldsymbol{k}\cdot\boldsymbol{r}} \left|e\right\rangle \left\langle g\right| + \text{H.c.}, \tag{3.6}$$

$$H_{AL}(t) = -\hbar\Omega e^{-i\omega_L t} e^{i\boldsymbol{k}_L\cdot\boldsymbol{r}} \left|e\right\rangle \left\langle g\right| + \text{H.c.}, \tag{3.7}$$

Here H_A is the Hamiltonian of a two-level atom, and m, $\boldsymbol{p}$, $\boldsymbol{r}$, ω_A are the mass, momentum, position, and the transition frequency of the atom; H_S describes long-lived system photon modes of interest associated with bosonic annihilation operators $a_{\boldsymbol{q}}$ and energies $\hbar\omega_{\boldsymbol{q}}$; H_B describes lossy bath modes with bosonic annihilation operators $b_{\boldsymbol{k}}$ and energies $\hbar\omega_{\boldsymbol{k}}$; H_{AS}, H_{AB}, and $H_{AL}(t)$ represent atom-system photon, atom-bath photon, and atom-laser interactions. Throughout the text $\boldsymbol{q}$ is the wave vector for system photons and $\boldsymbol{k}$ labels bath photons. $2\alpha_{\boldsymbol{q}}$ and $2\beta_{\boldsymbol{k}}$ are the single-photon Rabi frequencies of the system photons and bath photons. Note that all

coupling frequencies $\alpha_{\boldsymbol{q}}$, $\beta_{\boldsymbol{k}}$, and Ω are assumed to be real and are defined as a half of the usual Rabi frequencies to absorb the 1/2 factor for notational simplicity.

In what follows we separate the system and bath modes by including cavity end mirrors, and assume that the intrinsic optical depth of the atomic cloud is much smaller than 1, while the effective optical depth after including the cavity is greater than 1, so that the system photonic modes are now cavity modes. For simplicity, we make a plane-wave approximation for the cavity modes so that Eq. (3.5) still holds. In principle, our general concept of thermalizing system photons via laser cooling may also be realized in a cavity-free setting.

To obtain an effective Hamiltonian and the corresponding master equation describing the evolution of the atom and the system modes $a_{\boldsymbol{q}}$, we first integrate out the lossy bath modes $b_{\boldsymbol{k}}$ in the weak excitation limit $\Omega \ll |\Delta_L + i\Gamma/2|$. According to Fermi's golden rule and momentum conservation, the spontaneous emission rate from the atomic excited state with momentum $\boldsymbol{p}$ due to all bath modes $b_{\boldsymbol{k}}$ is

$$\Gamma_b(\boldsymbol{p}) = \frac{2\pi}{\hbar} \sum_{\boldsymbol{k}} |\hbar\beta_{\boldsymbol{k}}|^2 \delta\left(\Delta E_{eg}(\boldsymbol{k}, \boldsymbol{p})\right) \approx \Gamma_b(0) \equiv \Gamma_b, \tag{3.8}$$

with the energy difference between the initial excited and final ground states defined as

$$\Delta E_{eg}(\boldsymbol{k}, \boldsymbol{p}) = \frac{\boldsymbol{p}^2}{2m} + \hbar\omega_A - \frac{|\boldsymbol{p} - \hbar\boldsymbol{k}|^2}{2m} - \hbar\omega_{\boldsymbol{k}}. \tag{3.9}$$

The effect of atomic motion on the total decay rate is negligible, assuming the atomic transition energy $\hbar\omega_A$ is much larger than the Doppler shift and the recoil energy.

Similarly, the total spontaneous emission rate from the atomic excited state

with $\boldsymbol{p}$ due to system modes $a_{\boldsymbol{q}}$ is

$$\Gamma_a(\boldsymbol{p}) = \frac{2\pi}{\hbar}\sum_{\boldsymbol{q}} \frac{|\hbar\alpha_{\boldsymbol{q}}|^2\hbar\kappa_{\boldsymbol{q}}}{\Delta E_{eg}(\boldsymbol{q},\boldsymbol{p})^2 + \hbar^2\kappa_{\boldsymbol{q}}^2/4} \approx \Gamma_a(0) \equiv \Gamma_a. \tag{3.10}$$

Here $\kappa_{\boldsymbol{q}}$ is the cavity decay linewidth of the system photons $a_{\boldsymbol{q}}$. Note that the overall approach here can also apply to the case without a cavity by replacing the Lorentzian factor in Eq. (3.10) with a Dirac δ function. We work in the limit $\Gamma_b \gg \Gamma_a$ so that the spontaneous emission rate into bath modes is approximately the atomic natural linewidth of the atom, $\Gamma_b \approx \Gamma$.

Scattering between atomic ground states with different momenta is induced by the laser and the photon modes. Working in the weak excitation limit, we calculate the transition rates with time-dependent perturbation theory to the lowest order in $\frac{\Omega}{\Delta_L + i\Gamma/2}$ [124]. The relevant processes are illustrated diagrammatically in Fig. 3.3. For example, Fig. 3.3(b) represents the coupling from an initial ground-state atom in momentum state $\boldsymbol{p}$, $|g,\boldsymbol{p}\rangle$, to the new momentum state $\boldsymbol{p}+\hbar\boldsymbol{k}_L-\hbar\boldsymbol{k}$, $|g,\boldsymbol{p}+\hbar\boldsymbol{k}_L-\hbar\boldsymbol{k}\rangle$, with an additional emission of a bath photon with momentum $\hbar\boldsymbol{k}$ into the $b_{\boldsymbol{k}}$ modes. Using second-order time-dependent perturbation theory, represented diagrammatically in Fig. 3.3(b), we get an effective coupling between atomic motional ground states with momentum $\boldsymbol{p}$ and $\boldsymbol{p}+\hbar\boldsymbol{k}_L-\hbar\boldsymbol{k}$ as

$$R_{\boldsymbol{k}}(\boldsymbol{p}) = \frac{\Omega\beta_{\boldsymbol{k}}}{\omega_L - \omega_A - \frac{\boldsymbol{p}\cdot\boldsymbol{k}_L}{m} - \frac{E_r(\boldsymbol{k}_L)}{\hbar} + i\frac{\Gamma}{2}}. \tag{3.11}$$

Note that the term $-\frac{\boldsymbol{p}\cdot\boldsymbol{k}_L}{m} = -\mathbf{v}\cdot\boldsymbol{k}_L$ is the Doppler shift of the laser frequency as seen by the moving atom. The photon recoil energy, defined as

$$E_r(\boldsymbol{k}_L) = \frac{\hbar^2\boldsymbol{k}_L^2}{2m}, \tag{3.12}$$

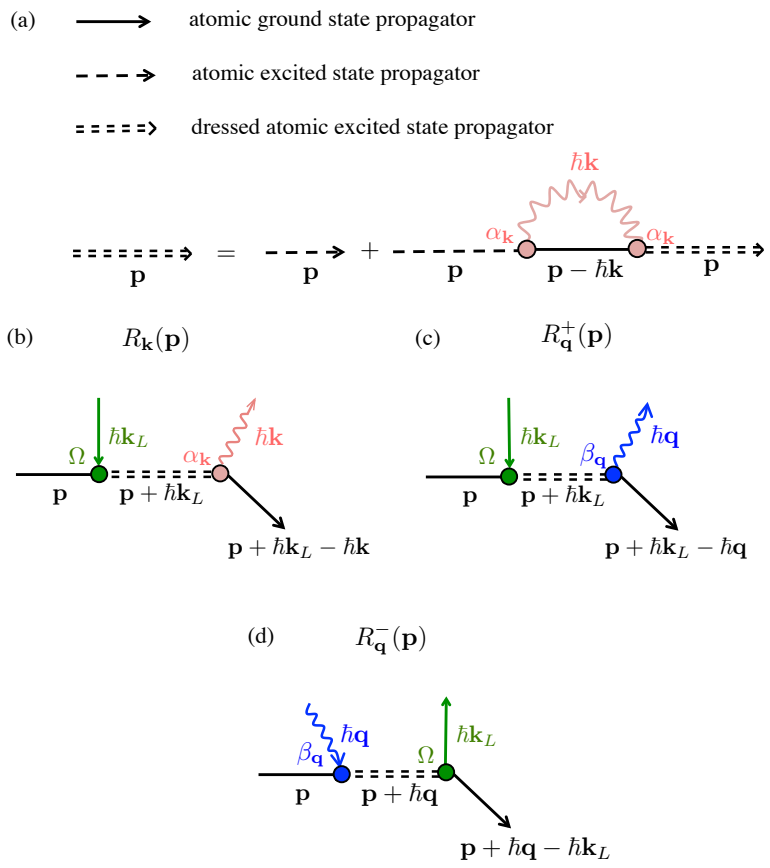

Figure 3.3: Diagrams for laser-induced scattering between atomic ground states with different momenta to lowest order in Ω. (a) The dressed atomic excited-state propagator (double dashed line) is defined by including nonperturbative effects due to the coupling to the bath photon modes $b_{\boldsymbol{k}}$ [red (gray) wavy arrow] and neglecting the effect of the system photons assuming $\Gamma_b \approx \Gamma \gg \Gamma_a$. (b) The diagrammatic representation of the scattering amplitude of a ground-state atom (solid black line) from an initial momentum state $\boldsymbol{p}$ to a final state $\boldsymbol{p} + \hbar\boldsymbol{k}_L - \hbar\boldsymbol{k}$ by absorbing a pump photon [green (gray) straight arrow] and emitting a bath photon. This process is associated with an effective coupling $R_{\boldsymbol{k}}(\boldsymbol{p})$ between momentum states $|g, \boldsymbol{p}\rangle$ and $|g, \boldsymbol{p} + \hbar\boldsymbol{k}_L - \hbar\boldsymbol{k}\rangle$. (c) The scattering amplitude from $|g, \boldsymbol{p}\rangle$ to $|g, \boldsymbol{p} + \hbar\boldsymbol{k}_L - \hbar\boldsymbol{q}\rangle$ by absorbing a pump photon and emitting a system photon $a_{\boldsymbol{q}}$ [blue (dark-gray) wavy arrow], associated with a coupling $R^{+}_{\boldsymbol{q}}(\boldsymbol{p})$. (d) The scattering amplitude from $|g, \boldsymbol{p}\rangle$ to $|g, \boldsymbol{p} + \hbar\boldsymbol{q} - \hbar\boldsymbol{k}_L\rangle$ by absorbing a system photon $a_{\boldsymbol{q}}$ and emitting a pump photon, associated with a coupling $R^{-}_{\boldsymbol{q}}(\boldsymbol{p})$. Not shown is the process in which a system photon is rescattered to a bath photon, which is treated in Fig. 3.5.

also shifts the laser frequency by an additional amount $\frac{\hbar \boldsymbol{k}_L^2}{2m}$.

Assuming the magnitude of the atom-bath photon coupling constants $\beta_{\boldsymbol{k}}$ are insensitive to the photon energy over the atomic linewidth, we calculate the total dissipation rate for an atom with momentum $\boldsymbol{p}$ due to laser-bath scattering using Fermi's golden rule. Diagrammatically this is equivalent to summing over the bath output states in Fig. 2(b) labeled by $\hbar\boldsymbol{k}$,

$$\begin{aligned}\gamma(\boldsymbol{p}) &= \frac{2\pi}{\hbar}\sum_{\boldsymbol{k}} |\hbar R_{\boldsymbol{k}}(\boldsymbol{p})|^2 \delta\left(\Delta E_{gg}(\boldsymbol{k},\boldsymbol{p})\right) \\ &\approx \frac{\Omega^2\Gamma}{(\bar{\Delta}_L - \frac{\boldsymbol{p}\cdot\boldsymbol{k}_L}{m})^2 + \frac{\Gamma^2}{4}},\end{aligned} \tag{3.13}$$

with the ground-to-ground energy difference defined as

$$\Delta E_{gg}(\boldsymbol{k},\boldsymbol{p}) = \frac{\boldsymbol{p}^2}{2m} + \hbar\omega_L - \frac{|\boldsymbol{p}+\hbar\boldsymbol{k}_L - \hbar\boldsymbol{k}|^2}{2m} - \hbar\omega_{\boldsymbol{k}}. \tag{3.14}$$

where $\bar{\Delta}_L = \omega_L - \omega_A - E_r(\boldsymbol{k}_L)/\hbar$ is the shifted detuning of the laser, including the recoil shift from the bare detuning Δ_L. This momentum-dependent dissipation rate can lead to Doppler cooling of the atomic motions for $\Delta_L < 0$ [74, 125]. In Appendix. A, we recover the results of the standard Doppler cooling theory applied to our two-mode (system and bath) configuration. More generally, when the Doppler-cooled atomic ensemble can be treated as a thermal bath for the system photons, the parametric (laser-induced) coupling between atomic motion and the system photons will bring the system photons to an equilibrium state describable using a grand canonical ensemble, leading to an effective nonzero chemical potential set by the pump frequency $\mu = \hbar\omega_L$ [38].

The system photons also give rise to an effective coupling between atomic

ground states $|g, \boldsymbol{p}\rangle$ and $|g, \boldsymbol{p} + \hbar\boldsymbol{k}_L - \hbar\boldsymbol{q}\rangle$, which to lowest order in $\frac{\Omega}{\Delta_L + i\Gamma}$ [see Fig. 3.3(c)] is

$$R_{\boldsymbol{q}}^{+}(\boldsymbol{p}) = \frac{\alpha_{\boldsymbol{q}}\Omega}{\bar{\Delta}_L - \frac{\boldsymbol{p}\cdot\boldsymbol{k}_L}{m} + i\frac{\Gamma}{2}}. \tag{3.15}$$

In contrast to the bath modes, the system modes have high effective optical depth and we must also take into account the reverse process of first absorbing a system photon and reemitting into the laser-cooling field. This gives rise to the effective coupling between atomic stateS $|g, \boldsymbol{p}\rangle$ and $|g, \boldsymbol{p} + \hbar\boldsymbol{q} - \hbar\boldsymbol{k}_L\rangle$ [Fig. 3.3(d)]

$$R_{\boldsymbol{q}}^{-}(\boldsymbol{p}) = \frac{\alpha_{\boldsymbol{q}}\Omega}{\bar{\Delta}_{\boldsymbol{q}} - \frac{\boldsymbol{p}\cdot\boldsymbol{q}}{m} + i\frac{\Gamma}{2}}, \tag{3.16}$$

where $\bar{\Delta}_{\boldsymbol{q}} = \omega_{\boldsymbol{q}} - \omega_A - \hbar\boldsymbol{q}^2/2m = \Delta_{\boldsymbol{q}} - E_r(\boldsymbol{q})/\hbar$ is the shifted detuning of the system photon, including the recoil shift. The combined effects of these momentum-changing transitions lead to broadening of the motional eigenstates of the atom.

To determine the transition rates leading to the detailed balance condition for the system photons, we require a similar sum over the outgoing states as in Eq. (3.13). If we can account for all the relevant processes—including the one not shown in Fig. 3.3 in which a system photon is rescattered into a bath mode—we would have a complete description of the master equation for the system modes. However, as we discuss in the next section, this requires a self-consistent treatment of the atomic-ground-state scattering to account for the broadening of the ground-state energies due to the Doppler-cooling process.

3.4 Self-Consistent Calculation of Transition Rates

To fully account for the finite lifetime of the motional eigenstates of the atoms in their electronic ground states due to laser-cooling-induced transitions, here we develop a formulation of FGR we call THE *self-consistent Fermi's golden rule* (SC-FGR) [126, 127], in which the effect of the rapid dissipation is treated self-consistently. As shown below, this leads to a replacement of the δ function in the usual sum over atomic states with an energy-broadened approximate δ function. This allows us to evaluate the rates for system photon emission and absorption, leading to a simple set of rate equations for system modes tracing over the atomic motion. Our SC-FGR approach yields a key result: For experimentally accessible parameters, the atomic temperature must be significantly higher than the Doppler cooling limit for our theory to apply.

The general concept of SC-FGR can be understood through an example illustrated in Fig. 3.4. As seen diagrammatically in Fig. 3.4(a), the ground-state propagator for the atoms becomes dressed with the excited state due to the presence of the Doppler cooling laser field. Solving this equation self-consistently, we find that the dressed propagator for the ground-state atoms is approximately

$$\frac{i}{\omega - \boldsymbol{p}^2/2m\hbar + i\gamma(\boldsymbol{p})/2} = \pi\delta_{\gamma(\boldsymbol{p})}(\omega - \boldsymbol{p}^2/2m\hbar) + i\text{P.V.}, \tag{3.17}$$

where $\delta_\epsilon(\omega) = \frac{\epsilon/2\pi}{\omega^2+\epsilon^2/4}$ is a broadened δ function for ω with width ϵ and P.V. corresponds to the principal value in the limit $\gamma(\boldsymbol{p}) \to 0$. When the broadening is neglected we recover the usual FGR transition rate shown in Fig. 3.4(b). In com-

parison, for our SC-FGR calculation [Fig. 3.4(c)], we replace the atomic-ground-state propagators with dressed ones. This way, we evaluate the system photon emission process over a finite time before the atoms are reset by the emission process (quantum jump) into bath modes, which leads to a broadening of the δ function that arises in the standard FGR, as detailed in Appendix. A. The treatment of such a lifetime broadening effect is crucial since the detailed balance equilibration to a grand canonical ensemble of photons relies upon energy-conserving transitions between system modes and their (parametrically) coupled bath – atomic motion, in our case.

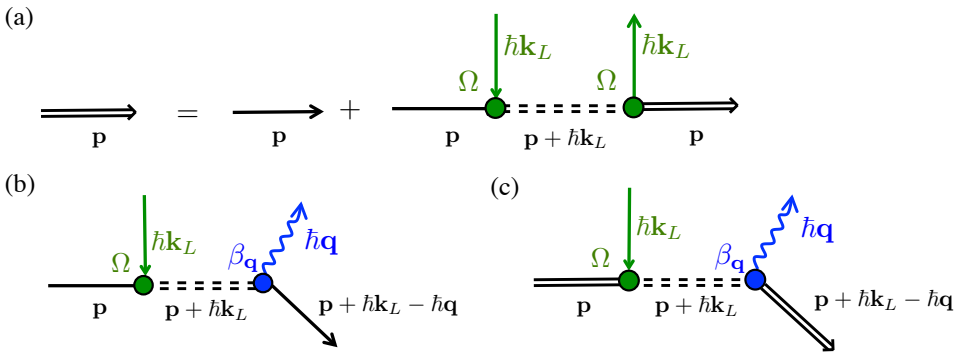

Figure 3.4: Diagrammatic comparison between Fermi's golden rule and self-consistent Fermi's golden rule. (a) The dressed state picture of the atomic-ground-state propagator (double black line) is defined by including nonperturbative effects due to the ground-state scattering induced by laser. The double dashed line is the atomic excited-state propagator dressed by the bath modes $b_{\boldsymbol{k}}$ as shown in Fig. 3.3(a). (b) For reference, we give the diagrammatic representation of the (regular) Fermi's golden rule scattering amplitude that involves a system photon $a_{\boldsymbol{q}}$ emission, using the dressed excited-state propagators which leads to a standard FGR result. (c) The diagrammatic representation of the self-consistent Fermi's golden rule scattering amplitude, in which we also replace the atomic-ground-state propagators with dressed ones to account for the finite lifetime of the original and final atomic motional states set by rapid emission processes into bath modes.

In the next two sections, we use the SC-FGR to derive the system photon emission rate, the system photon absorption rate mediated by the laser, and the system photon loss rate due to scattering into bath modes. We find that the system photons follow a grand canonical distribution when the photon losses due to scattering into bath modes or from the cavity mirror are negligible, and the SC-FGR analysis sets an additional high-temperature requirement on the atomic motion: $k_B T \gg \hbar\Gamma/2$. For a reader interested in the microscopic details, in Sec. A.2 we give an alternative derivation of the SC-FGR using the quantum jump picture, which agrees with this diagrammatic analysis.

3.4.1 Photon equilibration mediated by dressed atoms

Our analysis makes use of a Born approximation, which assumes that the atomic momentum thermalizes (due to laser cooling) after each emission or absorption event of system photons as shown in Sec. A.1, leading to no correlations between the motional distribution and the system photons. Thus we take the steady state motional distribution to be

$$\Pi(\boldsymbol{p})\mathrm{d}^3\boldsymbol{p} = \left(\frac{\beta}{2\pi m}\right)^{\frac{3}{2}} e^{-\beta|\boldsymbol{p}|^2/2m}\mathrm{d}^3\boldsymbol{p} \tag{3.18}$$

with a temperature $k_B T \approx \frac{\hbar}{2}\frac{\bar{\Delta}_L^2+\Gamma^2/4}{|\bar{\Delta}_L|}$ set by laser cooling. In this approximation we can use Eq. (3.18) to integrate over the atomic motion, and get an average rate for the thermalization of system photons. We first focus on the two processes involving system photon-laser photon scattering [see Fig. 3.1(b)- 3.1(c) and Fig. 3.5(b)-3.5(c)]. This steady-state distribution of the atoms effectively averages out the phase factor

$e^{i(\boldsymbol{k}_L-\boldsymbol{q})\cdot\boldsymbol{r}}$ in the atom-light coupling $V_{ASL}(t)$ (see Appendixes A and B). As a result, we can neglect coherent driving of the system photons, and the steady-state density matrix of the system photons is diagonal in the photon number basis. The long-time dynamics is then governed by incoherent transitions between photon number sectors with rates computed below.

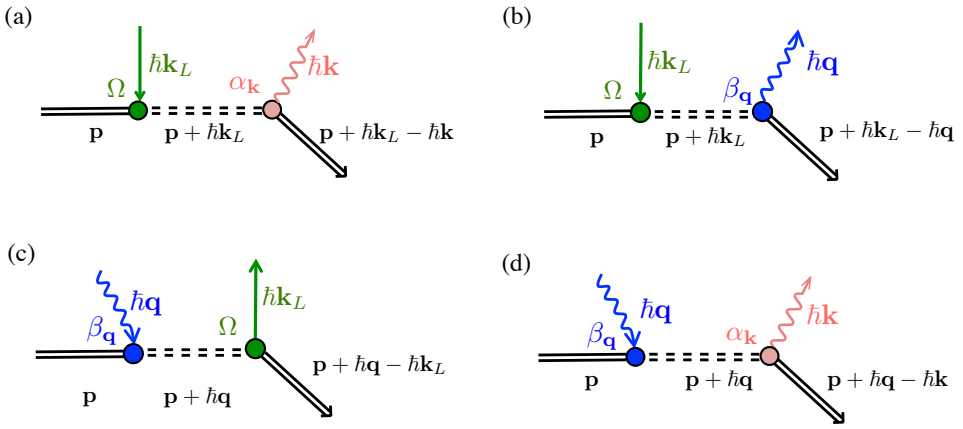

Figure 3.5: The diagrammatic representation of the scattering amplitude for four possible processes associated with transitions out of the initial state $|g,\boldsymbol{p}\rangle$ into final atomic states with a change in the ground-state momentum. (a) Scattering process that absorbs a laser photon and spontaneously decays into the bath modes. (b) Scattering process that absorbs a laser photon and emits a system photon. (c) Scattering process that absorbs a system photon and scatters back into the laser mode. (d) Scattering process that absorbs a system photon and scatters into the bath modes.

According to the SC-FGR and after integrating over the atomic momentum, the total rate to emit a system photon is given by $|\langle n_{\boldsymbol{q}}+1|\, a^\dagger_{\boldsymbol{q}}\, |n_{\boldsymbol{q}}\rangle|^2\Lambda^+_{\boldsymbol{q}} = (n_{\boldsymbol{q}}+1)\Lambda^+_{\boldsymbol{q}}$, with a laser-mediated single photon-emission rate given by the SC-FGR formula:

$$\Lambda^+_{\boldsymbol{q},L} = \int \mathrm{d}^3\boldsymbol{p}\Pi(\boldsymbol{p})|R^+_{\boldsymbol{q}}(\boldsymbol{p})|^2\delta_{\gamma(\boldsymbol{p})+\gamma(\boldsymbol{p}+\boldsymbol{k}_L-\boldsymbol{q})}\left(\Delta E_{gg}(\boldsymbol{q},\boldsymbol{p})\right) \tag{3.19}$$

The decay rates of the initial and final momentum states are summed together in the broadened δ function because we evaluate the propagator in Eq. (3.17) at the on-shell energy of the intermediate state, which includes the decay rate. By analogy to Eq. (3.13), we refer to Eq. (3.19) as an example of self-consistent Fermi's golden rule because of the appearance of the decay-broadened δ function $\delta_{\gamma(\boldsymbol{p})+\gamma(\boldsymbol{p}+\boldsymbol{k}_L-\boldsymbol{q})}$.

To evaluate Eq. (3.19), we will use the high-temperature approximation discussed in Sec. II. The primary reason we introduced the SC-FGR is to quantitatively determine the regime of validity of this approximation. In particular, we find the condition

$$\gamma(\boldsymbol{p}) \ll \sqrt{\frac{k_B T}{m}} |\boldsymbol{k}_L - \boldsymbol{q}|, \tag{3.20}$$

for which the decay-broadened δ function in Eq. (3.19) can be approximated by a true δ function since the integral over atomic momentum is much wider in energy than the decay broadening. More intuitively, this high-temperature limit can be interpreted as the condition that the momentum transfer to the atom is well defined, which requires that the Doppler broadening $v_{\text{th}}\delta q$ associated with the thermal velocity $v_{\text{th}} = \sqrt{k_B T/m}$ and atomic momentum transfer $\delta q = |\boldsymbol{k}_L - \boldsymbol{q}|$ is much greater than the motional decay rate of the ground states $\gamma(\boldsymbol{p})$. With the additional approximation $\gamma(\boldsymbol{p}) \ll \Gamma$ we find

$$\Lambda^{+}_{\boldsymbol{q},L} \approx \frac{\sqrt{2\pi\beta m}\Omega^2 |\alpha_{\boldsymbol{q}}|^2 e^{-\beta p_0^2/2m}}{|\boldsymbol{k}_L - \boldsymbol{q}| \left[(\bar{\Delta}_L - \frac{p_0 \hat{\boldsymbol{n}}\cdot\boldsymbol{k}_L}{m})^2 + \frac{\Gamma^2}{4}\right]}, \tag{3.21}$$

where p_0 is the magnitude of atomic momentum, satisfying the energy conservation

condition

$$\frac{p_0|\boldsymbol{k}_L-\boldsymbol{q}|}{m}+\frac{\hbar(\boldsymbol{k}_L-\boldsymbol{q})^2}{2m}+\omega_{\boldsymbol{q}}-\omega_L=0 \tag{3.22}$$

[the δ-function argument in Eq. (3.19)] and $\hat{\boldsymbol{n}}=\frac{\boldsymbol{k}_L-\boldsymbol{q}}{|\boldsymbol{k}_L-\boldsymbol{q}|}$ is the unit vector along the change between the initial and final momentum.

Similarly, one can find the total rate to absorb a system photon through the process that a system photon is first absorbed by the atom and then scattered back into the laser field [Fig. 3.5(c)], $n_{\boldsymbol{q}}\Lambda^-_{\boldsymbol{q},L}$, with a laser-mediated single-photon absorption rate in the high-temperature limit given by

$$\Lambda^-_{\boldsymbol{q},L}\approx\frac{\sqrt{2\pi\beta m}\Omega^2|\alpha_{\boldsymbol{q}}|^2e^{-\beta {p_0}'^2/2m}}{|\boldsymbol{k}_L-\boldsymbol{q}|\left[(\bar{\Delta}_{\boldsymbol{q}}-\frac{{p_0}'\hat{\boldsymbol{n}}\cdot\boldsymbol{q}}{m})^2+\frac{\Gamma^2}{4}\right]}. \tag{3.23}$$

Here ${p_0}'$ is the magnitude of the atomic momentum satisfying the energy conservation condition

$$\frac{{p_0}'|\boldsymbol{k}_L-\boldsymbol{q}|}{m}-\frac{\hbar(\boldsymbol{k}_L-\boldsymbol{q})^2}{2m}+\omega_{\boldsymbol{q}}-\omega_L=0. \tag{3.24}$$

If we consider the equilibration between these two processes only, the detailed balance condition reproduces the result of Eq. (3.1), which we motivated in Sec. II:

$$\frac{\bar{n}_{\boldsymbol{q}}+1}{\bar{n}_{\boldsymbol{q}}}=\frac{\Lambda^-_{\boldsymbol{q},L}}{\Lambda^+_{\boldsymbol{q},L}}=\frac{e^{-\beta\frac{{p_0}'^2}{2m}}}{e^{-\beta\frac{p_0^2}{2m}}}=e^{-\beta\frac{{p_0}'^2-p_0^2}{2m}}=e^{\beta\hbar(\omega_{\boldsymbol{q}}-\omega_L)}. \tag{3.25}$$

Here we have applied the equalities $\frac{{p_0}'^2}{2m}-\frac{p_0^2}{2m}=\hbar\omega_L-\hbar\omega_{\boldsymbol{q}}$, and $\bar{\Delta}_{\boldsymbol{q}}-\frac{{p_0}'\hat{\boldsymbol{n}}\cdot\boldsymbol{q}}{m}=\bar{\Delta}_L-\frac{p_0\hat{\boldsymbol{n}}\cdot\boldsymbol{k}_L}{m}$. For $\omega_{\boldsymbol{q}}>\omega_L$, we will have $\bar{n}_{\boldsymbol{q}}=\frac{1}{e^{\beta\hbar(\omega_{\boldsymbol{q}}-\omega_L)}-1}$, which corresponds to a Bose grand canonical distribution with temperature β and an effective chemical potential $\hbar\omega_L$. For $\omega_{\boldsymbol{q}}<\omega_L$, Eq. (3.25) suggests the onset of gain—higher photon numbers become ever more probable. A full treatment of that regime is beyond the

present work. However, the use of a cavity can modify the system photon density-of-states to prevent gain from contributing to the dynamics (e.g., by setting the relevant cavity resonant frequencies higher than the laser frequency). As shown in Fig. 3.2 and below, once loss is properly taken into account, there is only a finite range of frequencies where the gain exceeds the loss.

3.4.2 Accounting for additional photon loss mechanisms

The detailed balance condition we found in Eq. (3.25) will be modified by system photon loss associated with scattering into the bath modes [Fig. 3.5(d)] or via the cavity mirrors. Considering first the loss into bath modes using SC-FGR, we find the overall scattering rate $n_{\boldsymbol{q}}\Lambda^{-}_{\boldsymbol{q},B}$ in the high-temperature approximation, and neglecting the Doppler shift relative to the detuning $\bar{\Delta}_{\boldsymbol{q}}$,

$$\Lambda^{-}_{\boldsymbol{q},B} \equiv \int \mathrm{d}^3\boldsymbol{p} \frac{\Pi(\boldsymbol{p})|\alpha_{\boldsymbol{q}}|^2\Gamma}{(\bar{\Delta}_{\boldsymbol{q}} - \frac{\boldsymbol{p}\cdot\boldsymbol{q}}{m})^2 + \frac{\Gamma^2}{4}} \approx \frac{|\alpha_{\boldsymbol{q}}|^2\Gamma}{\bar{\Delta}^2_{\boldsymbol{q}} + \frac{\Gamma^2}{4}}. \tag{3.26}$$

Neglecting the Doppler shift in $\Lambda^{-}_{\boldsymbol{q},L}$, we find the modified detailed balance condition

$$\frac{\bar{n}_{\boldsymbol{q}}+1}{\bar{n}_{\boldsymbol{q}}} = \frac{\Lambda^{-}_{\boldsymbol{q},L}+\Lambda^{-}_{\boldsymbol{q},B}}{\Lambda^{+}_{\boldsymbol{q},L}} \approx e^{\beta\hbar(\omega_{\boldsymbol{q}}-\omega_L)} + \frac{\Gamma|\boldsymbol{k}_L-\boldsymbol{q}|}{\Omega^2\sqrt{2\pi\beta m}} e^{\frac{\beta}{2m}\left(-\frac{m(\omega_{\boldsymbol{q}}-\omega_L)}{|\boldsymbol{k}_L-\boldsymbol{q}|}-\frac{\hbar|\boldsymbol{k}_L-\boldsymbol{q}|}{2}\right)^2}. \tag{3.27}$$

If the scattering loss rate is small, $\Lambda^{-}_{\boldsymbol{q},B} \ll \Lambda^{-}_{\boldsymbol{q},L}$, one can treat the effect of loss as a small correction to Eq. (3.1) and identify an effective temperature for the cavity mode $k_B T_{\text{eff}} = \beta_{\text{eff}}^{-1}$ and an observed shift to the chemical potential $\delta\mu$ according to the modified condition Eq. (3.27):

$$\beta_{\text{eff}}(\hbar\omega_{\boldsymbol{q}} - \hbar\omega_L + \delta\mu) = \ln\left(\frac{\bar{n}_{\boldsymbol{q}}+1}{\bar{n}_{\boldsymbol{q}}}\right). \tag{3.28}$$

Here the observed shift in the chemical potential $\delta\mu$, typically much smaller than the atomic temperature, is formally defined such that $\hbar\omega_{\boldsymbol{q}} = \hbar\omega_L - \delta\mu$ is the transition frequency from equilibrium to gain,

$$\frac{\bar{n}_{\boldsymbol{q}} + 1}{\bar{n}_{\boldsymbol{q}}} = 1 = e^{-\beta\delta\mu} + \frac{\Gamma|\boldsymbol{k}_L - \boldsymbol{q}|}{\Omega^2\sqrt{2\pi\beta m}} e^{\frac{\beta}{2m}\left(\frac{m\delta\mu}{\hbar|\boldsymbol{k}_L - \boldsymbol{q}|} - \frac{\hbar|\boldsymbol{k}_L - \boldsymbol{q}|}{2}\right)^2}, \tag{3.29}$$

where $\delta\mu$ and β_{eff} can potentially depend on $\boldsymbol{q}$. In Sec. 3.5, we determine the conditions under which this $\boldsymbol{q}$-dependence can be neglected, in which case a single temperature and chemical potential [yellow region in Fig. 3.2 describe the relevant system modes over a wide range of frequencies.

To aid concreteness in the remaining discussion, we focus on a Fabry-Perot cavity design as illustrated in Fig. 3.1(a). In the regime of interest, the dependence of $\boldsymbol{q}$ on $\omega_{\boldsymbol{q}}$ is weak enough to neglect, and the only $\boldsymbol{q}$ dependence that remains is in its angle relative to $\boldsymbol{k}_L$. For a Fabry-Perot cavity, the system modes are nearly colinear and the angle dependence of $\delta\mu$ and β_{eff} can also be neglected. Equation (3.29) does not always have solutions; for a given $\boldsymbol{q}$ direction, there is a critical laser Rabi frequency Ω_c below which there are no solutions. This value determines the minimum power required to observe grand canonical ensemble behavior with a well-defined chemical potential, setting the bottom of the gain region in Fig. 3.2. Above this critical power, there are always two solutions, which determine the left and right boundaries of the gain region in Fig. 3.2. Finally, we use the left boundary as the definition of $\delta\mu$.

To thermalize close to a GCE with $\beta_{\text{eff}} \approx \beta$, we require the coefficient of the second term in Eq. (3.29) to be much less than 1. This is equivalent to the condition

$\Lambda^-_{\boldsymbol{q},B} \ll \Lambda^-_{\boldsymbol{q},L}$, which requires

$$\sqrt{\frac{k_B T}{m}}|\boldsymbol{k}_L - \boldsymbol{q}| \ll \frac{\Omega^2}{\Gamma}. \tag{3.30}$$

The high-temperature limit has already set a constraint on the left-hand side of this equation. Combining the inequality Eq. (3.30) with the high-temperature limit Eq. (3.20), using the explicit form of $\gamma(\boldsymbol{q})$ Eq. (3.13) and the approximation $|\boldsymbol{k}_L - \boldsymbol{q}| \approx |\boldsymbol{k}_L|\sqrt{2(1-\cos\theta)}$, the condition for the system photon to thermalize close to a grand canonical ensemble is

$$\frac{\Gamma^4}{\left(\bar{\Delta}_L^2 + \frac{\Gamma^2}{4}\right)^2} \ll \frac{\Gamma^2\left(\bar{\Delta}_L^2 + \frac{\Gamma^2}{4}\right) E_r(\boldsymbol{k}_L)}{\Omega^4\left|\bar{\Delta}_L\right|\hbar}(1-\cos\theta) \ll 1. \tag{3.31}$$

The above inequalities can be satisfied in the low-excitation limit with

$$\Gamma \ll \Omega \ll |\bar{\Delta}_L|, \tag{3.32}$$

with a finite angle θ, and assuming $E_r(\boldsymbol{k}_L)/\hbar \lesssim \Gamma$ as one typically finds for laser cooling transitions. This condition can be understood intuitively: In order for the laser photon-system photon scattering rate to dominate over the system photon scattering loss, one needs to increase the pump intensity until $\Gamma \ll \Omega$; a large detuning $\Omega \ll |\bar{\Delta}_L|$ is then required to stay in the low-excitation limit, leading to a higher atomic temperature than the standard detuning case with $\bar{\Delta}_L \approx -\Gamma/2$. For strong pump intensity, $\Omega > |\bar{\Delta}_L|, \Gamma$, we would need to revisit the problem nonperturbatively in $\Omega/\left|\bar{\Delta}_L + i\Gamma\right|$, which may remove this high-temperature tradeoff.

To account for a finite cavity loss $\kappa_{\boldsymbol{q}}$, the detailed balance condition is furthered modified as

$$\frac{\bar{n}_{\boldsymbol{q}} + 1}{\bar{n}_{\boldsymbol{q}}} = \frac{\Lambda^-_{\boldsymbol{q},L} + \Lambda^-_{\boldsymbol{q},B} + \kappa_{\boldsymbol{q}}}{\Lambda^+_{\boldsymbol{q},L}}. \tag{3.33}$$

The cavity loss will increase the critical laser Rabi frequency Ω_c, and further modify the observed shift in chemical potential $\delta\mu$ and the effective temperature T_{eff}. A cavity with small enough linewidth, i.e., with cavity loss rate much slower than the system photon emission and absorption rates, is thus also required to achieve a grand canonical distribution of system photons. In practice, one can increase the optical depth by adding more atoms into the ensemble to overcome the contribution from cavity loss since it is independent of the number of atoms. We neglect the cavity loss in our calculations for Fig. 3.2 and the next section.

3.5 Realizing the Grand Canonical Ensemble limit

We now numerically study the results of the modified detailed balance equation (Eq. (3.27)) to verify our previous analysis and characterize in which regimes the photon steady state is described by a single temperature and chemical potential. The equilibrium system photon occupation number for several conditions is shown in Fig. 3.6. In the standard Doppler cooling case, $\bar{\Delta}_L \simeq -\Gamma/2$, the mean system photon number is always small due to the rapid scattering of system photons into bath modes, and the grand-canonical-like distribution cannot be achieved, as suggested in Sec. 3.4 B. [See the dashed line in Fig. 3.6.]

On the other hand, in the large detuning regime, the photon occupation number at negative cavity detuning may approach the distribution for an ideal grand canonical ensemble, as described in Eq. (3.1). This occurs for a laser Rabi frequency larger than the critical value Ω_c [blue and orange curves in Fig. 3.6] in the negative

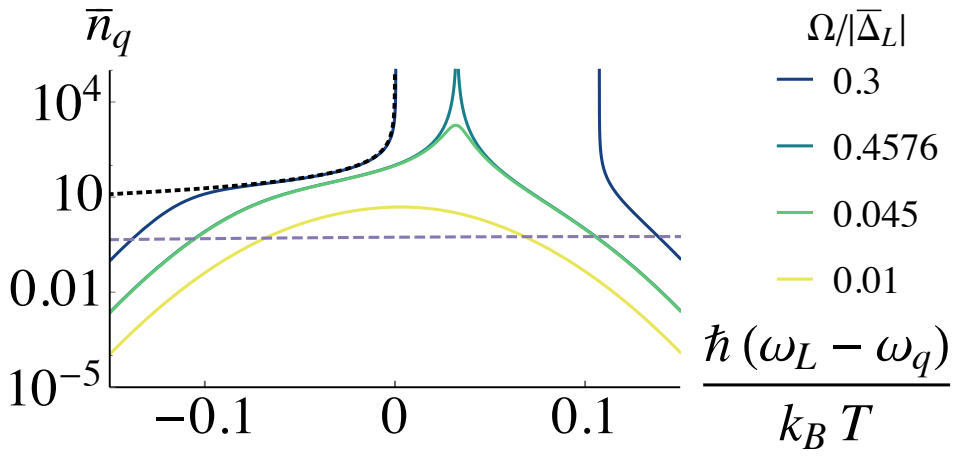

Figure 3.6: Equilibrium system photon occupation number ($\bar{n}_{\boldsymbol{q}}$) as a function of the laser detuning from the system photon frequency ($\omega_L - \omega_{\boldsymbol{q}}$). The ideal grand canonical ensemble result is plotted as the black solid line, the standard detuning with $\bar{\Delta}_L \approx -\frac{\Gamma}{2}$ and $\Omega = 0.15\Gamma$ is shown as the purple dashed line, and for large detuning with $\bar{\Delta}_L \approx -157\Gamma$ and varying Ω are shown with colored solid lines. We assume $|\boldsymbol{k}_L - \boldsymbol{q}| \approx \sqrt{2}|\boldsymbol{k}_L|$ and take the parameters for the Yb intercombination transition to ${}^3P_1$, $\omega_A/2\pi = 539$ THz, $\Gamma/2\pi = 180$ kHz, $E_{r,\boldsymbol{k}_L}/h = 3.74$ kHz.

detuning regime. We remark that the chemical potential is shifted from the laser frequency slightly by an amount $\delta\mu$, as discussed in Sec. 3.4 B. An example plot $\delta\mu$ as a function of Ω is shown in Fig. 3.7(a), where the critical end point at Ω_c is indicated as a dot. When the chemical potential exceeds the single-photon energy, gain is expected, leading to diverging photon numbers as seen in Fig. 3.6, which defines the green region in Fig. 3.2. By further increasing the laser frequency beyond the gain region to positive cavity detuning, the photon occupation number becomes finite again, indicating quasithermal behavior distinct from the grand canonical description. For laser intensity less than the critical value [green and red curves in Fig. 3.6], the photon occupation number never diverges and there is gain-free region.

In the large detuning regime, we characterize the steady-state behavior of system photons as a function of laser frequency and intensity by quantifying the degree to which T_{eff} is independent of $\boldsymbol{q}$. For a reference temperature we use the value of the effective temperature at the equilibrium-to-gain transition (T_o), defined as T_{eff} when $\omega_{\boldsymbol{q}} = \omega_L - \delta\mu/\hbar$, which is shown in Fig. 3.7(b) as a function of the laser intensity. Above Ω_c, T_o quickly approaches the atomic temperature. The calculated ratio T_{eff}/T_o as a function of mode frequency and laser intensity is shown in Fig. 3.7(c). This ratio quantifies the degree to which the system photons can be well characterized by a single chemical potential and temperature, with a ratio of 1 over a large range of $\boldsymbol{q}$ indicating perfect thermalization. We choose the yellow region in Fig. 3.7(c)—identified as the grand canonical ensemble (GCE) region in Fig. 3.2 as well—by defining the condition that $-1/2 \leq \log_{10}\left(\frac{T_{\text{eff}}}{T_o}\right) \leq 0$. Outside the gain and GCE region, i.e., at low laser powers or large detunings, photon loss

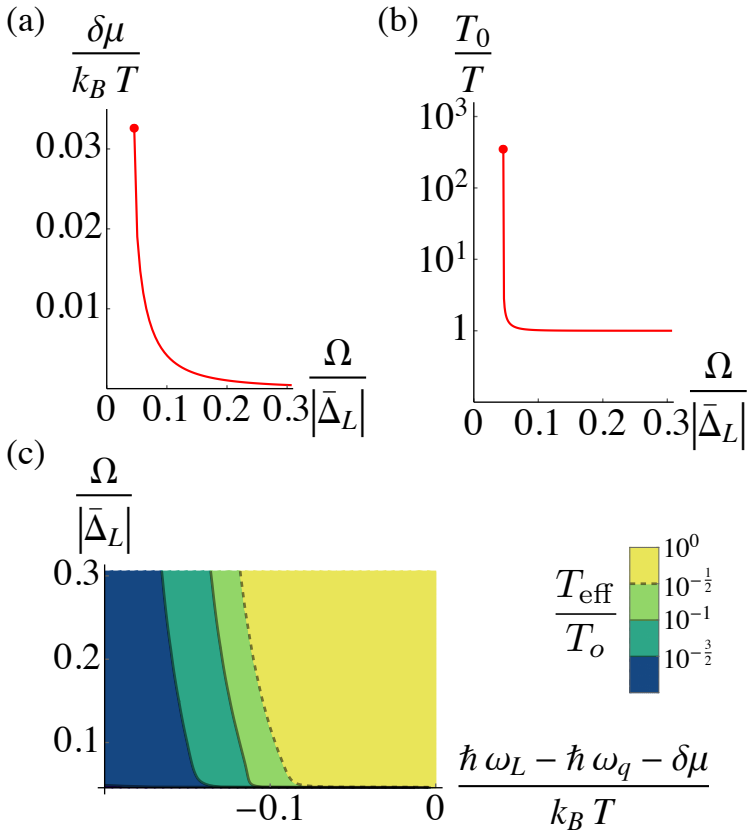

Figure 3.7: Grand canonical ensemble realization for a tunable-frequency single-mode cavity with a Yb gas. (a) The observed shift in the equilibrium-to-gain chemical potential ($\delta\mu$) as a function of the laser intensity (Ω) with $\bar{\Delta}_L \approx -157\Gamma$. (b) The effective temperature at the equilibrium-to-gain transition (T_o) as a function of the laser intensity (Ω) with $\bar{\Delta}_L \approx -157\Gamma$. (c) The ratio between the effective temperature T_{eff} and T_o as a function of the shifted laser detuning from the system photon frequency ($\omega_L - \omega_{\boldsymbol{q}} - \delta\mu/\hbar$) and the laser intensity (Ω) with $\bar{\Delta}_L \approx -157\Gamma$. The y-axis has a lower cutoff $\Omega_c/|\bar{\Delta}_L| = 0.04576$ which also corresponds to the end point (dot) in Figs. 3.7(a)-3.7(b). In these plots we assume $|\boldsymbol{k}_L - \boldsymbol{q}| \approx \sqrt{2}|\boldsymbol{k}_L|$ and take the parameters for the Yb intercombination transition to $^3P_1$, $\omega_A/2\pi = 539$ THz, $\Gamma/2\pi = 180$ kHz, $E_{r,\boldsymbol{k}_L}/h = 3.74$ kHz.

prevents detailed balance with the atomic motion, and only quasithermal light is expected [blue region in Fig. 3.2].

3.6 Outlook

We have identified an application of Doppler cooling of atoms by considering the steady state of the re-emitted light and showed this light can be described as a grand canonical ensemble with a laser-controlled chemical potential and a temperature set by the atomic motional temperature. Our analysis offers a framework to study the behavior of optically thick ensembles. Looking forward, the simplicity of our approach—using an ensemble of two-level atoms contained within an optical cavity, and maintaining a balance between optical depth and transparency—will admit a variety of extensions and expansions. For example, we can examine sub-Doppler regimes, cavity-assisted cooling, and related phenomena. An immediate consequence of this paper is that Bose condensation of noninteracting photons via laser cooling of atoms inside a multimode cavity should be possible; we defer the details of this for a later work. With a fully microscopic treatment and thermodynamic detailed balance arguments, our approach can be directly applied to more exotic interacting photonic systems [38]. For example, adding synthetic gauge fields to the problem would map the cavity system to an interacting quantum Hall system. Another promising future direction will be studying Rydberg-polariton thermalization with laser-cooled Rydberg atoms working in the electromagnetically induced transparency (EIT) regime. This may provide a cavity-free setting for observing

equilibrium behavior of interacting photons, where intriguing many-body phenomena can arise.

Chapter 4: Bose Condensation of Photons Thermalized via Laser Cooling of Atoms

4.1 Introduction

A Bose-Einstein condensation (BEC) is a striking example of quantum behavior where a macroscopic number of bosons occupy the same single-particle state. Traditionally, BEC occurs in systems with particle number conservation, either represented by a grand canonical ensemble (GCE) or in a system closed to particle exchange. Thus, we would expect photons, whose number is not conserved and which do not generally admit a GCE description, not to condense. For example, when one cools a blackbody, photons disappear; instead of forming a condensate, one reaches a vacuum state at $T = 0$.

There are several exceptions to this, however. For example, light can acquire nonzero chemical potential and form a BEC via mutual interactions mediated by matter in the form of hybridized light-matter particles called polaritons [20, 25, 26, 92, 128–130], photons in a plasma [110, 131], cavity photons in a nonlinear resonator [113], and propagation of light in a nonlinear medium [132–135]. Photons can also thermalize with a number-conserving reservoir, and condense [136],

in a dye-filled microcavity [21, 93, 95, 97, 99, 100, 111, 137, 138], an optomechanical cavity [33, 112], an ideal gases composed of two kinds of atoms [139], a 1D microtube [140], and a fiber [141]. In all of these cases, the average photon number is approximately conserved either by photon confinement in a cavity or through the compensation of loss via nonequilibrium pumping.

We recently found a different photon thermalization mechanism that occurs in Doppler laser cooling of a high optical depth atomic ensemble [142], which requires neither matter-matter nor effective photon-photon interactions. Here we show that this thermalization mechanism can lead to Bose condensation of photons. Specifically, in our scenario the laser-cooled atoms serve as a thermal reservoir while the laser photons serve as a particle reservoir for the reemitted photons, leading to a grand canonical ensemble of photons at the atomic temperature and with a chemical potential very close to the energy of a single laser photon.

To give a practical setting for our work, we adopt the now standard approach to controlling the photon dispersion relation by using a Fabry-Perot cavity where transverse excitations of a single longitudinal mode can be mapped onto a 2D massive bosonic gas with a harmonic trapping potential. While previous theoretical analysis of BEC has been mostly focused on the identification of a critical temperature or critical number (density) [21, 95, 96, 111, 143, 144], here we consider the photon condensate fraction as a function of temperature and chemical potential (set effectively by the cooling laser detuning from the cavity). By carefully treating the modification due to loss, we are able to construct a phase diagram as a function of laser frequency and field strength, showing condensate, thermal, quasithermal

and gain regimes for cavity photons with calculated values appropriate for the Yb intercombination transition.

4.2 Photon Thermalization

Consider 3D Doppler cooling of noninteracting two-level atoms in a long cavity [i.e. the cavity subtends a small solid angle as illustrated in Fig. 4.1(a)]. The cavity separates the emitted photons into long-lived cavity modes and lossy, free-space modes. When the atom is excited by a laser photon, it is most likely to de-excite by emitting a photon into free-space, and this scattering process induces Doppler cooling of atoms [76–78]. A rarer event is the spontaneous emission into the cavity. However, the high quality of the cavity mirrors allows those cavity photons to be reabsorbed by the atoms and preferentially emitted into the cooling beam, if the cooling laser is sufficiently intense. Both processes produce light whose coherence is described as thermal, in the quantum optics sense of having a photon autocorrelation that is peaked at short times. However, multiple scattering also leads to photon thermalization in an energetic sense across different transverse cavity modes. Photons thermalize with the atomic motion in an approximate particle number-conserving way where the cooling laser acts as a photon reservoir.

In the low excitation limit for Doppler cooling, $\Omega^2 \ll \left|\bar{\Delta}_L + i\Gamma/2\right|^2$ [124], the scattering between the red-detuned laser fields and the free-space modes will lead to cooling of atoms to a temperature $k_B T = \beta^{-1} = \hbar(\bar{\Delta}_L^2 + \Gamma^2/4)/2|\bar{\Delta}_L|$ [125]. Here 2Ω is the Rabi frequency of the cooling laser field, $\bar{\Delta}_L = \omega_L - \omega_A - \frac{\hbar \boldsymbol{k}_L^2}{2m_A} < 0$ is

the laser detuning including the recoil shift $\frac{\hbar \boldsymbol{k}_L^2}{2m_A}$; Γ, ω_A, and m_A are the natural linewidth, two-level transition frequency, and the mass of the atoms; ω_L and $\hbar \boldsymbol{k}_L$ are the frequency and momentum of the laser photons.

In addition to the timescale set by photon scattering rate in the Doppler-cooling process there is the slower dynamics associated with emission and absorption of the cavity photons by atoms. In the large detuning and high power limit $\left|\bar{\Delta}_L\right|^2 \gg \Omega^2 \gg \Gamma^2$, the dominant processes involving creation and annihilation of cavity photons are the scatterings between a laser photon and a cavity photon as illustrated in Fig. 4.1(c)-(d). For a single longitudinal mode with a longitudinal momentum $\boldsymbol{q}_\parallel = q_\parallel \hat{z}$, the transverse modes of the cavity can be expressed in terms of Laguerre-Gauss modes labeled by the radial index $l \in \mathbb{N}$ and azimuthal index $m \in \mathbb{Z}$ [145, 146]. According to Fermi's golden rule, the total rate that an atom scatters laser photons into a cavity mode with mode frequency $\omega_{q_\parallel lm}$ [145] [Fig. 4.1(c)] is, in the large detuing limit,

$$(n_{q_\parallel lm}+1)\Lambda^+_{q_\parallel lm,L} \approx \sum_{\boldsymbol{p}} \frac{2\pi}{\hbar} \frac{\hbar^2\Omega^2\alpha^2_{q_\parallel}}{\left|\bar{\Delta}_L\right|^2} (n_{q_\parallel lm}+1)\delta\left(\hbar\omega_L + K(\boldsymbol{p}) - \hbar\omega_{q_\parallel lm} - K(\boldsymbol{p}')\right), \tag{4.1}$$

where $\alpha^2_{q_\parallel}$ is the spatial average of $\alpha^2_{q_\parallel lm}$ ($2\alpha_{q_\parallel lm}$ is the single-photon Rabi frequency of the transverse cavity mode $q_\parallel lm$), $n_{q_\parallel lm}$ is the cavity photon occupation number, $\Lambda^+_{q_\parallel lm,L}$ is the single-cavity-photon emission rate mediated by the laser, $\boldsymbol{p}$ and $\boldsymbol{p}' = \boldsymbol{p} + \hbar\boldsymbol{k}_L - \hbar\boldsymbol{q}_\parallel$ are the atomic momentum before and after the scattering event, and $K(\boldsymbol{p}) = \boldsymbol{p}^2/2m_A$ is the kinetic energy of the atom. We are working in the paraxial limit so that $q_{q_\parallel lm} \equiv \omega_{q_\parallel lm}/c \approx q_\parallel$. Furthermore, the atoms are taken to have

a uniform spatial distribution within the cavity mode volume so that the spatial average of $\alpha^2_{q_\parallel lm}$ is independent of l and m.

Similarly, the total rate that an atom scatters cavity photons into the laser field [Fig. 4.1(d)] is

$$n_{q_\parallel lm}\Lambda^-_{q_\parallel lm,L} \approx \sum_{\boldsymbol{p}'} \frac{2\pi}{\hbar} \frac{\hbar^2\Omega^2\alpha^2_{q_\parallel}}{\left|\bar{\Delta}_L\right|^2} n_{q_\parallel lm}\delta\left(\hbar\omega_{q_\parallel lm} + K(\boldsymbol{p}') - \hbar\omega_L - K(\boldsymbol{p})\right), \tag{4.2}$$

where $\Lambda^-_{q_\parallel lm,L}$ is the single-cavity-photon absorption rate mediated by the laser, $\boldsymbol{p}'$ is the atomic momentum before the scattering event, and $\boldsymbol{p} = \boldsymbol{p}' + \hbar\boldsymbol{q}_\parallel - \hbar\boldsymbol{k}_L$ is the atomic momentum after the scattering event.

Equilibration between emission and absorption of cavity photons mediated by the cooling laser will lead to a detailed balance condition such that Eq. (4.1) equals Eq. (4.2), which gives

$$\frac{\bar{n}_{q_\parallel lm}+1}{\bar{n}_{q_\parallel lm}} = \frac{\Lambda^-_{q_\parallel lm,L}}{\Lambda^+_{q_\parallel lm,L}} = \sum_i \frac{e^{-\beta K(\boldsymbol{p}_i')}}{e^{-\beta K(\boldsymbol{p}_i)}} = e^{\beta\hbar(\omega_{q_\parallel lm}-\omega_L)}. \tag{4.3}$$

Here $\bar{n}_{q_\parallel lm}$ is the mean number of photons under detailed balance. The Boltzman factor is picked up by each pair of $\boldsymbol{p}_i$ and $\boldsymbol{p}_i{}'$ satisfying the energy conservation condition $K(\boldsymbol{p}_i{}')-K(\boldsymbol{p}_i) = \hbar(\omega_L-\omega_{q_\parallel lm})$ when summing over the atomic momentum distribution. This equilibration condition can be understood within the framework of photon thermalization with a parametrically coupled bath [38, 102, 103, 142], where the conservation of the total number of cavity plus laser photons during the scattering processes imposes a nonzero chemical potential $\hbar\omega_L$ to the cavity photons. For $\omega_{q_\parallel lm} > \omega_L$, one has $\bar{n}_{q_\parallel lm} = \frac{1}{e^{\beta\hbar(\omega_{q_\parallel lm}-\omega_L)}-1}$ corresponding to a grand canonical distribution; for $\omega_{q_\parallel lm} < \omega_L$, one expects gain or lasing instead of an equilibrium steady state since $\Lambda^+_{q_\parallel lm,L} > \Lambda^-_{q_\parallel lm,L}$.

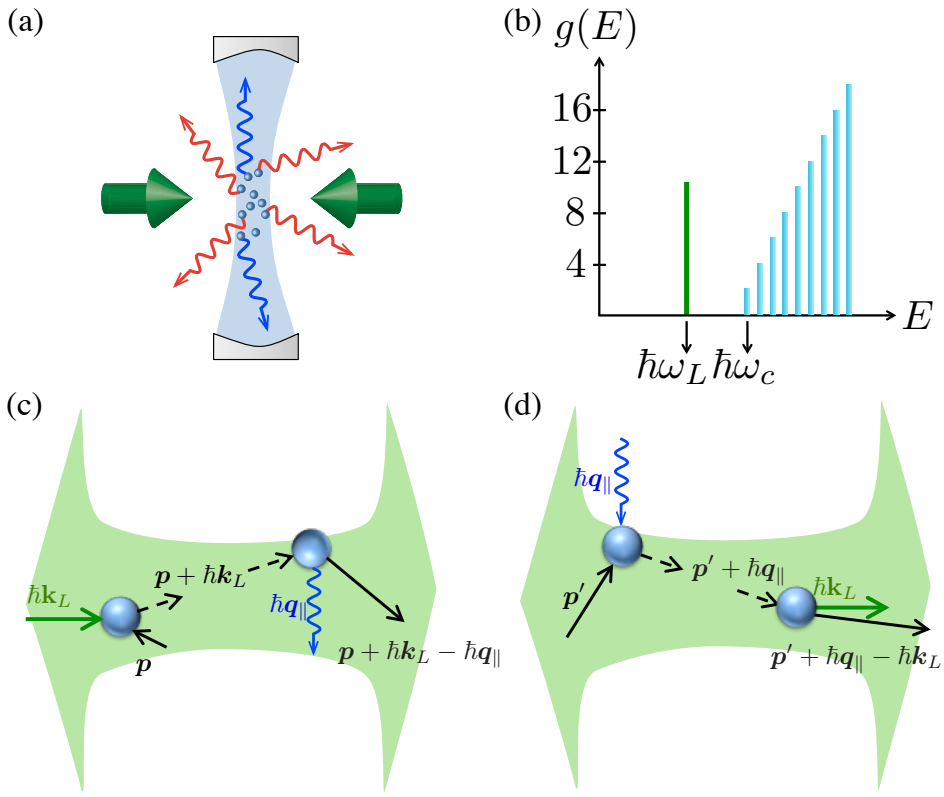

Figure 4.1: (a) Schematic of an ensemble of two-level atoms which are Doppler-cooled by laser fields (green arrows) and free-space photon modes (red arrows), while also interacting with cavity photon modes (blue arrows within the light-blue region). (b) The state degeneracy $g(E)$ (equivalent to density of states) of the transverse cavity modes is equivalent to that of a 2D massive particle in a harmonic trapping potential with a lower-cutoff energy $\hbar\omega_c = \hbar\omega_{q_\parallel 00}$ including polarization. The green line shows the energy of a single laser photon $\hbar\omega_L$. (c) The scattering process in which an atom is excited by the laser field and then emits a cavity photon. (d) The scattering process in which an atom absorbs a cavity photon and then scatters back into the laser field.

In reality, cavity photons also suffer from losses either due to scattering into the free space modes or dissipations at the cavity mirrors. Based on the theoretical tools developed in Ref. [142], assuming perfect cavity mirrors, the detailed balance condition is modified by the loss caused by scattering of the cavity photons into the free-space modes to

$$\frac{\bar{n}_{q_\parallel lm}+1}{\bar{n}_{q_\parallel lm}} \approx e^{\beta\hbar(\omega_{q_\parallel lm}-\omega_L)} + \frac{\Gamma}{\Omega^2}\frac{|\boldsymbol{k}_L-\boldsymbol{q}_\parallel|}{\sqrt{2\pi\beta m_A}} e^{\frac{\beta}{2m_A}\left(-\frac{m_A}{|\boldsymbol{k}_L-\boldsymbol{q}_\parallel|}(\omega_{q_\parallel lm}-\omega_L)-\frac{\hbar|\boldsymbol{k}_L-\boldsymbol{q}_\parallel|}{2}\right)^2}. \quad (4.4)$$

This loss-modified result represents a small correction to the grand-canonical form Eq. (4.3) in the high power limit $\Omega \gg \Gamma$, which is the focus of this work. Furthermore, the correction depends on the cavity mode frequency, and is larger for larger transverse cavity modes (when the frequency difference between the given cavity mode and the laser, $\omega_{q_\parallel lm} - \omega_L$, is larger). At large but finite power, we can incorporate the corrections from the second term on the right hand side of Eq. (4.4) into a shifted chemical potential $\hbar\omega_L - \delta\mu$ and a mode-dependent effective temperature β_{eff}^{-1}, where, formally, $\delta\mu$ and β_{eff} are defined by the equations [142]

$$1 = e^{-\beta\delta\mu} + \frac{\Gamma}{\Omega^2}\frac{|\boldsymbol{k}_L-\boldsymbol{q}_\parallel|}{\sqrt{2\pi\beta m_A}} e^{\frac{\beta}{2m}\left(\frac{m_A\delta\mu}{\hbar|\boldsymbol{k}_L-\boldsymbol{q}_\parallel|}-\frac{\hbar|\boldsymbol{k}_L-\boldsymbol{q}_\parallel|}{2}\right)^2}, \quad (4.5)$$

$$e^{\beta_{\text{eff}}(\hbar\omega_{q_\parallel lm}-\hbar\omega_L+\delta\mu)} = \frac{\bar{n}_{q_\parallel lm}+1}{\bar{n}_{q_\parallel lm}}. \quad (4.6)$$

Equation (4.6) predicts a transition from equilibrium to gain at the shifted frequency $\omega_{q_\parallel lm} = \omega_L - \delta\mu/\hbar$. For low power, $\Omega < \Omega_c$ for some critical value Ω_c, photon loss is large enough such that Eq. (4.5) has no solutions. In that case, $\delta\mu$ and β_{eff} are no longer well-defined and only quasithermal light (where the photon distribution cannot be described by a single well-defined temperature) is expected.

4.3 2D photonic BEC in a curved cavity

Restricting the cavity photon states to $\omega_{\boldsymbol{q}} \geq \omega_c > \omega_L - \delta\mu/\hbar$, for a cavity cut-off frequency ω_c equal to the lowest transverse mode frequency, can prevent the regime of gain and take us towards a photon BEC. Specifically, we control the photon density of states with a cavity and, further, consider a Fabrey-Perot cavity with curved mirrors to realize a quadratic dispersion relation for the energy of photons, as has been used to create a BEC of light [94, 113]. In contrast to prior work, here we consider a long cavity subtending a small solid angle, which makes the atoms emit mostly into the free-space modes, enabling Doppler cooling [Fig. 4.1(a)].

Specifically, the frequency of a cavity photon in a Laguerre-Gauss mode $(q_\parallel, l, m)$ is given by [145, 146]

$$\omega_{q_\parallel lm} \equiv c q_\parallel + \frac{c}{D_0}(2l + |m| + 1)\cos^{-1}\left(1 - \frac{D_0}{R}\right), \tag{4.7}$$

where D_0 is the distance between cavity mirrors and R is the radius of curvature of the mirrors. The transverse energy spectrum and the density of states of a single longitudinal mode inside the cavity is identical to that of a Hamiltonian for a (fictitious) massive 2D particle in a harmonic potential trap:

$$\hat{H}_\perp = \frac{(\hbar\hat{\boldsymbol{q}}_\perp)^2}{2M_{\rm ph}} + \frac{1}{2}M_{\rm ph}\omega_T^2\hat{r}_\perp^2, \tag{4.8}$$

where $M_{\rm ph} = \hbar q_\parallel/c$ is the mass of the 2D particle, $\hbar\hat{\boldsymbol{q}}_\perp$ and $\hat{r}_\perp$ are the corresponding momentum and position operators, and the trapping frequency is $\omega_T = \frac{c}{D_0}\cos^{-1}(1 - D_0/R)$.

As with 2D massive bosons in a harmonic trap, the cavity photons can undergo Bose condensation into the ground mode (the lowest transverse mode, which sets the cut-off frequency $\omega_c \equiv \omega_{q_\parallel 00}$ to the cavity modes). To make a direct connection to the typical BEC theory, we define a displaced chemical potential $\mu = \hbar(\omega_L - \omega_c)$ to compare the original chemical potential with the ground mode energy, such that in the absence of loss the whole system is in thermal equilibrium for $\mu < 0$, achieves BEC in the the thermodynamic limit[1] at $\mu = 0$, and exhibits gain when $\mu > 0$. The critical temperature of condensation is given by $T_c \approx \hbar\omega_T\sqrt{3n_{\text{tot}}}/\pi k_B$ where n_{tot} is the steady-state average photon number [94, 143, 144]. In contrast to many prior theoretical discussions of trapped atomic and photon BEC, there are two distinguishing features in photon BEC transitions under this laser cooling scenario. First, our system is better treated in the context of a grand canonical ensemble with a controlled chemical potential. Second, the energy-dependent loss mechanisms can affect the transition. We will first explore lossless BEC physics under the framework of a number reservoir with a controlled chemical potential, and later include the effect of loss.

In our laser cooling scenario, one can control T and μ independently by setting an approximately fixed temperature $k_B T \approx \hbar\left|\bar{\Delta}_L\right|/2$ for a large detuning from the atomic transition, and adjusting μ by the small laser detuning from ω_c. The analogous 2D massive bosonic gas experiences a fixed trapping frequency ω_T determined by the geometry of the cavity. We note that n_{tot} is determined jointly by T, μ, and

[1]The thermodynamic limit is reached by taking $n_{\text{tot}} \to \infty$ while keeping the 2D number density inside the trap, which is proportional to $n_{\text{tot}}\omega_T^2$, fixed.

ω_T, and we explore the BEC transition in the context of a fixed T and ω_T while varying μ.

For the ideal (lossless) grand canonical ensemble of a 2D massive Bose gas in a harmonic trap, $n_{\rm tot}$ is

$$n_{\rm tot} = \sum_{l=0}^{\infty} \sum_{m=-\infty}^{\infty} \frac{2}{e^{\beta\{(2l+|m|)\hbar\omega_T - \mu\}} - 1} = \sum_{j=0}^{\infty} \frac{2(j+1)}{e^{\beta(j\hbar\omega_T - \mu)} - 1}, \tag{4.9}$$

where the factor of 2 comes from polarization degeneracy and $j = 2l + |m|$. Each cavity mode with frequency $\omega_c + j\omega_T$ has degeneracy $2(j+1)$ as one expects for a 2D harmonic oscillator. The corresponding cavity state degeneracy is illustrated in Fig. 4.1(b). Defining n_0 as the average photon number in the ground mode, The black lines in Fig. 4.2(a)-(b) show the numerically calculated curves of the condensate fraction $n_0/n_{\rm tot}$ and $n_{\rm tot}$ as a function of μ in the absence of loss with T and ω_T fixed. In our finite system we do not have a sharp transition; We define the transition to BEC to be at the inflection point, where $d^2(n_0/n_{\rm tot})/d[\log(\mu)]^2 = 0$ in Fig. 4.2(a). Treating the total number of excited photons in the continuous limit [144], the phase transition according to this definition[2] occurs at the critical value $\mu = -3\hbar^2\omega_T^2/\pi^2 k_B T$, which coincides with the condition $n_0/n_{\rm tot} \approx 1/2$. The total number of photons at the transition point in this lossless limit for these parameters is $\sim 26\,000$.

The position of the inflection point in $n_0/n_{\rm tot}$ [Fig. 4.2(a)] will shift in the presence of loss—due to both cavity loss and scattering into the free-space modes—whose effects become important at lower laser power. In the regime we focus on in

[2]Here we study the scenario with varying $n_{\rm tot}$ while keeping ω_T constant, which is different from the usual case to approach thermodynamic limit with a fixed number density.

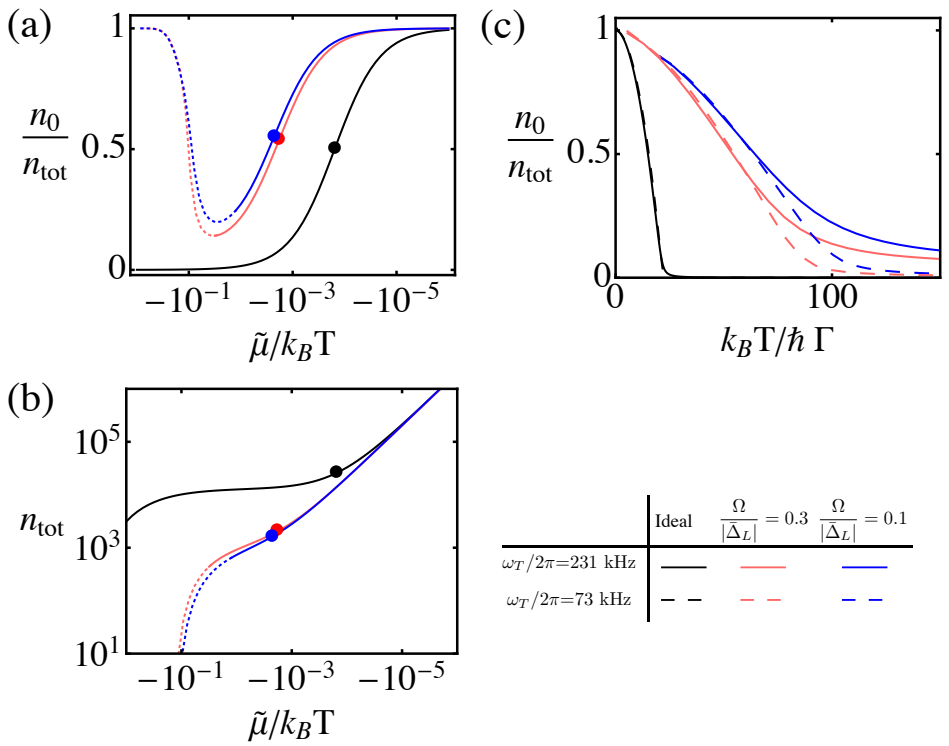

Figure 4.2: (a),(b) The condensate fraction $n_0/n_{\rm tot}$ [shown in (a)] and the total average number of photons $n_{\rm tot}$ [shown in (b)] at a fixed temperature as a function of the loss-shifted chemical potential $\tilde{\mu}$ plotted on a logarithmic scale. The ideal grand canonical ensemble result is shown in black lines, and the colored lines represent the modified results with two different Rabi frequencies. The critical points representing the onset of the BEC phase are identified by dots. We take parameters for the $^1S_0 - {}^3P_1$ Yb intercombination transition [109], $\omega_L/2\pi \approx \omega_A/2\pi = 539$ THz, $\Gamma/2\pi = 180$ kHz, $E_{r,\boldsymbol{k}_L}/h = 3.74$ kHz, and assume $|\boldsymbol{k}_L - \boldsymbol{q}| \approx \sqrt{2}|\boldsymbol{k}_L|$, $\bar{\Delta}_L \approx -157\Gamma$, and a cavity trapping frequency $\omega_T/2\pi$= 231 kHz. (c) The condensate fraction $n_0/n_{\rm tot}$ as a function of temperature while keeping the total number of photons fixed. The ideal grand canonical distribution is shown in black lines while the colored lines indicate loss-modified results with two different Rabi frequencies. We take parameters for the Yb intercombination transition with $\omega_T/2\pi = 231$ kHz for $n_{\rm tot} = 10^3$ and $\omega_T/2\pi = 73$ kHz for $n_{\rm tot} = 10^4$ such that $n_{\rm tot}(\omega_T/2\pi)^2 = 5.33 \times 10^{13}\mathrm{s}^{-2}$, proportional to the 2D number density, is fixed, which leaves the critical temperature essentially unchanged.

this work, the cavity loss at the mirrors can be neglected because the effective optical depth is taken to be large enough that the cavity photons will interact with an atom before being lost at the mirrors. The effect of cavity photon loss by scattering into the free-space modes can be suppressed by increasing the cooling laser intensity. However, higher order effects will need to be considered if one works beyond the low excitation limit $\Omega^2 \ll \left|\bar{\Delta}_L\right|^2$.

For $\Omega > \Omega_c$, the loss-modified total number of photons is given by replacing μ with $\tilde{\mu} \equiv (\hbar\omega_L - \hbar\omega_c - \delta\mu)$, which is the loss-modified displaced chemical potential, and replacing β with $\beta_{\text{eff}}[j]$ in Eq. (4.9). The effective temperature $\beta_{\text{eff}}[j]^{-1}$ is mode-dependent, and decreases as $j = 2l + |m|$ increases. We study the BEC transition with scattering loss numerically as shown in the colored lines in Fig. 4.2. For scenarios with a fixed total number of photons, which is a closer analogy to atomic BEC, the condensate fraction n_0/n_{tot} is shown as the colored lines in Fig. 4.2(c). The modified curves resemble qualitatively the ideal grand canonical ensemble case [black lines in Fig. 4.2(c)] at large n_{tot} and large $\Omega/|\bar{\Delta}_L|$, but with a higher transition temperature. The increase in the transition temperature arises from the loss-induced truncation of the populations of the higher frequency modes leading to these modes no longer being in thermal equilibrium. These populations are significantly lower than would be predicted by a single temperature equal to the atom temperature (see Fig. 5 in [142]). Thus, for a fixed n_{tot} and T, the mode occupation of the lower modes is significantly higher than in the untruncated case, which increases the transition temperature. Just as in a trapped atomic gas BEC, higher central density (ground mode occupation) leads to a higher transition temperature.

The loss-modified condensate fraction and the corresponding total number of photons as a function of $\tilde{\mu}$, at fixed T and ω_T, are shown in colored lines in Fig. 4.2(a)-(b). The transition between solid and dotted segments marks the distinction between GCE-like and quasithermal regimes as described below. The solid segments of the colored lines are qualitatively similar to the ideal result (black) with the inflection points of Fig. 4.2(a) left-shifted, which also arises from the loss-induced truncation of the populations of the higher frequency modes. On the other hand, the dotted part of our modified result is showing drastically different features from the ideal curve: Instead of being a monotonic function of $\tilde{\mu}$, the modified n_0/n_{tot} reaches a minimum then eventually increases to 1 when $\tilde{\mu}$ decreases further away from zero. The total number of photons also decreases substantially in this regime. This behavior is due to the fact that higher frequency modes have lower effective temperature because of loss; the occupation will tend toward the limit of $n_0/n_{\text{tot}} = 1$ for large, negative $\tilde{\mu}$ not because of a high degree of condensation but rather because only one mode survives the loss. We again define the BEC boundary to be at the inflection points of the condensation fraction curves. We then define an empirical condition that separates the GCE-like (solid line) region from the quasithermal (dotted line) region in Fig. 4.2(a)-(b): We define a grand canonical ensemble phase in which $-1/2 \leq \log_{10}\left(\frac{T_{\text{eff}}[5]}{T_o}\right) \leq 0$, where T_o is a reference temperature at the equilibrium-to-gain transition, such that there are at least $\sum_{j=0}^{5} 2(j+1) = 42$ modes that can be effectively described by a single temperature. For larger negative $\tilde{\mu}$ or lower laser intensities, the scattering loss prevents detailed balance of the cavity photons with atomic motion, and only quasithermal light (where the photon distribution cannot

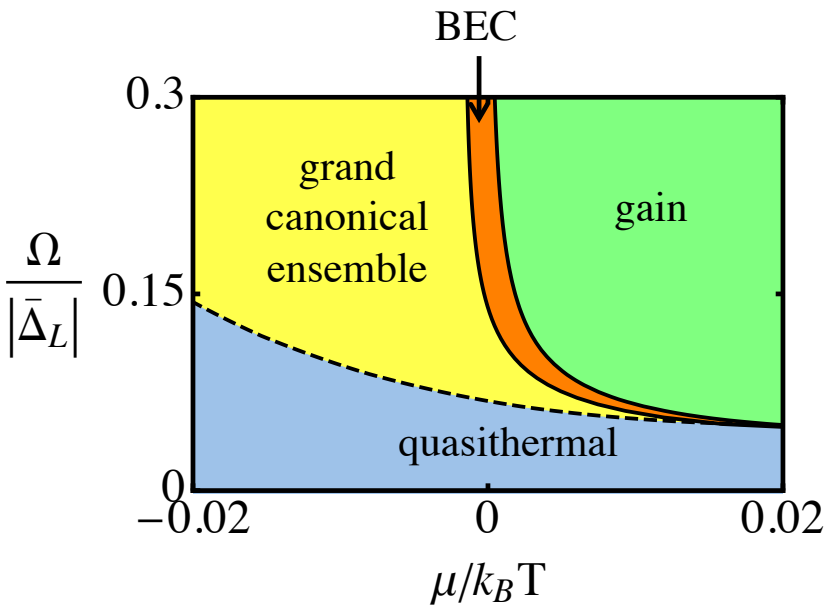

Figure 4.3: Calculated phase diagram of cavity photons as a function of Ω and μ. At high power, photon generation can exceed loss leading to gain (green region) and possibly lasing; cavity photons can be described as a grand canonical ensemble (yellow) at equilibrium, and we find the formation of a photon BEC (orange) within the GCE area and near the gain boundary. For low power, photon loss prevents equilibration of photons to a single temperature corresponding to that of the atomic motion, and only quasithermal light (blue) is expected. In this diagram we use the same parameters as in Fig. 4.2(a).

be described by a single temperature even for a moderate number of modes) is expected. For $\tilde{\mu} > 0$, one expects the onset of gain for the ground mode. The calculated phase diagram of the cavity photons is summarized in Fig. 4.3 with the phase boundaries defined above.

What can one observe in an experiment? In atomic BEC experiments, a typical technique to observe a BEC transition is to use the time-of-flight method to measure the momentum distribution of atoms. Here, the photonic version of "time-of-flight" is the far-field distribution of light emitted from the cavity, which

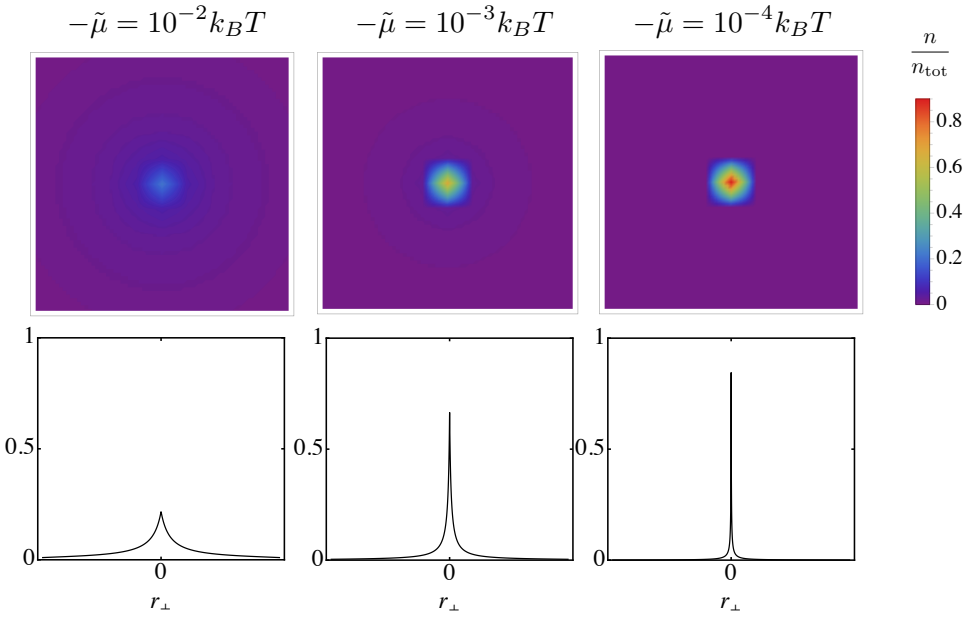

Figure 4.4: Simulations of the far-field photonic "time-of-flight" images and corresponding cross-sections through the center, where $r_\perp$ is the far-field transverse position. The parameters are the same as in Fig. 4.2(a) with $\Omega = 0.3\left|\bar{\Delta}_L\right|$.

reflects the momentum distribution of the cavity transverse modes. Simulations of the photonic "time-of-flight" images according to Eq. (4.4) are shown in Fig. 4.4. One expects a sharp central peak when $\tilde{\mu}$ is near zero, representing condensation into the ground mode.

4.4 Summary and Outlook

We have shown that Doppler cooling of a dilute, two-level, atomic ensemble inside an optical cavity can lead to 2D Bose-Einstein condensation of light. By studying the condensate fraction and the total photon number with values appropriate for the Yb intercombination transition, we have constructed a phase diagram

as a function of laser frequency and field strength showing gain, condensate, thermal, and quasithermal regimes for cavity photons. The simplicity as well as the high degree of control of our approach open up opportunities in exploring quantum phenomena with light. In particular, the thermalization arguments can be directly generalized to include nonlinear interactions, and thus are relevant to applications such as Rydberg-polariton thermalization with laser-cooled Rydberg atoms, photon superfluidity, and nonequilibrium phase transitions.

Chapter 5: Nonequilibrium Photon Transport in Driven Systems [1]

5.1 Quantum Transport Theory

Transport properties are among the key attributes of many important quantum phenomena in condensed matter physics including superconductivity, quantum Hall effect, Coulomb blockade, topological insulators, and localized phases [147]. Recent development of photonic technologies has allowed emulation of transport physics, such as photon blockade, using cavity [148, 149] and circuit quantum electrodynamics [15, 150]. However, the vacuum is the typical ground state for photonic systems, and thus efforts for quantum simulation with light have focused on driving systems far from equilibrium to provide sufficient numbers of photons. This makes predicting the dynamics and steady state behavior an outstanding challenge [35, 36].

On the other hand, electronic transport theory, pioneered in the works of Landauer [151–153], Büttiker [154], and Imry [153], has successfully dealt with a different problem: What is the quantum version of Ohm's law, i.e., the relationship between chemical potential difference (voltage) and particle flux (current), for describing the motion of electrons in mesoscopic systems [151–157]? Of particular

[1] This chapter has part of "Landauer formulation of photon transport in driven systems," by C.-H. Wang and J. M. Taylor in Phys. Rev. B **94**, 155437 (2016)

use have been mathematical tools such as nonequilibirum Green's function (NEGF) methods [156–159], which enable predictions for systems even at large voltage bias and with strong interactions.

In this chapter we consider whether a photonic version of the Landauer-type transport exists, and find that for parametrically coupled semi-infinite leads (transmission lines), a natural photonic voltage arises with an associated Ohm's law-type behavior for the photon flux. Our results rely upon the most recent of several approaches for developing a photonic equivalent to this voltage-bias [137, 160–162], including equilibration of light coupled to electrons flowing in a diode [161, 163, 164] and, more recently, parametrically coupled photonic systems [38]. Specifically, we derive the nonequilibrium transport of light under the parametric coupling scheme using nonequilibrium Green's function formalism. We study the photon flux as the equivalent of a current through a parametrically driven mesoscopic region, and show that the photon flux formula can be understood in the Landauer sense, as a transport from a chemical potential imbalance from the parametric coupling, with the addition of an anomalous particle-nonconserving squeezing term. Intuitively, our result connects the photon flow between a low frequency bath and an optical bath as mediated by a mesoscopic, interacting region. Thus we provide a rigorous framework for studying such near-equilibrium photonic systems without resorting to *ad hoc* tools for steady-state dynamics. Furthermore, our result predicts a quantitative link between the photon flux and the Green's function, which provides a possible testing ground for photonic quantum simulations even without particle number conservation.

5.2 Photon Transport Through a Trivial Scatterer

We start by developing our photonic analog to voltage bias. Consider a photonic (optical or microwave) system coupled to two baths: one associated with the typical decay of excitations into other modes via, e.g., imperfect mirrors, while the other is associated with a second bath coupled time-dependently with fast sinusoidal variation of the coupling constant at angular frequency ω_p. In particular, in Ref. [38], one of us showed that a time-dependent bath coupling can lead to the equilibration of a small system best described by a grand canonical ensemble distribution, i.e., a system of photons with a chemical potential. However, in that work crucial questions—such as what happens when coupled to two baths—were largely detailed heuristically. Here we focus on building a formalism, analogous to the finite-bias Green's function approach for electronic transport. In particular, we describe the two baths as semi-infinite transmission lines for our purposes, with the parametrically coupled bath being the left lead, and the natural bath corresponding to photon loss being the right lead, which could correspond to an outgoing optical signal to be measured with a photodetector (Fig. 5.1). This is now analogous to electronic transport at finite voltage bias, where the voltage is equivalent to the chemical potential $\hbar\omega_p$.

As a toy model, and to help develop the formalism, we start with the simplest setup in which the scatterer is trivial—a section of transmission line—and the problem now reduces to the case with left and right semi-infinite leads coupled parametrically (see Fig. 5.1). The Hamiltonian of the the system is $H = H_L + H_R + H_T(t)$,

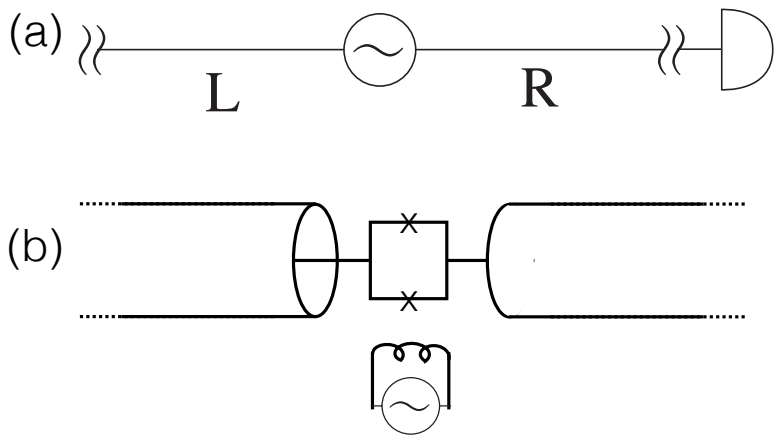

Figure 5.1: (a) Our conceptually simplest system of two semi-infinite leads, with a time-dependent coupling between them and a photodetector connecting to the right lead. (b) A potential physical implementation with a Josephson parametric coupler, driven with a flux bias line, between two transmission lines.

with

$$H_L = \sum_\alpha \epsilon_\alpha a_\alpha^\dagger a_\alpha,\ H_R = \sum_\beta \epsilon_\beta b_\beta^\dagger b_\beta,$$

$$H_T(t) = \cos(\omega_p t) \sum_{\alpha,\beta} \lambda_{\alpha\beta} u_\alpha u_\beta. \tag{5.1}$$

Here H_L and H_R are Hamiltonians of left and right transmission lines respectively, and $H_T(t)$ is the time-dependent tunneling coupling between the two subsystems. The summation index α labels the states in the left transmission line with energies $\hbar\omega_\alpha = \epsilon_\alpha$, photon annihilation operators a_α, displacement operators $u_\alpha = \sqrt{\frac{\hbar}{2\omega_\alpha}}\left(a_\alpha^\dagger + a_\alpha\right)$, and momentum operators $p_\alpha = i\sqrt{\frac{\hbar\omega_\alpha}{2}}\left(a_\alpha^\dagger - a_\alpha\right)$, while β, $\hbar\omega_\beta = \epsilon_\beta$, b_β, u_β, and p_β represent states in the right. $\lambda_{\alpha,\beta}$ are the coupling constants.

We may organize the Hamiltonian in a matrix form

$$H = \frac{1}{2}\vec{p}^{\mathrm{T}}\vec{p} + \frac{1}{2}\vec{u}^{\mathrm{T}}\mathbf{K}\vec{u} \tag{5.2}$$

by introducing displacement and momentum vectors

$$\vec{u} = \begin{pmatrix} \vec{u}_L \\ \\ \vec{u}_R \end{pmatrix}, \vec{p} = \begin{pmatrix} \vec{p}_L \\ \\ \vec{p}_R \end{pmatrix}, \tag{5.3}$$

with elements $(u_{L(R)})_{\alpha(\beta)} \equiv u_{\alpha(\beta)}$ and $(p_{L(R)})_{\alpha(\beta)} \equiv p_{\alpha(\beta)}$. $\vec{u}$ and $\vec{p}$ follow the equal time commutation relation

$$\left[\vec{u}(t), \vec{p}^{\mathrm{T}}(t)\right] = i\hbar\mathbf{I}. \tag{5.4}$$

Here $\mathbf{I}$ is the identity matrix, and T denotes the matrix transpose. $\mathbf{K}$ is a symmetric spring's constant matrix and can be further separated into diagonal and off-diagonal parts $\mathbf{K} = \mathbf{D} + \mathbf{V}(t) = \mathbf{D} + \mathbf{V}\cos(\omega_p t)$, where

$$\mathbf{D} = \begin{pmatrix} \mathbf{D}^L & 0 \\ \\ 0 & \mathbf{D}^R \end{pmatrix}, \mathbf{V}(t) = \begin{pmatrix} 0 & \mathbf{V}^{LR}(t) \\ \\ \mathbf{V}^{RL}(t) & 0 \end{pmatrix}. \tag{5.5}$$

Here $D^L_{\alpha\alpha'} = \omega^2_\alpha \delta_{\alpha\alpha'}$, $D^R_{\beta\beta'} = \omega^2_\beta \delta_{\beta\beta'}$, and $V^{LR}_{\alpha\beta}(t) = V^{RL}_{\beta\alpha}(t) = \cos(\omega_p t)\lambda_{\alpha\beta}$.

Assume the two subsystems were initially decoupled and in their own thermal equilibrium, and the parametric coupling is adiabatically turned on at $t = -\infty$ and turned off at $t = \infty$. Our goal is to find the photonic current transported between the two ends and express it in a Landauer-like formula in order to predict the current based on an effective chemical potential difference analogous to a voltage bias.

The current on the right at some later time t is defined as the temporal change of the total number of photons in the right transmission line $N_R = \sum_\beta b^\dagger_\beta b_\beta$, which

corresponds to an expected photodetector signal. We have

$$J_R(t) \equiv \left\langle \dot{N}_R(t) \right\rangle = \left\langle \frac{\mathrm{d}\sum_\beta b_\beta^\dagger b_\beta(t)}{\mathrm{d}t} \right\rangle . \tag{5.6}$$

The angular bracket denotes ensemble average over the initial equilibrium density of states, while the operators are in the Heisenberg picture. According to the Heisenberg equation of motion,

$$\dot{N}_R(t) = -\frac{1}{\hbar}\left(\frac{\partial}{\partial t'} \left[\vec{u}_R^{\mathrm{T}}(t') \tilde{\mathbf{V}}^{RL}(t) \vec{u}_L(t) \right] \right) \Big|_{t'=t}, \tag{5.7}$$

where $\tilde{V}_{\beta\alpha}^{RL}(t) \equiv V_{\beta\alpha}^{RL}(t)/\omega_\beta = \cos(\omega_p t)\lambda_{\alpha\beta}/\omega_\beta$.

One can connect the current expression with Keldysh Green's functions [158] by introducing the nonequilibrium lesser Green's function defined as

$$\mathbf{G}^<(t,t') \equiv -\frac{i}{\hbar} \left\langle \vec{u}(t') \vec{u}^{\mathrm{T}}(t) \right\rangle^{\mathrm{T}}, \tag{5.8}$$

which can also be split into four blocks associated with left and right transmission lines. We can write the current using the lesser Green's function as

$$J_R(t) = -i \left(\frac{\partial}{\partial t'} \mathrm{Tr} \left[\mathbf{G}_{LR}^<(t,t') \tilde{\mathbf{V}}^{RL}(t) \right] \right) \Big|_{t'=t}. \tag{5.9}$$

The trace here means tracing over photon states α.

We now follow the standard Keldysh formalism (NEGF formalism) [158] to study the transport formula [155–157, 165]. Since we define our Green's functions on displacement operators u instead of photon creation operators $a^\dagger$, our problem structurally resembles more the thermal transport cases [165] than electronic ones. We remind the reader here that since the parametric coupling varies with time and allows pair production and annihilation mechanisms, many identities and tricks in

previous works involving steady-state or particle-conserving assumptions cannnot be applied here.

The equation of motion of the contour ordered Green's function defined on the Keldysh contour C follows

$$\frac{\partial^2}{\partial\tau^2}\mathbf{G}^c(\tau,\tau') + \mathbf{K}\mathbf{G}^c(\tau,\tau') = -\delta(\tau,\tau')\mathbf{I}, \tag{5.10}$$

while the noninteracting equilibrium Green's function $\mathbf{g}^c(\tau,\tau')$ follows the equation of motion

$$\frac{\partial^2}{\partial\tau^2}\mathbf{g}^c(\tau,\tau') + \mathbf{D}\mathbf{g}^c(\tau,\tau') = -\delta(\tau,\tau')\mathbf{I}. \tag{5.11}$$

One can easily verify that $\mathbf{G}^c(\tau,\tau')$ follows the Dyson equation

$$\mathbf{G}^c(\tau,\tau') = \mathbf{g}^c(\tau,\tau') + \int_C d\tau''\mathbf{g}^c(\tau,\tau'')\mathbf{V}(\tau'')\mathbf{G}^c(\tau'',\tau'). \tag{5.12}$$

Using the Langreth theorem of analytic continuation [159], the lesser Green's function can be expressed as an integral form on the real axis

$$\mathbf{G}^<_{LR}(t,t') \approx \int_{-\infty}^{\infty} \mathrm{d}t_1 \left\{\mathbf{g}^r_L(t,t_1)\mathbf{V}^{LR}(t_1)\mathbf{g}^<_R(t_1,t')\mathbf{g}^<_L(t,t_1)\mathbf{V}^{LR}(t_1)\mathbf{g}^a_R(t_1,t')\right\} + \mathcal{O}(\lambda^2). \tag{5.13}$$

Here the r and a superscripts stand for retarded and advanced Green's functions, and we treat λ as a perturbation. The equilibrium Green's functions used in the

$\mathbf{G}^{<}_{LR}(t,t')$ expression are given by

$$
\begin{aligned}
(g^r_L)_\alpha(t,t_1) &= \frac{-i}{2\omega_\alpha}\theta(t-t_1)\left(e^{-i\omega_\alpha(t-t_1)} - e^{i\omega_\alpha(t-t_1)}\right), \\
(g^<_R)_\beta(t_1,t') &= \frac{-i}{2\omega_\beta}\left\{n_R(\epsilon_\beta)e^{-i\omega_\beta(t_1-t')} + [1+n_R(\epsilon_\beta)]e^{i\omega_\beta(t_1-t')}\right\}, \\
(g^<_L)_\alpha(t,t_1) &= \frac{-i}{2\omega_\alpha}\left\{n_L(\epsilon_\alpha)e^{-i\omega_\alpha(t-t_1)} + [1+n_L(\epsilon_\alpha)]e^{i\omega_\alpha(t-t_1)}\right\}, \\
(g^a_R)_\beta(t_1,t') &= \frac{-i}{2\omega_\beta}\theta(t'-t_1)\left(e^{i\omega_\beta(t_1-t')} - e^{-i\omega_\beta(t_1-t')}\right)
\end{aligned}
\tag{5.14}
$$

Here $n_{L(R)}(\epsilon_{\alpha(\beta)}) = (e^{(\epsilon_{\alpha(\beta)}-\mu_{L(R)})/k_BT}-1)^{-1}$ are the bosonic occupation number in left and right transmission lines. The chemical potentials $\mu_L = \mu_R = 0$ for photons, k_B is the Boltzmann constant, and T is the initial temperature of the system.

By inserting the expression for $\mathbf{G}^{<}_{LR}(t,t')$, the current is now

$$
\begin{aligned}
J_R(t) =& -i\left(\frac{\partial}{\partial t'}\mathrm{Tr}\left[\int_{-\infty}^{\infty}\mathrm{d}t_1\left\{\mathbf{g}^r_L(t,t_1)\mathbf{V}^{LR}(t_1)\mathbf{g}^<_R(t_1,t')\right.\right.\right. \\
&\left.\left.\left. + \ \mathbf{g}^<_L(t,t_1)\mathbf{V}^{LR}(t_1)\mathbf{g}^a_R(t_1,t')\right\}\tilde{\mathbf{V}}^{RL}(t)\right]\right)\Big|_{t'=t} \\
=& -i\left(\frac{\partial}{\partial t'}\sum_{\alpha,\beta}\int_{-\infty}^{\infty}\mathrm{d}t_1\frac{\lambda^2_{\alpha\beta}}{\omega_\beta}\cos(\omega_p t_1)\cos(\omega_p t)\right. \\
&\left.\times\left\{(g^r_L)_\alpha(t,t_1)(g^<_R)_\beta(t_1,t') + (g^<_L)_\alpha(t,t_1)(g^a_R)_\beta(t_1,t')\right\}\right)\Big|_{t'=t} \\
=& \sum_{\alpha,\beta}\frac{\lambda^2_{\alpha\beta}}{4\omega_\alpha\omega_\beta}\int_0^\infty \mathrm{d}\tau\Big(\left\{\cos(\omega_p\tau) + \cos[\omega_p(2t-\tau)]\right\} \\
&\times\left\{\cos[(\omega_\beta-\omega_\alpha)\tau]\left[n_L(\epsilon_\alpha) - n_R(\epsilon_\beta)\right]\right. \\
&\left.+\cos[(\omega_\beta+\omega_\alpha)\tau]\left[n_L(\epsilon_\alpha)+n_R(\epsilon_\beta)+1\right]\right\}\Big).
\end{aligned}
\tag{5.15}
$$

In the last equality we have used the identity $\cos(\omega_p t_1)\cos(\omega_p t) = \cos(\omega_p\tau)/2 + \cos[\omega_p(2t-\tau)]/2$, and changed the integral variable to $\tau = t - t_1$. The only explicit t dependence arises in the $\cos[\omega_p(2t-\tau)]$ factor. Averaging over one pump cycle

$2\pi/\omega_p$ takes this factor to zero. We thus neglect those terms with $\cos[\omega_p(2t-\tau)]$ in the spirit of the rotating wave approximation.

We assume the coupling constant only depends on the mode energy, $\lambda_{\alpha\beta} = \lambda(\epsilon_\alpha, \epsilon_\beta)$, and take the continuum limit of energy so that $\sum_{\alpha,\beta} = \int_0^\infty \mathrm{d}\epsilon_\alpha \rho_L(\epsilon_\alpha)$ $\times \int_0^\infty \mathrm{d}\epsilon_\beta \rho_R(\epsilon_\beta)$. Here ρ_L and ρ_R are the energy density of states in the left and right transmission lines. Note that $\int_0^\infty \cos[(\omega-\omega_1)\tau]d\tau = \pi\delta(\omega-\omega_1)$. We now arrive at a current formula with three terms:

$$\begin{aligned}\bar{J}_R = &\int_{\hbar\omega_p}^\infty \mathrm{d}\epsilon\, T(\epsilon, \epsilon-\hbar\omega_p)\left[n_L(\epsilon) - n_R(\epsilon-\hbar\omega_p)\right] \\ &+ \int_{\hbar\omega_p}^\infty \mathrm{d}\epsilon\, T(\epsilon-\hbar\omega_p, \epsilon)\left[n_L(\epsilon-\hbar\omega_p) - n_R(\epsilon)\right] \\ &+ \int_0^{\hbar\omega_p} \mathrm{d}\epsilon\, T(\epsilon, \hbar\omega_p-\epsilon)\left[n_L(\epsilon) + n_R(\hbar\omega_p-\epsilon) + 1\right] \end{aligned} \tag{5.16}$$

Here $\bar{J}_R$ represents the time-averaged current under the rotating wave approximation, and $T(\epsilon_1, \epsilon_2)$ is the transmission function defined as $T(\epsilon_1, \epsilon_2) = \frac{\hbar^3\pi}{8\epsilon_1\epsilon_2}\lambda^2(\epsilon_1, \epsilon_2)$ $\times \rho_L(\epsilon_1)\rho_R(\epsilon_2)$. $\bar{J}_L$ can be calculated with similar formulations.

Note that the $1/\epsilon$ factor in the transmission function and the bosonic occupation numbers $n_{L(R)}(\epsilon)$ go to infinity as the photon energy approaches zero. One can ensure the convergence of our model by the choice of a three-dimensional reservoir on the low-frequency side. The presence of the nonlinear interaction in the case of an interacting mesoscopic region can regulate the problem as well [38]. The power from the pump that generates the parametric coupling should be finite, and as the IR divergence is approached for lower dimensional systems, an appropriate inclusion of pump depletion will be necessary to develop a complete understanding of the problem.

The first line of Eq. (5.16) can be interpreted as a Landauer-like transport with an effective chemical potential $\hbar\omega_p$ on the right transmission line, and the second line represents a Landauer-like transport with an effective chemical potential $\hbar\omega_p$ on the left. The third line is a particle-nonconserving term due to pair creation and annihilation mechanisms allowed by the oscillating u-u type coupling. Two-mode squeezed states of light [166] are generated through this mechanism with the photon pairs entangled. One will expect a thermal state when tracing over the output modes on one side of such photon pairs.

Note that the current formula is consistent with Fermi's golden rule: The parametric coupling $\cos(\omega_p t)$ only allows transition with $E_f - E_i = \Delta E = \pm\hbar\omega_p$, where E_f and E_i are the energies of the final and initial states. For $\omega_p = 0$, the current equation reduces to the usual Landauer form proportional to $n_L(\epsilon) - n_R(\epsilon)$, which is essentially zero when the two transmission lines are at the same temperature.

The particle-nonconserving nature of the problem is manifested by identifying the anomalous current $\bar{J}_A \equiv \frac{\bar{J}_R + \bar{J}_L}{2} = \int_0^{\hbar\omega_p} \mathrm{d}\epsilon T(\epsilon, \hbar\omega_p - \epsilon)\,[n_L(\epsilon) + n_R(\hbar\omega_p - \epsilon) + 1]$, which is only zero when $T(\epsilon, \hbar\omega_p - \epsilon) = 0$ throughout the range, as is the case in Fig. 5.2(b). This term can also be understood in Fermi's golden rule point of view, considering the harmonic perturbation $H_T(t)$. According to Fermi's golden rule, the pair creation (annihilation) rates R_c (R_a) are:

$$\begin{aligned} R_c &= \int_0^{\hbar\omega_p} \mathrm{d}\epsilon\, T(\epsilon, \hbar\omega_p - \epsilon)\,[n_L(\epsilon) + 1]\,[n_R(\hbar\omega_p - \epsilon) + 1]\,, \\ R_a &= \int_0^{\hbar\omega_p} \mathrm{d}\epsilon\, T(\epsilon, \hbar\omega_p - \epsilon) n_L(\epsilon) n_R(\hbar\omega_p - \epsilon). \end{aligned} \tag{5.17}$$

The net creation rate is thus $R_c - R_a = \bar{J}_A$.

One can find the nonequilibrium transport part of the current by subtracting the anomalous squeezing (particle-nonconserving) term $\bar{J}_A$, and we are left with the normal current $\bar{J}_N \equiv (\bar{J}_R - \bar{J}_L)/2$, the first two lines of Eq. (5.16). We note here that the asymmetry between right and left is necessary for the transport to occur; the first two lines of Eq. (5.16) will cancel each other otherwise.

To focus on the transport mechanism only, we consider an energy gap on the right transmission line [see Fig. 5.2(b)] such that $\forall\alpha, \beta, \epsilon_\beta > \hbar\omega_p, \epsilon_\beta > \epsilon_\alpha$. This gap setup prevents the pair creation and annihilation mechanisms, leaves us with a conserved current and permits a direct photonic analog to electronic transport. The system follows the transport formula $\bar{J}_R = \int_{\epsilon_{\beta,\min}}^{\epsilon_{\alpha,\max}+\hbar\omega_p} \mathrm{d}\epsilon T\left(\epsilon - \hbar\omega_p, \epsilon\right)$ $\times [n_L(\epsilon - \hbar\omega_p) - n_R(\epsilon)]$, which is equivalent to a nonequilibirum transport current under a chemical potential imbalance $\mu_L = \hbar\omega_p, \mu_R = 0$.

One can see the resemblance between our gapped transport equation and the I-V (current-voltage) characteristic of an ideal light emitting diode (LED) [161] by relating the chemical potential $\hbar\omega_p$ to qV, and the gap energy $\epsilon_{\beta,\min}$ to the photon energy threshold e_g, and working under the region $\epsilon_{\alpha,\max} + \hbar\omega_p \gg k_B T$. However, we cannot yet make a direct connection mathematically with the somewhat different problem of electron transport through a diode combined with emission of photon into an interacting region.

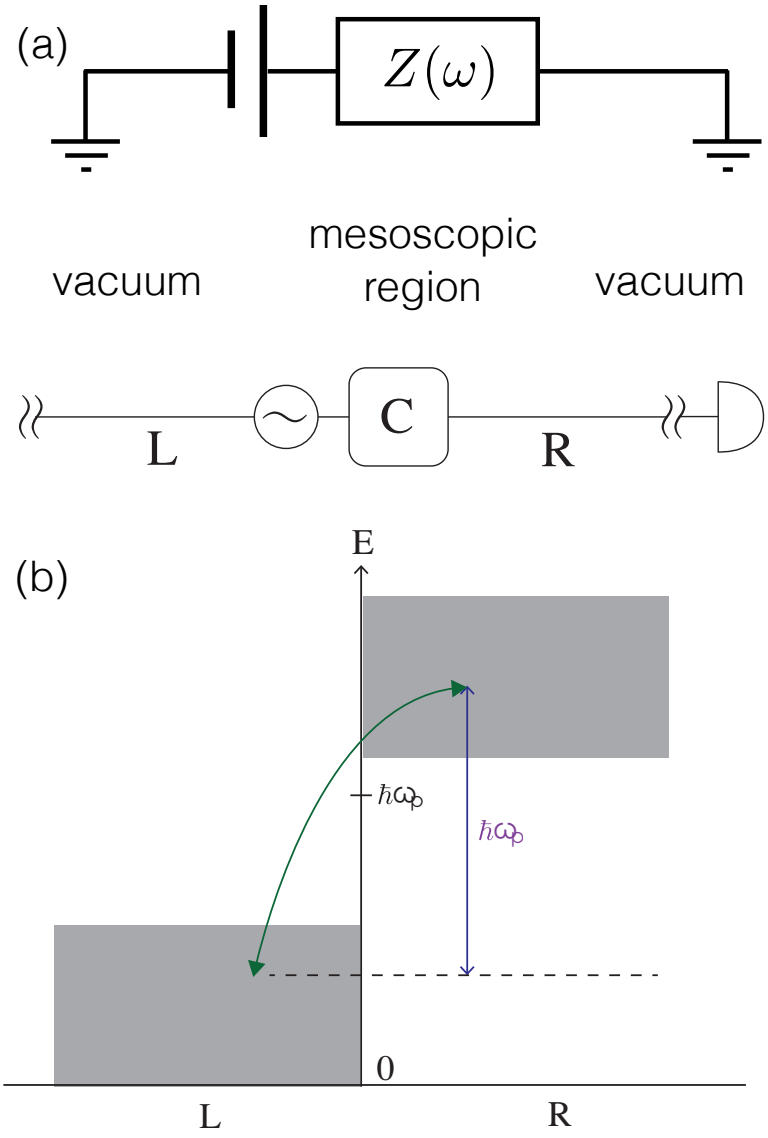

Figure 5.2: (a) The generic mesoscopic scenario, with two semi-infinite leads coupled parametrically to an intermediate mesoscopic region C, provides a photonic equivalent to a voltage bias and a (nonlinear) impedance provided by the region C. (b) A schematic diagram of the parametric coupling mechanism, in which a low-energy photonic mode on the left side is up-converted via the pump photon with energy $\hbar\omega_p$ to a higher energy mode on the right. The case where L and R leads have a high (left) and low (right) frequency cutoff is shown, to prevent anomalous squeezing terms.

5.3 Photon Transport Through a Mesoscopic Central Region

Now we consider a more generic case with a center mesoscopic region placed between the transmission lines, with parametric coupling between the center region and the left transmission line (see Fig. 5.2). We replace the time-dependent barrier $H_T(t)$ with $H_C + H_{CL}(t) + H_{CR}$, and the Hamiltonian becomes

$$H = H_L + H_C + H_R + H_{CL}(t) + H_{CR}, \tag{5.18}$$

$$\begin{aligned} H_L &= \sum_\alpha \epsilon_\alpha a_\alpha^\dagger a_\alpha,\ H_R = \sum_\beta \epsilon_\beta b_\beta^\dagger b_\beta, \\ H_C &= \sum_{\gamma,\gamma'} t_{\gamma\gamma'} c_\gamma^\dagger c_{\gamma'} + H_{\text{int}}, \\ H_{CL}(t) &= \cos(\omega_p t) \sum_{\alpha,\gamma} \lambda_{\alpha\gamma} u_\alpha u_\gamma, \\ H_{CR} &= \sum_{\beta,\gamma} \breve{\lambda}_{\beta\gamma} u_\beta u_\gamma. \end{aligned} \tag{5.19}$$

The summation index γ labels the states in the center with energies $\hbar\omega_\gamma = \epsilon_\gamma$ and photon annihilation operators c_γ. Note that we place all time dependence in the center to left coupling $H_{CL}(t)$. The central region can contain some nonlinear interacting term H_{int} as well as nontrivial single-particle potential effects from $t_{\gamma\gamma'}$. We again assume the subsystems were initially in their own thermal equilibrium before the parametric coupling adiabatically turned on at $t = -\infty$.

The current on the right can be expressed as

$$J_R(t) = -i \left(\frac{\partial}{\partial t'} \text{Tr} \left[\mathbf{G}_{CR}^<(t,t') \tilde{\mathbf{V}}^{RC} \right] \right) \Big|_{t'=t}. \tag{5.20}$$

Here $\tilde{V}^{RC}_{\beta\gamma} = V^{RC}_{\beta\gamma}/\omega_\beta = \breve{\lambda}_{\beta\gamma}/\omega_\beta$.

Accordingly to the Dyson equation, $\mathbf{G}^c_{CR}(\tau,\tau') = \int_C \mathbf{G}^c_{CC}(\tau,\tau'')\mathbf{V}^{CR}\mathbf{g}^c_R(\tau'',\tau')$. Using the Langreth theorem of analytic continuation and defining $\tilde{\mathbf{\Sigma}}_R(t_1,t') = \mathbf{V}^{CR}\mathbf{g}_R(t_1,t')\tilde{\mathbf{V}}^{RC}$, we have

$$J_R(t) = -i\int_{-\infty}^{\infty} \mathrm{d}t_1 \Big(\frac{\partial}{\partial t'}\mathrm{Tr}\left[\mathbf{G}^r_{CC}(t,t_1)\tilde{\mathbf{\Sigma}}^<_R(t_1,t') + \mathbf{G}^<_{CC}(t,t_1)\tilde{\mathbf{\Sigma}}^a_R(t_1,t')\right]\Big)\Big|_{t'=t}. \tag{5.21}$$

This is our generic current expression analogous to the Meir-Wingreen equation in the electronic transport theory [156].

One can reformulate the current through Fourier transform

$$J_R(t) = \int_{-\infty}^{\infty} \frac{\omega\,\mathrm{d}\omega}{2\pi}\mathrm{Tr}\left[\mathbf{G}^r_{CC}(t,\omega)\tilde{\mathbf{\Sigma}}^<_R(\omega) + \mathbf{G}^<_{CC}(t,\omega)\tilde{\mathbf{\Sigma}}^a_R(\omega)\right]. \tag{5.22}$$

Here $\mathbf{G}_{CC}(t,t') \equiv \int_{-\infty}^{\infty}\frac{\mathrm{d}\omega}{2\pi}e^{-i\omega(t-t')}\mathbf{G}_{CC}(t,\omega)$, $\mathbf{G}_{CC}(t,\omega) \equiv \int_{-\infty}^{\infty} dt' e^{i\omega(t-t')}\mathbf{G}_{CC}(t,t')$. We note here that due to the time-dependent coupling, the center Green's function is not in a steady state, and its Fourier transform function therefore depends on the initial (or ending) time index.

We now examine the simplified case of noninteracting center, and the main result of this work follows through. Non-interacting mesoscopic transport theory provides interesting phenomena such as weak localization, ballistic-to-diffusive transitions, and weak-antilocalization [167–169]. For $H_{\mathrm{int}} = 0$, the center Green's function follows the Dyson equation

$$\mathbf{G}^c_{CC}(\tau,\tau') = \mathbf{g}^c_C(\tau,\tau') + \int_C \mathbf{g}^c_C(\tau,\tau_1)\mathbf{\Sigma}^c_{\mathrm{tot}}(\tau_1,\tau_2)\mathbf{G}^c_{CC}(\tau_2,\tau'). \tag{5.23}$$

Here $\mathbf{\Sigma}^c_{\rm tot}(\tau_1,\tau_2)$ is the total self-energy of the center,

$$\begin{aligned}
&\mathbf{\Sigma}^c_{\rm tot}(\tau_1,\tau_2) = \mathbf{\Sigma}^c_L(\tau_1,\tau_2) + \mathbf{\Sigma}^c_R(\tau_1,\tau_2),\\
&\mathbf{\Sigma}^c_L(\tau_1,\tau_2) \equiv \mathbf{V}^{CL}\cos(\omega_p\tau_1)\mathbf{g}^c_L(\tau_1,\tau_2)\cos(\omega_p\tau_2)\mathbf{V}^{LC},\\
&\mathbf{\Sigma}^c_R(\tau_1,\tau_2) \equiv \mathbf{V}^{CR}\mathbf{g}^c_R(\tau_1,\tau_2)\mathbf{V}^{RC}.
\end{aligned} \tag{5.24}$$

Note that for the case of interacting center, there will be additional contribution to the self-energy depending on the details of $H_{\rm int}$.

Specifically, the center greater and lesser Green's function follows

$$\mathbf{G}^{\gtrless}_{CC}(t,t') = \int \mathrm{d}t_1\,\mathrm{d}t_2 \mathbf{G}^r_{CC}(t,t_1)\mathbf{\Sigma}^{\gtrless}_{\rm tot}(t_1,t_2)\mathbf{G}^a_{CC}(t_2,t'), \tag{5.25}$$

which allows us to further simplify the current expression.

The center Green's function under parametric coupling can be expanded with the harmonics of the coupling frequency ω_p. Specifically, $\mathbf{G}_{CC}(t,\omega) = \sum_n \mathbf{G}_{CC,n}(\omega)$ $\times e^{2ni\omega_p t}$, $n \in \mathbb{Z}$. Under the rotating wave approximation, we neglect fast oscillating terms with $n \neq 0$ and keep only the $n = 0$ steady part of the current. The time averaged current is now

$$\bar{J}_R = \int_{-\infty}^{\infty} \frac{\mathrm{d}\omega}{2\pi}\omega \mathrm{Tr}\left[\mathbf{G}^r_{CC,0}(\omega)\tilde{\mathbf{\Sigma}}^<_R(\omega) + \mathbf{G}^<_{CC,0}(\omega)\tilde{\mathbf{\Sigma}}^a_R(\omega)\right]. \tag{5.26}$$

Since the current is real, $\bar{J}_R = (\bar{J}_R + \bar{J}^*_R)/2$. Using the general identity $G^> - G^< = G^r - G^a$ and identities for steady state Green's functions in the frequency domain $[G^r(\omega)]^\dagger = G^a(\omega)$, $[G^<(\omega)]^\dagger = -G^<(\omega)$,

$$\bar{J}_R = \int_{-\infty}^{\infty} \frac{\mathrm{d}\omega}{4\pi}\omega \mathrm{Tr}\left\{\left[\mathbf{G}^>_{CC,0}(\omega) - \mathbf{G}^<_{CC,0}(\omega)\right]\tilde{\mathbf{\Sigma}}^<_R(\omega) - \mathbf{G}^<_{CC,0}(\omega)\left[\tilde{\mathbf{\Sigma}}^r_R(\omega) - \tilde{\mathbf{\Sigma}}^a_R(\omega)\right]\right\}. \tag{5.27}$$

Expanding the non-interacting center greater and lesser Green's functions to the leading order term yields:

$$\mathbf{G}^{\gtrless}_{CC}(t,t') \approx \int \mathrm{d}t_1\,\mathrm{d}t_2 \mathbf{g}^r_{CC}(t,t_1)\mathbf{\Sigma}^{\gtrless}_{\mathrm{tot}}(t_1,t_2)\mathbf{g}^a_{CC}(t_2,t') + \mathcal{O}(\lambda^3),$$

$$\mathbf{G}^{\gtrless}_{CC,0}(\omega) \approx \mathbf{g}^r_C(\omega)\mathbf{\Sigma}^{\gtrless}_{\mathrm{tot},0}(\omega)\mathbf{g}^a_C(\omega)$$

$$= \mathbf{g}^r_C(\omega)\left(\mathbf{V}^{CR}\mathbf{g}^{\gtrless}_R(\omega)\mathbf{V}^{RC} + \frac{1}{4}\mathbf{V}^{CL}\mathbf{g}^{\gtrless}_L(\omega+\omega_p)\mathbf{V}^{LC} + \frac{1}{4}\mathbf{V}^{CL}\mathbf{g}^{\gtrless}_L(\omega-\omega_p)\mathbf{V}^{LC}\right)\mathbf{g}^a_C(\omega). \tag{5.28}$$

By inserting the equilibrium Green's function for left and right transmission lines g_L and g_R, we arrive at a formula similar to the trivial scatterer problem:

$$\begin{aligned}\bar{J}_R = &\int_{\hbar\omega_p}^{\infty} \mathrm{d}\epsilon T_C(\epsilon, \epsilon-\hbar\omega_p)\left[n_L(\epsilon) - n_R(\epsilon-\hbar\omega_p)\right] \\ &+ \int_{\hbar\omega_p}^{\infty} \mathrm{d}\epsilon T_C(\epsilon-\hbar\omega_p, \epsilon)\left[n_L(\epsilon-\hbar\omega_p) - n_R(\epsilon)\right] \\ &+ \int_{0}^{\hbar\omega_p} \mathrm{d}\epsilon T_C(\epsilon, \hbar\omega_p-\epsilon)\left[n_L(\epsilon) + n_R(\hbar\omega_p-\epsilon) + 1\right].\end{aligned} \tag{5.29}$$

where the center transmission function is

$$\begin{aligned}T_C(\epsilon_\alpha,\epsilon_\beta) &= \frac{\pi\hbar^3}{8}\mathrm{Tr}\left[\mathbf{g}^r_c(\epsilon_\beta)\mathbf{\Lambda}_R(\epsilon_\beta)\mathbf{g}^a_c(\epsilon_\beta)\mathbf{\Lambda}_L(\epsilon_\alpha)\right], \\ [\Lambda_L(\epsilon_\alpha)]_{\gamma_1,\gamma_2} &= \rho_L(\epsilon_\alpha)\lambda_{\gamma_1}(\epsilon_\alpha)\lambda_{\gamma_2}(\epsilon_\alpha)/\epsilon_\alpha, \\ [\Lambda_R(\epsilon_\beta)]_{\gamma_1,\gamma_2} &= \rho_R(\epsilon_\beta)\breve{\lambda}_{\gamma_1}(\epsilon_\beta)\breve{\lambda}_{\gamma_2}(\epsilon_\beta)/\epsilon_\beta.\end{aligned} \tag{5.30}$$

We again have the first two lines of Eq. (5.29) as the Landauer-like transport terms, and the last line is the particle-nonconserving part due to the oscillating u-u type coupling. The system will undergo nonequilibirum transport with an effective chemical potential imbalance $\hbar\omega_p$ under specific gap setups, and the current expression resembles the I-V characteristic of an ideal light-emitting diode.

5.4 Outlook

We have derived the photonic flux between different baths parametrically coupled to an intermediate system and found a Landauer-like transport formula for non-interacting centers. However, we also have another regime, with a particle-nonconserving term, which we can interpret as a two-mode squeezing output. The consequences of this latter regime for observation and even application remain to be explored and are beyond the scope of the present work. We have also shown a potential extension of these techniques at the formal level to the interacting case, but suggest that applying these results, e.g., to photon-blockaded systems to see the nonclassical light output would be an intriguing next step.

Appendix A: Self-Consistent Analysis of Laser Cooling with Optically Thick and Thin Modes [1]

A.1 The Master Equation

The rapid decay of the lossy bath modes $b_{\boldsymbol{k}}$ leads to dissipative effects for the atoms (e.g., excited-state decay) and the system photons $a_{\boldsymbol{q}}$ (via scattering into bath modes). We describe the resulting dissipative dynamics with a Lindblad-form master equation. Each Lindblad-form damping term has a jump operator $\hat{c}_j$ and an associated rate r_j. Formally, the master equation for a density matrix ρ_{T} describing the atoms and the system photons is [106]

$$\begin{aligned}\frac{\mathrm{d}\rho_{\mathrm{T}}}{\mathrm{d}t} &= \frac{1}{i\hbar}(H_{\mathrm{eff}}\rho_{\mathrm{T}} - \rho_{\mathrm{T}}H_{\mathrm{eff}}^{\dagger}) + \sum_j r_j \hat{c}_j \rho_{\mathrm{T}} \hat{c}_j^{\dagger}, \\ H_{\mathrm{eff}} &= H_{\mathrm{T}} - i\hbar \sum_j \frac{r_j}{2}\hat{c}_j^{\dagger}\hat{c}_j, \end{aligned} \tag{A.1}$$

where H_{T} is the combined system and atom Hamiltonian.

We now identify the jump operators and corresponding rates for atomic states due to bath modes based on the above analysis. Due to spontaneous decay into bath modes, for each bath mode $b_{\boldsymbol{k}}$, we have an excited-state jump operator $\hat{c}_{\boldsymbol{k}}^{e}$ with

[1] This chapter has part of "Photon thermalization via laser cooling of atoms," by C.-H. Wang, M. J. Gullans, J. V. Porto, W. D. Phillips and J. M. Taylor in Phys. Rev. A **98**, 013834 (2018)

a jump rate $r^e_{\boldsymbol{k}}$:

$$\hat{c}^e_{\boldsymbol{k}} = e^{-i\boldsymbol{k}\cdot\boldsymbol{r}} \left|g\right\rangle \left\langle e\right|, \; r^e_{\boldsymbol{k}}(\boldsymbol{p}) = \frac{2\pi}{\hbar}|\hbar\beta_{\boldsymbol{k}}|^2\delta(\Delta E_{eg}(\boldsymbol{k},\boldsymbol{p})). \tag{A.2}$$

The sum of all jump rates leads to an overall decay rate of the excited state, $\sum_{\boldsymbol{k}} r^e_{\boldsymbol{k}} = \Gamma$, as expected. The second-order transitions due to laser-bath scattering with modes $b_{\boldsymbol{k}}$ will also lead to ground state–ground state jump operators $\hat{c}^g_{\boldsymbol{k}}$ and jump rates $r^g_{\boldsymbol{k}}$,

$$\hat{c}^g_{\boldsymbol{k}} = e^{i(\boldsymbol{k}_L-\boldsymbol{k})\cdot\boldsymbol{r}} \left|g\right\rangle \left\langle g\right|, \; r^g_{\boldsymbol{k}}(\boldsymbol{p}) = \frac{2\pi}{\hbar}|\hbar R_{\boldsymbol{k}}(\boldsymbol{p})|^2\delta(\Delta E_{gg}(\boldsymbol{k},\boldsymbol{p})), \tag{A.3}$$

where $R_{\boldsymbol{k}}(\boldsymbol{p})$ is given by Eq. (3.11). The sum of all jump rates leads to a laser-induced decay of the atomic ground state, $\sum_{\boldsymbol{k}} r^g_{\boldsymbol{k}}(\boldsymbol{p}) = \gamma(\boldsymbol{p})$. Note that the groun-state decay rate is momentum dependent. The overall effect of the cavity decay of the system photons can be described as jump operators $\hat{c}_{\boldsymbol{q}} = a_{\boldsymbol{q}}$, and jump rates $\kappa_{\boldsymbol{q}}$.

When applying the ground-state jump operators and rates, the lowest order effect in Ω of the bath modes $b_{\boldsymbol{k}}$ has been included. To treat the overall problem consistently, we have to express the Hamiltonian to the lowest order in Ω for the system modes $a_{\boldsymbol{q}}$ as well. Specifically, we have

$$\begin{aligned} V_{ASL}(t) = &-\sum_{\boldsymbol{q}} a^\dagger_{\boldsymbol{q}} e^{-i\omega_L t} e^{i(\boldsymbol{k}_L-\boldsymbol{q})\cdot\boldsymbol{r}} \hbar R^+_{\boldsymbol{q}}(\boldsymbol{p}) \left|g\right\rangle \left\langle g\right| \\ &-\sum_{\boldsymbol{q}} a_{\boldsymbol{q}} e^{i\omega_L t} e^{-i(\boldsymbol{k}_L-\boldsymbol{q})\cdot\boldsymbol{r}} \hbar R^-_{\boldsymbol{q}}(\boldsymbol{p}) \left|g\right\rangle \left\langle g\right|, \end{aligned} \tag{A.4}$$

where $R^+_{\boldsymbol{q}}(\boldsymbol{p})$ and $R^-_{\boldsymbol{q}}(\boldsymbol{p})$ are given by Eqs. (3.15) and (3.16).

We can then write down the effective Hamiltonian after integrating out the

lossy bath modes $b_{\boldsymbol{k}}$ as

$$\begin{aligned} H_{\text{eff}} =& \hbar\left(\omega_A - i\frac{\Gamma}{2}\right)|e\rangle\langle e| + \frac{\boldsymbol{p}^2}{2m} - \frac{i\hbar\gamma(\boldsymbol{p})}{2}|g\rangle\langle g| + \sum_{\boldsymbol{q}}\hbar\left(\omega_{\boldsymbol{q}} - i\frac{\kappa_{\boldsymbol{q}}}{2}\right)a_{\boldsymbol{q}}^\dagger a_{\boldsymbol{q}} \\ &- \sum_{\boldsymbol{q}}\hbar\alpha_{\boldsymbol{q}}\left(a_{\boldsymbol{q}}e^{i\boldsymbol{q}\cdot\boldsymbol{r}}|e\rangle\langle g| + |g\rangle\langle e|\, a_{\boldsymbol{q}}^\dagger e^{-i\boldsymbol{q}\cdot\boldsymbol{r}}\right) \\ &- \sum_{\boldsymbol{q}} a_{\boldsymbol{q}}^\dagger e^{-i\omega_L t}e^{i(\boldsymbol{k}_L-\boldsymbol{q})\cdot\boldsymbol{r}}\hbar R_{\boldsymbol{q}}^+(\boldsymbol{p})|g\rangle\langle g| \\ &- \sum_{\boldsymbol{q}} a_{\boldsymbol{q}}e^{i\omega_L t}e^{-i(\boldsymbol{k}_L-\boldsymbol{q})\cdot\boldsymbol{r}}\hbar R_{\boldsymbol{q}}^-(\boldsymbol{p})|g\rangle\langle g|\,. \end{aligned} \tag{A.5}$$

From the $V_{ASL}(t)$ term in the effective Hamiltonian, we see explicitly that the laser mediates time-dependent (parametric) coupling between the system photons and the atomic ground state. We will study how the atomic motional state evolves later in this section, which determines the dynamics of the bath. In Appendix B we will find the emission and absorption rates of the system photons on top of the rapid thermalization of atoms due to laser and bath modes.

Working from Eq. (A.1), we write the full master equation for the atoms and system photons:

$$\begin{aligned} \frac{\mathrm{d}\rho_{\mathrm{T}}}{\mathrm{d}t} =& \frac{1}{i\hbar}(H_{\text{eff}}\rho_{\mathrm{T}} - \rho_{\mathrm{T}}H_{\text{eff}}^\dagger) + \sum_{\boldsymbol{q}}\kappa_{\boldsymbol{q}}a_{\boldsymbol{q}}\rho_{\mathrm{T}}a_{\boldsymbol{q}}^\dagger. \\ &+ \sum_{\boldsymbol{k}}\left\{\frac{r_{\boldsymbol{k}}^e}{2}, e^{-i\boldsymbol{k}\cdot\boldsymbol{r}}|g\rangle\langle e|\,\rho_{\mathrm{T}}\,|e\rangle\langle g|\,e^{i\boldsymbol{k}\cdot\boldsymbol{r}}\right\} \\ &+ \sum_{\boldsymbol{k}}\left\{\frac{r_{\boldsymbol{k}}^g}{2}, e^{i(\boldsymbol{k}_L-\boldsymbol{k})\cdot\boldsymbol{r}}|g\rangle\langle g|\,\rho_{\mathrm{T}}\,|g\rangle\langle g|\,e^{-i(\boldsymbol{k}_L-\boldsymbol{k})\cdot\boldsymbol{r}}\right\} \end{aligned} \tag{A.6}$$

Since the jump rates depend on the atomic momentum, we treat them as operators and symmetrize them around $\hat{c}_j\rho_{\mathrm{T}}\hat{c}_j^\dagger$ terms using the anticommutator $\{,\}$.

The system density matrix now describes the atoms and the system photons $a_{\boldsymbol{q}}$ only, and can be further separated as $\rho_{\mathrm{T}} = \rho_{\mathrm{ee}}|e\rangle\langle e| + \rho_{\mathrm{gg}}|g\rangle\langle g| + \rho_{\mathrm{eg}}|e\rangle\langle g| +$

$\rho_{\mathrm{ge}} |g\rangle \langle e|$, where ρ_{ij} is an operator acting in the atomic momentum and photon number Hilbert space. According to the master equation, the excited component ρ_{ee} is rapidly decaying with a rate Γ while the off-diagonal terms ρ_{eg}, ρ_{ge} dephase with a rate $\Gamma/2 + \gamma(\boldsymbol{p})/2 \approx \Gamma/2$.

We now focus on the ground state component ρ_{gg} only. We start with the simplest case that the overall space is one dimensional (1D) along the $\hat{x}$ axis. In the limit $(\boldsymbol{k}_L - \boldsymbol{k}) \cdot \boldsymbol{r} \ll 1$, we can make a Lamb-Dicke approximation because the distance the atom moves during scattering events is much shorter than the wavelength of the photons. This leads to the approximate expression

$$e^{i(\boldsymbol{k}_L - \boldsymbol{k})\cdot \boldsymbol{r}} \rho_{gg} e^{-i(\boldsymbol{k}_L - \boldsymbol{k})\cdot \boldsymbol{r}} \approx \rho_{gg} + i[(\boldsymbol{k}_L - \boldsymbol{k}) \cdot \boldsymbol{r}, \rho_{gg}] - \frac{1}{2}[(\boldsymbol{k}_L - \boldsymbol{k}) \cdot \boldsymbol{r}, [(\boldsymbol{k}_L - \boldsymbol{k}) \cdot \boldsymbol{r}, \rho_{gg}]]. \tag{A.7}$$

Applying the first term in Eq. (A.7) to Eq. (A.6) produces $\left\{\frac{\gamma(\boldsymbol{p})}{2}, \rho_{\mathrm{gg}}\right\}$, which cancels with $-\left\{\frac{\gamma(\boldsymbol{p})}{2}, \rho_{\mathrm{gg}}\right\}$ from the imaginary part of the effective Hamiltonian in ground state, $-\frac{i\hbar\gamma(\boldsymbol{p})}{2} |g\rangle \langle g|$.

The second term in Eq. (A.7) is imaginary and will lead to an effective force in Eq. (A.6). Assuming the recoil effect is small as in the usual Doppler cooling scheme, the relevant bath modes are photons with momentum about the same magnitude as $\hbar k_L$ but nearly isotropic. Therefore, we have $\sum_{\boldsymbol{k}} \boldsymbol{k} |\beta_{\boldsymbol{k}}^2| \delta(\Delta E_{gg}(\boldsymbol{k}, \boldsymbol{p})) \approx 0$. For $\boldsymbol{k}_L = k_L \hat{x}$, the second term leads to

$$\sum_{\boldsymbol{k}} i k_L [x, \{r_{\boldsymbol{k}}^g, \rho_{\mathrm{gg}}\}] \approx \frac{i k_L \Omega^2 \Gamma}{\bar{\Delta}_L^2 + \Gamma^2/4} \left([x, \rho_{\mathrm{gg}}] + \frac{\bar{\Delta}_L k_L}{(\bar{\Delta}_L^2 + \Gamma^2/4) m} [x, \{p_x, \rho_{\mathrm{gg}}\}] \right). \tag{A.8}$$

The approximation follows by assuming the Doppler shift and the recoil shift are much smaller than $\bar{\Delta}_L$ or Γ. The part proportional to $[x, \rho_{\mathrm{gg}}]$ corresponds to a

dc force $\frac{\Omega^2\Gamma}{\bar{\Delta}_L^2+\Gamma^2/4}\hbar\boldsymbol{k}_L$, and the $[x,\{p_x,\rho_{\rm gg}\}]$ part will create a velocity-dependent damping term for p_x with a rate $\frac{-2\hbar\Omega^2\Gamma\bar{\Delta}_L k_L^2}{(\bar{\Delta}_L^2+\Gamma^2/4)^2 m}$. Note that the rate is positive with a negative detuning $\bar{\Delta}_L$ appropriate for laser cooling.

We then examine the third term in Eq. (A.7), $-\frac{1}{2}[(\boldsymbol{k}_L-\boldsymbol{k})\cdot\boldsymbol{r},[(\boldsymbol{k}_L-\boldsymbol{k})\cdot\boldsymbol{r},\rho_{\rm gg}]]$. Recall that we are considering the 1D case, we have $\sum_{\boldsymbol{k}}(\boldsymbol{k}_L-\boldsymbol{k})^2\frac{2\pi}{\hbar}|\hbar\beta_{\boldsymbol{k}}^2|\delta(\Delta E_{gg}(\boldsymbol{k},\boldsymbol{p}))$ $\approx 2k_L^2\Gamma$. We have again neglected the recoil effect for the relevant bath modes. The leading order contribution from this term to Eq. (A.6) is $-\frac{\Omega^2\Gamma k_L^2}{\bar{\Delta}_L^2+\Gamma^2/4}[x,[x,\rho_{\rm gg}]]$, which corresponds to a diffusion term for the atomic momentum.

The master equation in 1D for the atoms after elimination of the excited state now reads

$$\begin{aligned}\frac{\mathrm{d}\rho_{\rm gg}}{\mathrm{d}t}=&\frac{1}{i\hbar}\left[H_{\rm T}-i\hbar\sum_{\boldsymbol{q}}\frac{\kappa_{\boldsymbol{q}}}{2}a_{\boldsymbol{q}}^\dagger a_{\boldsymbol{q}},\rho_{\rm gg}\right]+\frac{1}{i\hbar}[-F_0(\boldsymbol{k}_L)x,\rho_{\rm gg}]-\frac{i\zeta}{\hbar}\left[x,\{p_x,\rho_{\rm gg}\}_+\right]\\&-\frac{2m\zeta k_BT}{\hbar^2}[x,[x,\rho_{\rm gg}]]+\sum_{\boldsymbol{q}}\kappa_{\boldsymbol{q}}a_{\boldsymbol{q}}\rho_{\rm gg}a_{\boldsymbol{q}}^\dagger.\end{aligned}\tag{A.9}$$

Here $H_{\rm T}=\frac{\boldsymbol{p}^2}{2m}+\hbar\omega_A|e\rangle\langle e|+H_S+H_{AS}+V_{ASL}(t)$. The above equation is in fact the master equation for quantum Brownian motion theory with a damping constant $\zeta=\frac{\hbar\Omega^2\Gamma|\bar{\Delta}_L|k_L^2}{(\bar{\Delta}_L^2+\Gamma^2/4)^2m}$ and temperature $k_BT=\frac{\hbar}{2}\frac{\bar{\Delta}_L^2+\Gamma^2/4}{|\bar{\Delta}_L|}$ given by the momentum diffusion up to a DC force term $F_0(\boldsymbol{k}_L)=\frac{\hbar k_L\Omega^2\Gamma}{\bar{\Delta}_L^2+\Gamma^2/4}$. The dc force term (a drift) can be compensated for by another dc force term or by including a counter-propagating laser. This master equation can be easily generalized to three dimensions. In practice, the use of multiple laser beams will remove the drift term and recover the standard Doppler cooling theory of two-level atoms in the low-excitation limit.

A.2 Self-Consistent Fermi's Golden Rule using Time-Dependent Perturbation Theory

To treat the dynamics of the atoms and the system photons self-consistently, we here calculate the transition rates associated with system photon emission and absorption using the quantum jump master equation and time-dependent perturbation theory. This complements—and indeed is equivalent to—the diagrammatic approach followed in the main text. For simplicity, we consider the case of a single laser mode $\boldsymbol{k}_L$, a single system photon mode $a_{\boldsymbol{q}}$, and an initial state with a definite atomic momentum $|\psi(t=0)\rangle = |n_{\boldsymbol{q}}\rangle\,|g,\boldsymbol{p}\rangle$. Here $\{n_{\boldsymbol{q}}\}$ denotes the Fock state of system photons. We also neglect cavity loss for the moment. Under the effective Hamiltonian, the time evolution of the unnormalized state is

$$\begin{aligned}|\psi(t)\rangle \approx& e^{-iz_{g_0}t}\,|\psi(0)\rangle - \frac{i}{\hbar}\sum_n |n\rangle \int_0^t \mathrm{d}t_a e^{-iz_n(t-t_a)-iz_{g_0}t_a}\,\langle n|\,V(t_a)\,|\psi(0)\rangle \\ =& e^{-iz_{g_0}t}\,|g_0\rangle + i\alpha_{\boldsymbol{q}}\sqrt{n_{\boldsymbol{q}}} f_{e^-_{\boldsymbol{q}}}(t)\left|e^-_{\boldsymbol{q}}\right\rangle + iR^+_{\boldsymbol{q}}(\boldsymbol{p})\sqrt{n_{\boldsymbol{q}}+1} f_{g^+_{\boldsymbol{q},L}}(t)\left|g^+_{\boldsymbol{q},L}\right\rangle \\ &+ iR^-_{\boldsymbol{q}}(\boldsymbol{p})\sqrt{n_{\boldsymbol{q}}} f_{g^-_{\boldsymbol{q},L}}(t)\left|g^-_{\boldsymbol{q},L}\right\rangle. \end{aligned} \tag{A.10}$$

According to the effective Hamiltonian, the evolution of each state has a complex frequency $z_i = \omega_i - i\gamma_i/2$; the real part corresponds to the state energy and the imaginary part denotes the damping. The short hand notations of the possible

states are

$$
\begin{aligned}
&|g_0\rangle = |n_{\boldsymbol{q}}\rangle\,|g,\boldsymbol{p}\rangle\,,\\
&\left|g^{+}_{\boldsymbol{q},L}\right\rangle = |n_{\boldsymbol{q}}+1\rangle\,|g,\boldsymbol{p}+\hbar\boldsymbol{k}_L-\hbar\boldsymbol{q}\rangle\,,\\
&\left|g^{-}_{\boldsymbol{q},L}\right\rangle = |n_{\boldsymbol{q}}-1\rangle\,|g,\boldsymbol{p}+\hbar\boldsymbol{q}-\hbar\boldsymbol{k}_L\rangle\,,\\
&\left|e^{-}_{\boldsymbol{q}}\right\rangle = |n_{\boldsymbol{q}}-1\rangle\,|e,\boldsymbol{p}+\hbar\boldsymbol{q}\rangle\,,
\end{aligned}
\tag{A.11}
$$

and their corresponding complex frequencies are defined as

$$
\begin{aligned}
z_{g_0} &= \frac{\boldsymbol{p}^2}{2m\hbar} + n_{\boldsymbol{q}}\omega_{\boldsymbol{q}} - \frac{i\gamma(\boldsymbol{p})}{2},\\
z_{g^{+}_{\boldsymbol{q},L}} &= \frac{|\boldsymbol{p}+\hbar\boldsymbol{k}_L-\hbar\boldsymbol{q}|^2}{2m\hbar} + (n_{\boldsymbol{q}}+1)\omega_{\boldsymbol{q}} - \frac{i\gamma(\boldsymbol{p}+\hbar\boldsymbol{k}_L-\hbar\boldsymbol{q})}{2},\\
z_{g^{-}_{\boldsymbol{q},L}} &= \frac{|\boldsymbol{p}+\hbar\boldsymbol{q}-\hbar\boldsymbol{k}_L|^2}{2m\hbar} + (n_{\boldsymbol{q}}-1)\omega_{\boldsymbol{q}} - \frac{i\gamma(\boldsymbol{p}+\hbar\boldsymbol{q}-\hbar\boldsymbol{k}_L)}{2},\\
z_{e^{-}_{\boldsymbol{q}}} &= \frac{|\boldsymbol{p}+\hbar\boldsymbol{q}|^2}{2m\hbar} + (n_{\boldsymbol{q}}-1)\omega_{\boldsymbol{q}} + \omega_A - \frac{i\Gamma}{2}.
\end{aligned}
\tag{A.12}
$$

Here the superscript " + " again denotes emission of a system photon ($|n_{\boldsymbol{q}}\rangle \to |n_{\boldsymbol{q}}+1\rangle$) and " − " for absorption ($|n_{\boldsymbol{q}}\rangle \to |n_{\boldsymbol{q}}-1\rangle$).

The time-dependent functions $f_i(t)$ are

$$
f_{g^{+}_{\boldsymbol{q},L}}(t) = \int_0^t \mathrm{d}t_a e^{-iz_{g^{+}_{\boldsymbol{q},L}}(t-t_a)} e^{-i\omega_L t_a - iz_{g_0}t_a}, \tag{A.13}
$$

$$
f_{g^{-}_{\boldsymbol{q},L}}(t) = \int_0^t \mathrm{d}t_a e^{-iz_{g^{-}_{\boldsymbol{q},L}}(t-t_a)} e^{i\omega_L t_a - iz_{g_0}t_a}, \tag{A.14}
$$

$$
f_{e^{-}_{\boldsymbol{q}}}(t) = \int_0^t \mathrm{d}t_a e^{-iz_{e^{-}_{\boldsymbol{q}}}(t-t_a)} e^{-iz_{g_0}t_a}. \tag{A.15}
$$

Compared to the usual time-dependent perturbation theory, the above time-dependent functions include the dissipative part of the Hamiltonian, and shall lead to modifications from the usual Fermi's golden rule.

First, since $\langle\psi(t)\,|\psi(t)\rangle \approx e^{-\gamma_{\boldsymbol{p}}t}$, we find the jump time t_J by solving $r = e^{-\gamma_{\boldsymbol{p}}t_J}$, $0 \leq r \leq 1$, where r is randomly distributed in $(0,1)$. The average total jump rate from the initial state is $\approx \gamma(\boldsymbol{p})$ up to a correction at order V^2. At the time of the jump, we need to evaluate the different possible jump outcomes, according to the un-normalized probability distributions $P_j \propto \mathcal{P}_j = \gamma_j \langle\psi(t_J)|\,\hat{c}_j^\dagger \hat{c}_j\,|\psi(t_J)\rangle\,/r$, and here we have included the $1/r$ factor to normalize the wave vector. We see

$$\mathcal{P}_0(\boldsymbol{p}) = \sum_{\boldsymbol{k}} r_{\boldsymbol{k}}^g(\boldsymbol{p})\,\langle g|\,\hat{c}_{\boldsymbol{k}}^{g\dagger}\hat{c}_{\boldsymbol{k}}^g\,|g\rangle\,\frac{|e^{-iz_{g_0}t_J}|^2}{r} = \gamma(\boldsymbol{p}), \tag{A.16}$$

$$\mathcal{P}_{\boldsymbol{q},L}^+(\boldsymbol{p}) = \gamma(\boldsymbol{p}+\hbar\boldsymbol{k}_L-\hbar\boldsymbol{q})|R_{\boldsymbol{q}}^+(\boldsymbol{p})|^2(n_{\boldsymbol{q}}+1)\frac{|f_{g_{\boldsymbol{q},L}^+}(t_J)|^2}{r}, \tag{A.17}$$

$$\mathcal{P}_{\boldsymbol{q},L}^-(\boldsymbol{p}) = \gamma(\boldsymbol{p}-\hbar\boldsymbol{k}_L+\hbar\boldsymbol{q})|R_{\boldsymbol{q}}^-(\boldsymbol{p})|^2 n_{\boldsymbol{q}}\frac{|f_{g_{\boldsymbol{q},L}^-}(t_J)|^2}{r}, \tag{A.18}$$

$$\mathcal{P}_{\boldsymbol{q},B}^-(\boldsymbol{p}) = \Gamma|\alpha_{\boldsymbol{q}}|^2 n_{\boldsymbol{q}}\frac{|f_{e_{\boldsymbol{q}}^-}(t_J)|^2}{r}. \tag{A.19}$$

We interpret the possible jump outcomes as the following processes (see Fig.3.5): (a) $\mathcal{P}_0(\boldsymbol{p})$: scattering process that absorbs a laser photon and spontaneously decays into the bath modes; (b) $\mathcal{P}_{\boldsymbol{q},L}^+(\boldsymbol{p})$: scattering process that absorbs a laser photon and emits a system photon; (c) $\mathcal{P}_{\boldsymbol{q},L}^-(\boldsymbol{p})$: scattering process that absorbs a system photon and scatters back into the laser mode; (d) $\mathcal{P}_{\boldsymbol{q},B}^-(\boldsymbol{p})$: scattering process that absorbs a system photon and scatters into the bath modes. The average rates for those processes will be evaluated in details.

Since $|\psi(t_J)\rangle \approx e^{-iz_{g_0}t_J}\,|\psi(0)\rangle + O(V^2)$, the scattering process that absorbs a laser photon and emits a system photon [Eq. (A.16)] is the leading-order effect. Therefore, $\sum_i \mathcal{P}_i \approx \mathcal{P}_0(\boldsymbol{p})$, and the normalized probability distribution is thus $P_j \equiv$

$\mathcal{P}_j/\sum_i \mathcal{P}_i \approx \mathcal{P}_j/\mathcal{P}_0(\boldsymbol{p})$. The transition rate associated with $\mathcal{P}_j$ can be found by $\Gamma_j(\boldsymbol{p}) = \int_0^1 \gamma(\boldsymbol{p}) P_j \mathrm{d}r$, which is the overall decay rate $\gamma(\boldsymbol{p})$ times the normalized probability P_j averaging over possible jump time.

The leading-order jump outcome associated with Eq. (A.16) happens at a rate $\Gamma_0(\boldsymbol{p}) = \gamma(\boldsymbol{p}) \int_0^1 \mathrm{d}r \frac{\mathcal{P}_0(\boldsymbol{p})}{\mathcal{P}_0(\boldsymbol{p})} = \gamma(\boldsymbol{p})$. This corresponds to the laser-bath scattering process [Fig.3.5(a)] with a rate consistent with our analysis in Sec 3.3. We can identify this rate as the "thermalizing jump rate," the jump rate that leads to the thermalization of atoms. In addition, since the laser-bath scattering leads to Doppler cooling of atoms, we can assume that the atomic motion reequilibrates to a steady state $\rho^B_{\text{atom}} = \int \mathrm{d}^3\boldsymbol{p} \Pi(\boldsymbol{p}) |g, \boldsymbol{p}\rangle \langle g, \boldsymbol{p}|$ before other processes involving the change of system photonic state occurs, where $\Pi(\boldsymbol{p})$ follows the Boltzmann distribution as defined in Eq. (3.18). This steady-state distribution due to Doppler cooling of atoms averages out the phase factor $e^{i(\boldsymbol{k}_L - \boldsymbol{q})\cdot \boldsymbol{r}}$ in the coupling $V_{ASL}(t)$; one can thus neglect the coherent part of the system photons. The long-time dynamics of the system photons is then governed by incoherent transitions between photon number states with rates calculated below.

The average rate of emitting one system photon from a specific atomic momentum state $|g, \boldsymbol{p}\rangle$, start from $|g_0\rangle$ and ending in $\left|g^+_{\boldsymbol{q},L}\right\rangle$ on top of the rapid jumps [Fig. 3.5(b)], is

$$\Gamma^+_{\boldsymbol{q},L}(\boldsymbol{p}) \equiv \gamma(\boldsymbol{p}) \int \frac{\mathcal{P}^+_{\boldsymbol{q},L}(\boldsymbol{p})}{\mathcal{P}_0(\boldsymbol{p})} \mathrm{d}r = \gamma(\boldsymbol{p} + \hbar\boldsymbol{k}_L - \hbar\boldsymbol{q}) |R^+_{\boldsymbol{q}}(\boldsymbol{p})|^2 (n_{\boldsymbol{q}} + 1) \int_0^1 \frac{\mathrm{d}r |f_{g^+_{\boldsymbol{q},L}}(r)|^2}{r}. \tag{A.20}$$

This rate corresponds to the emission process of a system photon over a finite

time before the atoms being reset (thermalized) by the emission process into bath modes. We see a simpler interpretation here: a new jump operator that acts directly on the system photon state, with a jump rate $\kappa^+_{\boldsymbol{q},L}(\boldsymbol{p}) = \Pi(\boldsymbol{p})\gamma(\boldsymbol{p}+\hbar\boldsymbol{k}_L - \hbar\boldsymbol{q})|R^+_{\boldsymbol{q}}(\boldsymbol{p})|^2 \int_0^1 |f_{g^+_{\boldsymbol{q},L}}(r)|^2 \mathrm{d}r/r$ and a jump term $a^\dagger_{\boldsymbol{q}}$.

Evaluating $\int_0^1 |f_{g^+_{\boldsymbol{q},L}}(r)|^2 \mathrm{d}r/r$, we have

$$\begin{aligned}\int_0^1 |f_{g^+_{\boldsymbol{q},L}}(r)|^2 \mathrm{d}r/r &= \gamma(\boldsymbol{p}) \int_0^\infty |f_{g^+_{\boldsymbol{q},L}}(t_J)|^2 \mathrm{d}t_J \\ &= \frac{\gamma_{g_0} + \gamma_{g^+_{\boldsymbol{q},L}}}{\gamma_{g^+_{\boldsymbol{q},L}} \left[(\omega_{g_0} + \omega_L - \omega_{g^+_{\boldsymbol{q},L}})^2 + (\gamma_{g_0} + \gamma_{g^+_{\boldsymbol{q},L}})^2/4\right]},\end{aligned} \tag{A.21}$$

where we used $r = e^{-\gamma(\boldsymbol{p})t} \to \frac{\mathrm{d}r}{r} = -\gamma(\boldsymbol{p})\mathrm{d}t$. The total system photon emission rate is $(n_{\boldsymbol{q}}+1)\Lambda^+_{\boldsymbol{q},L}$ with

$$\Lambda^+_{\boldsymbol{q},L} \equiv \int \mathrm{d}^3\boldsymbol{p}\kappa^+_{\boldsymbol{q},L}(\boldsymbol{p}) = \int \mathrm{d}^3\boldsymbol{p}\,\Pi(\boldsymbol{p})|R^+_{\boldsymbol{q}}(\boldsymbol{p})|^2 \delta_{\gamma(\boldsymbol{p})+\gamma(\boldsymbol{p}+\boldsymbol{k}_L-\boldsymbol{q})}\left(\Delta E_{gg}(\boldsymbol{q},\boldsymbol{p})\right). \tag{A.22}$$

Recall that $\delta_\epsilon(\omega) = \frac{\epsilon/2\pi}{\omega^2+\epsilon^2/4}$ is a broadened δ function of ω with a width ϵ. We call the result in Eq. (A.22) an example of the *self-consistent Fermi's golden rule*, in which the δ function in the usual Fermi's golden rule is now replaced by the decay-broadened δ function $\delta_{\gamma(\boldsymbol{p})+\gamma(\boldsymbol{p}+\boldsymbol{k}_L-\boldsymbol{q})}$ due to the finite lifetime of the initial and final states. The system photons absorption rates according to Eqs. (A.18) and (A.19) can be found analogously as presented in Sec. A.2.

Bibliography

[1] M. K. E. L. Planck, Verhandl. Dtsc. Phys. Ges. **2**, 237 (1900).

[2] M. Planck, Ann. Phys. (Berlin) **309**, 553 (1901).

[3] G. Kirchhoff, Ann. Phys. (Berlin) **185**, 275 (1860).

[4] W. Wien, Ann. Phys. (Berlin) **294**, 662 (1896).

[5] L. Rayleigh, Phil. Mag. **49**, 539 (1900).

[6] P. Ehrenfest, Ann. Phys. (Berlin) **341**, 91 (1911).

[7] P. A. M. Dirac, Proc. R. Soc. London, Ser. A **114**, 243 (1927).

[8] R. P. Feynman, Int. J. Theor. Phys. **21**, 467 (1982).

[9] I. M. Georgescu, S. Ashhab, and F. Nori, Rev. Mod. Phys. **86**, 153 (2014).

[10] A. Aspuru-Guzik and P. Walther, Nat. Phys. **8**, 285 (2012).

[11] C. Noh and D. G. Angelakis, Rep. Prog. Phys. **80**, 016401 (2017).

[12] R. Heidemann, U. Raitzsch, V. Bendkowsky, B. Butscher, R. Löw, L. Santos, and T. Pfau, Phys. Rev. Lett. **99**, 163601 (2007).

[13] T. Peyronel, O. Firstenberg, Q.-Y. Liang, S. Hofferberth, A. V. Gorshkov, T. Pohl, M. D. Lukin, and V. Vuletić, Nature (London) **488**, 57 (2012).

[14] M. J. Hartmann, J. Opt. **18**, 104005 (2016).

[15] A. A. Houck, H. E. Türeci, and J. Koch, Nat. Phys. **8**, 292 (2012).

[16] K. Hennessy, A. Badolato, M. Winger, D. Gerace, M. Atatüre, S. Gulde, S. Fält, E. L. Hu, and A. Imamoğlu, Nature (London) **445**, 896 (2007).

[17] H. Kim, R. Bose, T. C. Shen, G. S. Solomon, and E. Waks, Nat. Photon. **7**, 373 (2013).

[18] D. E. Chang, V. Vuletic, and M. D. Lukin, Nat. Photon. **8**, 685 (2014).

[19] O. Firstenberg, C. S. Adams, and S. Hofferberth, J. Phys. B **49**, 152003 (2016).

[20] J. Kasprzak, M. Richard, S. Kundermann, A. Baas, P. Jeambrun, J. M. Keeling, F. M. Marchetti, M. H. Szymańska, R. André, J. L. Staehli, V. Savona, P. B. Littlewood, B. Deveaud, and L. S. Dang, Nature (London) **443**, 409 (2006).

[21] J. Klaers, J. Schmitt, F. Vewinger, and M. Weitz, Nature (London) **468**, 545 (2010).

[22] S. Raghu and F. D. M. Haldane, Phys. Rev. A **78**, 33834 (2008).

[23] M. Hafezi, E. A. Demler, M. D. Lukin, and J. M. Taylor, Nat. Phys. **7**, 907 (2011).

[24] K. Fang, Z. Yu, and S. Fan, Nat. Photon. **6**, 782 (2012).

[25] R. Balili, V. Hartwell, D. Snoke, L. Pfeiffer, and K. West, Science **316**, 1007 (2007).

[26] H. Deng, H. Haug, and Y. Yamamoto, Rev. Mod. Phys. **82**, 1489 (2010).

[27] G. Tosi, G. Christmann, N. G. Berloff, P. Tsotsis, T. Gao, Z. Hatzopoulos, P. G. Savvidis, and J. J. Baumberg, Nat. Phys. **8**, 190 (2012).

[28] A. T. Black, H. W. Chan, and V. Vuletić, Phys. Rev. Lett. **91**, 203001 (2003).

[29] F. Dimer, B. Estienne, A. S. Parkins, and H. J. Carmichael, Phys. Rev. A **75**, 013804 (2007).

[30] D. Nagy, G. Szirmai, and P. Domokos, Eur. Phys. J. D **48**, 127 (2008).

[31] K. Baumann, C. Guerlin, F. Brennecke, and T. Esslinger, Nature (London) **464**, 1301 (2010).

[32] M. Fitzpatrick, N. M. Sundaresan, A. C. Y. Li, J. Koch, and A. A. Houck, Phys. Rev. X **7**, 011016 (2017).

[33] M. Weitz, J. Klaers, and F. Vewinger, Phys. Rev. A **88**, 045601 (2013).

[34] R. Ma, C. Owens, A. Houck, D. I. Schuster, and J. Simon, Phys. Rev. A **95**, 043811 (2017).

[35] J. Keeling and N. G. Berloff, Contemp. Phys. **52**, 131 (2011).

[36] F. Nissen, S. Schmidt, M. Biondi, G. Blatter, H. E. Türeci, and J. Keeling, Phys. Rev. Lett. **108**, 233603 (2012).

[37] J. W. Gibbs, *Elementary principles in statistical mechanics* (Yale University Press, London, 1928).

[38] M. Hafezi, P. Adhikari, and J. M. Taylor, Phys. Rev. B **92**, 174305 (2015).

[39] Y. Subaşı, C. H. Fleming, J. M. Taylor, and B. L. Hu, Phys. Rev. E **86**, 61132 (2012).

[40] T. J. Kippenberg and K. J. Vahala, Science **321**, 1172 (2008).

[41] F. Marquardt and S. M. Girvin, Physics **2**, 40 (2009).

[42] A. A. Clerk, M. H. Devoret, S. M. Girvin, F. Marquardt, and R. J. Schoelkopf, Rev. Mod. Phys. **82**, 1155 (2010).

[43] M. Aspelmeyer, T. J. Kippenberg, and F. Marquardt, Rev. Mod. Phys. **86**, 1391 (2014).

[44] F. Marquardt, J. P. Chen, A. A. Clerk, and S. M. Girvin, Phys. Rev. Lett. **99**, 093902 (2007).

[45] I. Wilson-Rae, N. Nooshi, W. Zwerger, and T. J. Kippenberg, Phys. Rev. Lett. **99**, 093901 (2007).

[46] F. Marquardt, A. A. Clerk, and S. M. Girvin, J. Mod. Opt. **55**, 3329 (2008).

[47] F. Elste, S. M. Girvin, and A. A. Clerk, Phys. Rev. Lett. **102**, 207209 (2009).

[48] R. W. Peterson, T. P. Purdy, N. S. Kampel, R. W. Andrews, P.-L. Yu, K. W. Lehnert, and C. A. Regal, Phys. Rev. Lett. **116**, 063601 (2016).

[49] A. D. O'Connell, M. Hofheinz, M. Ansmann, R. C. Bialczak, M. Lenander, E. Lucero, M. Neeley, D. Sank, H. Wang, M. Weides, J. Wenner, J. M. Martinis, and A. N. Cleland, Nature (London) **464**, 697 (2010).

[50] J. Chan, T. P. M. Alegre, A. H. Safavi-Naeini, J. T. Hill, A. Krause, S. Gröblacher, M. Aspelmeyer, and O. Painter, Nature (London) **478**, 89 (2011).

[51] J. D. Teufel, T. Donner, D. Li, J. W. Harlow, M. S. Allman, K. Cicak, A. J. Sirois, J. D. Whittaker, K. W. Lehnert, and R. W. Simmonds, Nature (London) **475**, 359 (2011).

[52] P. Rabl, A. Shnirman, and P. Zoller, Phys. Rev. B **70**, 205304 (2004).

[53] T. P. Purdy, P.-L. Yu, R. W. Peterson, N. S. Kampel, and C. A. Regal, Phys. Rev. X **3**, 031012 (2013).

[54] A. H. Safavi-Naeini, S. Gröblacher, J. T. Hill, J. Chan, M. Aspelmeyer, and O. Painter, Nature (London) **500**, 185 (2013).

[55] A. Nunnenkamp, K. Børkje, and S. M. Girvin, Phys. Rev. Lett. **107**, 063602 (2011).

[56] P. Rabl, Phys. Rev. Lett. **107**, 063601 (2011).

[57] K. Børkje, A. Nunnenkamp, J. D. Teufel, and S. M. Girvin, Phys. Rev. Lett. **111**, 053603 (2013).

[58] M.-A. Lemonde, N. Didier, and A. A. Clerk, Phys. Rev. Lett. **111**, 053602 (2013).

[59] X. Xu, M. Gullans, and J. M. Taylor, Phys. Rev. A **91**, 013818 (2015).

[60] M.-A. Lemonde, N. Didier, and A. A. Clerk, Nat. Commun. **7**, 11338 (2016).

[61] L. D. Tóth, N. R. Bernier, A. Nunnenkamp, A. K. Feofanov, and T. J. Kippenberg, Nat. Phys. **13**, 787 (2017).

[62] K. Yamamoto, D. Friedrich, T. Westphal, S. Goßler, K. Danzmann, K. Somiya, S. L. Danilishin, and R. Schnabel, Phys. Rev. A **81**, 033849 (2010).

[63] A. Sawadsky, H. Kaufer, R. M. Nia, S. P. Tarabrin, F. Y. Khalili, K. Hammerer, and R. Schnabel, Phys. Rev. Lett. **114**, 043601 (2015).

[64] A. M. Jayich, J. C. Sankey, B. M. Zwickl, C. Yang, J. D. Thompson, S. M. Girvin, A. A. Clerk, F. Marquardt, and J. G. E. Harris, New J. Phys. **10**, 095008 (2008).

[65] X. Xu and J. M. Taylor, Phys. Rev. A **90**, 043848 (2014).

[66] C. Stambaugh, H. Xu, U. Kemiktarak, J. Taylor, and J. Lawall, Ann. Phys. (Berlin) **527**, 81 (2015).

[67] M. Paternostro, S. Gigan, M. S. Kim, F. Blaser, H. R. Böhm, and M. Aspelmeyer, New J. Phys. **8**, 107 (2006).

[68] C. W. Gardiner and M. J. Collett, Phys. Rev. A **31**, 3761 (1985).

[69] H. Grabert, U. Weiss, and P. Talkner, Z. Phys. B **55**, 87 (1984).

[70] P. Hänggi and G.-L. Ingold, Chaos **15**, 026105 (2005).

[71] U. Weiss, *Quantum Dissipative Systems*, 3rd ed. (World Scientific, Singapore, 2008).

[72] C. W. Gardiner and P. Zoller, *Quantum Noise : a Handbook of Markovian and Non-Markovian Quantum Stochastic Methods with Applications to Quantum Optics*, Springer Series in Synergetics, Vol. 56 (Springer, Berlin, 2004).

[73] H. Xu, U. Kemiktarak, J. Fan, S. Ragole, J. Lawall, and J. M. Taylor, Nat. Commun. **8**, 14481 (2017).

[74] D. J. Wineland and W. M. Itano, Phys. Rev. A **20**, 1521 (1979).

[75] J. Dalibard and C. Cohen-Tannoudji, J. Opt. Soc. Am. B **2**, 1707 (1985).

[76] S. Chu, Rev. Mod. Phys. **70**, 685 (1998).

[77] C. N. Cohen-Tannoudji, Rev. Mod. Phys. **70**, 707 (1998).

[78] W. D. Phillips, Rev. Mod. Phys. **70**, 721 (1998).

[79] H. J. Metcalf and P. van der Straten, J. Opt. Soc. Am. **20**, 887 (2003).

[80] I. Bloch, J. Dalibard, and W. Zwerger, Rev. Mod. Phys. **80**, 885 (2008).

[81] M. Saffman, T. G. Walker, and K. Mølmer, Rev. Mod. Phys. **82**, 2313 (2010).

[82] H. Weimer, M. Muller, I. Lesanovsky, P. Zoller, and H. P. Buchler, Nat. Phys. **6**, 382 (2010).

[83] D. J. Heinzen, J. J. Childs, J. E. Thomas, and M. S. Feld, Phys. Rev. Lett. **58**, 1320 (1987).

[84] V. Vuletić and S. Chu, Phys. Rev. Lett. **84**, 3787 (2000).

[85] V. Vuletić, H. W. Chan, and A. T. Black, Phys. Rev. A **64**, 033405 (2001).

[86] E. A. Curtis, C. W. Oates, and L. Hollberg, Phys. Rev. A **64**, 031403 (2001).

[87] A. Beige, P. L. Knight, and G. Vitiello, Braz. J. Phys. **35**, 403 (2005).

[88] B. L. Lev, A. Vukics, E. R. Hudson, B. C. Sawyer, P. Domokos, H. Ritsch, and J. Ye, Phys. Rev. A **77**, 023402 (2008).

[89] D. V. Seletskiy, S. D. Melgaard, S. Bigotta, A. Di Lieto, M. Tonelli, and M. Sheik-Bahae, Nat. Photon. **4**, 161 (2010).

[90] M. Xu, S. B. Jäger, S. Schütz, J. Cooper, G. Morigi, and M. J. Holland, Phys. Rev. Lett. **116**, 153002 (2016).

[91] M. Hosseini, Y. Duan, K. M. Beck, Y.-T. T. Chen, and V. Vuletić, Phys. Rev. Lett. **118**, 183601 (2017).

[92] M. Fleischhauer, J. Otterbach, and R. G. Unanyan, Phys. Rev. Lett. **101**, 163601 (2008).

[93] J. Klaers, F. Vewinger, and M. Weitz, Nat. Phys. **6**, 512 (2010).

[94] J. Klaers, J. Schmitt, T. Damm, F. Vewinger, and M. Weitz, Appl. Phys. B **105**, 17 (2011).

[95] P. Kirton and J. Keeling, Phys. Rev. Lett. **111**, 100404 (2013).

[96] J. Klaers, J. Phys. B **47**, 243001 (2014).

[97] J. Marelic and R. A. Nyman, Phys. Rev. A **91**, 033813 (2015).

[98] J. Schmitt, T. Damm, D. Dung, F. Vewinger, J. Klaers, and M. Weitz, in *Laser Spectrosc.* (World ScientificSingapore, 2016) pp. 85–96.

[99] S. Greveling, K. L. Perrier, and D. van Oosten, (2017), arXiv:1712.08426 .

[100] J. Klaers, J. Schmitt, T. Damm, F. Vewinger, and M. Weitz, Phys. Rev. Lett. **108**, 160403 (2012).

[101] V. I. Yukalov, Laser Phys. **22**, 1145 (2012).

[102] M. J. J. Gullans, J. Stehlik, Y.-Y. Liu, C. Eichler, J. R. Petta, and J. M. Taylor, Phys. Rev. Lett. **117**, 056801 (2016).

[103] C.-H. Wang and J. M. Taylor, Phys. Rev. A **97**, 033850 (2018).

[104] K. I. Seetharam, C.-E. Bardyn, N. H. Lindner, M. S. Rudner, and G. Refael, Phys. Rev. X **5**, 041050 (2015).

[105] J. Dalibard, Y. Castin, and K. Molmer, Phys. Rev. Lett. **68**, 580 (1992).

[106] H. Carmichael, *An Open Systems Approach to Quantum Optics: Lectures Presented at the Université Libre de Bruxelles, October 28 to November 4, 1991* (Springer Berlin, 1993) p. 192.

[107] S. Stellmer, B. Pasquiou, R. Grimm, and F. Schreck, Phys. Rev. Lett. **110**, 263003 (2013).

[108] C. I. Westbrook, R. N. Watts, C. E. Tanner, S. L. Rolston, W. D. Phillips, P. D. Lett, and P. L. Gould, Phys. Rev. Lett. **65**, 33 (1990).

[109] A. D. Ludlow, M. M. Boyd, J. Ye, E. Peik, and P. O. Schmidt, Rev. Mod. Phys. **87**, 637 (2015).

[110] Y. B. Zel'Dovich and E. V. Levich, Sov. Phys. JETP **28**, 1287 (1969).

[111] A.-W. de Leeuw, H. T. C. Stoof, and R. A. Duine, Phys. Rev. A **88**, 033829 (2013).

[112] M. Fani and M. H. Naderi, J. Opt. Soc. Am. B **33**, 1242 (2016).

[113] R. Y. Chiao, Opt. Commun. **179**, 157 (2000).

[114] J. Lebreuilly, A. Chiocchetta, and I. Carusotto, Phys. Rev. A **97**, 033603 (2018).

[115] D. Kilda and J. Keeling, (2017), arXiv:1709.06361 .

[116] L. M. Sieberer, S. D. Huber, E. Altman, and S. Diehl, Phys. Rev. Lett. **110**, 195301 (2013) (2013).

[117] U. C. Täuber and S. Diehl, Phys. Rev. X **4**, 021010 (2014).

[118] M. F. Maghrebi and A. V. Gorshkov, Phys. Rev. B **93**, 014307 (2016).

[119] L. M. Sieberer, M. Buchhold, and S. Diehl, Rep. Prog. Phys. **79**, 096001 (2016).

[120] T. Walker, D. Sesko, and C. Wieman, Phys. Rev. Lett. **64**, 408 (1990).

[121] G. Labeyrie, F. de Tomasi, J. C. Bernard, C. A. Müller, C. Miniatura, and R. Kaiser, Phys. Rev. Lett. **83**, 5266 (1999).

[122] W. Guerin, M. T. Rouabah, and R. Kaiser, J. Mod. Opt. **64**, 895 (2017).

[123] R. Saint-Jalm, M. Aidelsburger, J. L. Ville, L. Corman, Z. Hadzibabic, D. Delande, S. Nascimbene, N. Cherroret, J. Dalibard, and J. Beugnon, Phys. Rev. A **97**, 061801 (2018).

[124] C. Cohen-Tannoudji, J. Dupont-Roc, and G. Grynberg, *Atom-Photon Interactions: Basic Processes and Applications* (Wiley, New York, 1998).

[125] P. D. Lett, W. D. Phillips, S. L. Rolston, C. E. Tanner, R. N. Watts, and C. I. Westbrook, J. Opt. Soc. Am. B **6**, 2084 (1989).

[126] H. M. Pastawski, Phys. B (Amsterdam, Neth.) **398**, 278 (2007).

[127] B. Gumhalter, A. Šiber, H. Buljan, and T. Fauster, Phys. Rev. B **78**, 155410 (2008).

[128] Imamoğlu, A. and Ram, R J and Pau, S and Yamamoto, Y, Phys. Rev. A **53**, 4250 (1996).

[129] H. Deng, G. Weihs, C. Santori, J. Bloch, and Y. Yamamoto, Science **298**, 199 (2002).

[130] J. Keeling, F. M. Marchetti, M. H. Szymańska, and P. B. Littlewood, Semicond. Sci. Technol. **22**, R1 (2007).

[131] J. T. Mendonça and H. Terças, Phys. Rev. A **95**, 063611 (2017).

[132] C. Connaughton, C. Josserand, A. Picozzi, Y. Pomeau, and S. Rica, Phys. Rev. Lett. **95**, 263901 (2005).

[133] C. Sun, S. Jia, C. Barsi, S. Rica, A. Picozzi, and J. W. Fleischer, Nat. Phys. **8**, 470 (2012).

[134] I. Chiocchetta, A and Larré, P-É and Carusotto, EPL **115**, 24002 (2016).

[135] N. Šantić, A. Fusaro, S. Salem, J. Garnier, A. Picozzi, and R. Kaiser, Phys. Rev. Lett. **120**, 055301 (2018).

[136] D. W. Snoke and S. M. Girvin, J. Low Temp. Phys. **171**, 1 (2013).

[137] J. Schmitt, T. Damm, D. Dung, F. Vewinger, J. Klaers, and M. Weitz, Phys. Rev. Lett. **112**, 030401 (2014).

[138] B. T. Walker, L. C. Flatten, H. J. Hesten, F. Mintert, D. Hunger, J. M. Smith, and R. A. Nyman, (2017), arXiv:1711.11087 .

[139] A. Kruchkov and Y. Slyusarenko, Phys. Rev. A **88**, 013615 (2013).

[140] A. J. Kruchkov, Phys. Rev. A **93**, 1 (2016).

[141] R. Weill, A. Bekker, B. Levit, M. Zhurahov, and B. Fischer, Opt. Express **25**, 18963 (2017).

[142] C.-H. Wang, M. J. Gullans, J. V. Porto, W. D. Phillips, and J. M. Taylor, Phys. Rev. A **98**, 013834 (2018).

[143] V. Bagnato and D. Kleppner, Phys. Rev. A **44**, 7439 (1991).

[144] W. J. Mullin, J. Low Temp. Phys. **106**, 615 (1997).

[145] H. Kogelnik and T. Li, Appl. Opt. **5**, 1550 (1966).

[146] A. E. Siegman, *Lasers* (University Science Books, Sausalito, California, 1986).

[147] U. Schneider, L. Hackermüller, J. P. Ronzheimer, S. Will, S. Braun, T. Best, I. Bloch, E. Demler, S. Mandt, D. Rasch, and A. Rosch, Nat. Phys. **8**, 213 (2012).

[148] K. M. Birnbaum, A. Boca, R. Miller, A. D. Boozer, T. E. Northup, and H. J. Kimble, Nature (London) **436**, 87 (2005).

[149] M. Hartmann, F. Brandão, and M. Plenio, Laser Photonics Rev. **2**, 527 (2008).

[150] A. J. Hoffman, S. J. Srinivasan, S. Schmidt, L. Spietz, J. Aumentado, H. E. Türeci, and A. A. Houck, Phys. Rev. Lett. **107** (2011), 10.1103/PhysRevLett.107.053602.

[151] R. Landauer, IBM J. Res. Dev. **1**, 223 (1957).

[152] R. Landauer, Philos. Mag. **21**, 863 (1970).

[153] Y. Imry and R. Landauer, Rev. Mod. Phys. **71**, S306 (1999).

[154] M. Büttiker, Phys. Rev. Lett. **57**, 1761 (1986).

[155] C. Caroli, R. Combescot, P. Nozieres, and D. Saint-James, J. Phys. C **4**, 916 (1971).

[156] Y. Meir and N. S. Wingreen, Phys. Rev. Lett. **68**, 2512 (1992).

[157] H. Haug, A.-P. Jauho, and M. Cardona, *Quantum Kinetics in Transport and Optics of Semiconductors*, Vol. 14 (Springer, Berlin Heidelberg, 2008).

[158] L. V. Keldysh, Sov. Phys. JETP **20**, 1018 (1965).

[159] D. C. Langreth, in *Linear Nonlinear Electron Transp. Solids*, edited by J. T. Devreese and V. E. van Doren (Plenum, New York, 1976) pp. 3–32.

[160] P. Wurfel, J. Phys. C **15**, 3967 (1982).

[161] H. Ries and A. J. McEvoy, J. Photochem. Photobiol. Chem. **59**, 11 (1991).

[162] F. Herrmann and P. Würfel, Am. J. Phys. **73**, 717 (2005).

[163] G. Smestad and H. Ries, Sol. Energy Mater. Sol. Cells **25**, 51 (1992).

[164] P. Berdahl, J. Appl. Phys. **58**, 1369 (1985).

[165] J.-S. Wang, B. K. Agarwalla, H. Li, and J. Thingna, Front. Phys. **9**, 673 (2014).

[166] G. J. Milburn, J. Phys. A **17**, 737 (1984).

[167] P. A. Lee and T. V. Ramakrishnan, Rev. Mod. Phys. **57**, 287 (1985).

[168] Y. Imry, *Introduction to Mesoscopic Physics*, 2nd ed. (Oxford University Press, Oxford, UK, 2002).

[169] E. Akkermans and G. Montambaux, *Mesoscopic Physics of Electrons and Photons* (Cambridge University Press, Cambridge, UK, 2007).